EFFECTS OF RADIATION SHELTERING AND SCATTERING FROM DISTANT LANDSCAPES ON THE ACCUMULATION AND ABLATION OF SNOW IN LA JARA CATCHMENT IN THE VALLES CALDERA

By

Alex J. Rinehart

Submitted in Partial Fulfillment of Requirements for the

Masters of Science in Hydrology

New Mexico Institute of Mining and Technology
Department of Earth and Environmental Sciences

Socorro, New Mexico

August 2008

This thesis is accepted on behalf of the
Faculty of the Institute by the following committee:

Enrique R. Vivoni
Advisor

Date

I release this document to the New Mexico Institute of Mining and Technology.

Student's Signature

August 1, 2008
Date

To my parents, Eric and Leslie Rinehart

ABSTRACT

Scattering of, and sheltering from, incoming shortwave radiation by the surrounding landscape, including topography, vegetation and snow, is an under-emphasized process in snow-dominated montane catchments, especially in regions of higher solar flux such as the southwestern United States. The sensitivity of the distribution of snow in space and time to different representations of these processes has not been clearly evaluated. I have developed a single-layer distributed snow model (DSM) that includes snow interception in the canopy and multiple representations of sheltering and scattering of shortwave radiation. Representations of sheltering include (1) only local controls by slope and aspect, (2) both local controls and remote shading where distant topography may directly block the sun and restricts the amount of visible sky, (3) both local controls and remote scattering where distant topography reflects light onto other points, and (4) combined local controls, and remote shading and scattering. There is no scattering when only local controls are considered. The visible surface controls the amount of scattered light by changing the effective landscape albedo. I have represented the effective landscape albedo as (1) local vegetation albedo, (2) local snow albedo, and (3) a dynamic mixed albedo that captures both the varying conditions of the canopy and the vegetative fraction.

I have applied the model to La Jara catchment (35.858°N 106.521°W) in the Valles Caldera in the Jemez Mountains of central New Mexico. La Jara drains from

the regional topographic high, Redondo Peak, and is a fairly homogenously forest of subalpine fir (*Abies lasiocarpa*). La Jara contains a wide range of slopes and aspect with a predominantly south-southeast aspect. Nonetheless, Redondo Peak is highly visible to most of the catchment. The radiation sheltering on the flank of Redondo Peak, conversely, is dominated by local shading (e.g., slope and aspect). Given the homogeneity of vegetation and topographic setting, La Jara is appropriate for this sensitivity study.

I have simulated four cases between 1 November 2004 and 5 June 2005: (1) local controls; (2) remote controls (shading and scattering) with vegetation landscape albedo; (3) remote controls with snow landscape albedo; and (4) remote controls with dynamic mixed landscape albedo. The remotely controlled case with vegetation landscape albedo has shown few differences from the local case, implying that scattered light compensates for the decrease in radiation from remote sheltering. When using snow albedo, large deviations in the dynamics of both radiation and snow-cover have been found. The absorbed shortwave radiation differed from -11 W/m^2 to +6.5 W/m^2. The season maximal SWE differed by ±26 cm, while the date of maximum SWE differed from –37 days to +41 days. The total number of snow covered days over the simulation period decreased by 40 days at most. Thus, when snow albedo is used, almost all deviations indicate that scattered radiation far exceeds the effects of sheltering by remote topography. When the mixed albedo was used, the radiation and SWE were found to be nearly identical to the case when snow albedo is used.

For completeness, 16 other simulations were completed. Four of these consisted of using a uniform surface albedo of 0.6 and modeling absorbed shortwave radiation for (1) local controls, (2) local controls and remote shading, (3) local controls and remote scattering. Parallel simulations were completed with a snow dynamics modeled, incorporating transient albedo. Remote shading was found to decrease the absorbed shortwave radiation, leading to more persistent snow pack through the simulation including snow dynamics. Remote scattering increased the absorbed radiation. When snow dynamics were used, this led to a less persistent snow pack. When vegetation hillslope albedo was used, smaller, less spatially extensive increases in absorbed radiation occurred. When snow or mixed hillslope albedo was used, the increases in absorbed radiation were found to be of greater magnitude and covering more catchment area. By comparing the cases incorporating both remote shading and scattering, and the cases applying only either shading or scattering, it was clear that the combined case was a composite of the latter cases. The hillslope representation controlled which case was more dominant. If vegetation albedo was used, then the combined case was closer to the shading case than the scattering-only case. If snow or mixed albedo was used, the converse was true. It is clear that for La Jara, distant interactions of radiation, snow, vegetation and topography are critical to consider in regions of high radiative fluxes and rugged topography.

ACKNOWLEDGEMENTS

Many people contributed to this work. I would like to thank my committee, Paul Brooks, Fred Phillips and John Wilson, and my advisor, Enrique Vivoni, for their guidance. Bayani Cardenas, Kate Duke, Carlos Aragon, Casey Elliott, Laura Rosales-Lagarde, Marty Frisbee, Matthew Bailie, Lisa Majkowski-Taylor, Ricardo Mantilla, Soni Yatheendradas and Sammy Ndur all endured many hours as I talked through problems with the implementation of the model and deserve special acknowledgement; all also formed a major part of my life through their friendship. Robert Bowman provided support both financially and morally by allowing me to work on his property. Keith Musselman and the participants of Univeristy of Arizona's 2005 snow camp collected the raw data used for verification and helped begin building my understanding of snow processes. Gary Axen and Peter Mozley deserve thanks for their engaging conversation about society and science in general.

Bruce Harrison, Robert Wyckoff, Michael Jennings, Penny Boston, Robert Bowman, John Wilson and my family, Eric, Leslie, Elizabeth and Adam Rinehart, deserve special thanks for their unwavering support and advice during critical times. Without them, this thesis would not have been completed.

Robert Parmenter and the staff of the Valles Caldera National Preserve provided access to the meteorological data and Arc GIS layer used to force and

generate the model applications in this thesis. Their responsiveness and general good cheer always made working with them a pleasure.

This work was supported under the National Science Foundation (NSF) Graduate Research Fellowship, NSF Grant EAR 0342526, and the New Mexico Water Resources Research Institute--Student Grant Program. I also received financial support from the New Mexico Institute of Mining and Technology's Department of Earth and Environmental Sciences for assisting in the instruction of Hydrology 508—Flow and Transport in Geologic Settings with John Wilson.

TABLE OF CONTENTS

LIST OF TABLES

LIST OF FIGURES

CHAPTER 1: INTRODUCTION

1.1 Background and Motivation

Snowmelt from headwaters in montane regions is one of the primary sources of usable surface water in the semiarid southwestern United States and throughout the West (Bales et al., 2006; Rango, 2006). Changing climate, however, has caused winter snowpacks during the late twentieth and early twenty first centuries to become shallower and more intermittent in much of the western United States (Mote et al., 2005). While the long-term effects of decreasing snowpack in semiarid continental basins may be foreseeable, it is necessary for water-management purposes to develop a clear understanding of the spatial distribution of snow during both accumulation and melt periods, and what effects different spatial and temporal patterns have on the timing and magnitude melt-dominated spring runoff.

Many of the areas that face decreasing seasonal snow pack are in the semiarid Southwest, which faces increasing population with rapidly diminishing water supplies. At the same time, the dynamics of snow in the headwaters of these regions has not been addressed by either modeling or field efforts (Bales et al., 2006). The lack of extensive study leads to uncertainty as to what are the dominant controls on the distribution of snow within headwater catchments. These catchments are in mountainous terrain, which has classically been difficult to study and poorly

understood due to rugged topography and the multiple closely located and intermingled ecosystems (Bales et al., 2006). These gaps in knowledge have led to a critical need to better understand the processes controlling the partitioning of mass and energy in the montane headwater catchments of the semiarid Southwest.

Given equal snow fall, the partitioning of water and energy determines the distribution of snow (Anderson, 1976). Different areas of the landscape may receive significantly different proportions and magnitudes of snow, rain, and incoming solar radiation. Air temperature, air pressure, wind speed and ground heat flux also control the energy partitioning and they vary dramatically in space (Dozier, 1980; Male and Gray, 1981; Williams and Tarboton, 1999). Vegetation and topography both have important controls on the fluxes into or from the snowpack. For example, vegetation increases the effective surface area from which snow can be sublimated by intercepting it in the canopy, but also decreases the amount of solar radiation reaching the ground and shelters areas from high winds (Gelfan et al., 2004; Pomeroy et al., 1998).

Rugged topography can shelter the snowpack by limiting the incoming diffuse radiation, shading snow from direct solar radiation, and decreasing wind velocities (Dozier, 1980; Marks et al., 2002). Topographic features also can expose snow to increased sublimation when there is an exposed ridgeline or plain with high winds, and also can expose distant snow packs to increased incoming longwave radiation and scattered light (Oke, 1987).

Most previous studies addressing the coupling of vegetation, topography and snow, whether model or field based, have been conducted in the Canadian prairie and

tundra (Liston and Elder, 2006; Liston et al., 2002; Pomeroy et al., 2006; Pomeroy et al., 1997; Strack et al., 2007; Sturm et al., 2005a; Sturm et al., 2001; Sturm et al., 2005b; Tape et al., 2006), in alpine maritime settings (Hubbart et al., 2007; Storck et al., 2002; Whitaker and Sugiyama, 2005), and the boreal forest (Brundl et al., 1999; Gelfan et al., 2004; Harding and Pomeroy, 1996; Liston and Elder, 2006; Pomeroy and Dion, 1996; Pomeroy et al., 2002; Pomeroy et al., 1998a; Pomeroy et al., 1998b; Zhang et al., 2004). Other studies have examined the effects of topography on the wind redistribution of snow in the northern portions of the semiarid Basin and Range and continental alpine settings (Baron et al., 1998; Hiemstra et al., 2002; Hubbart et al., 2007; Koivusalo and Kokkonen, 2002; Liston and Elder, 2006; Marks and Winstral, 2001; Marks et al., 2002; Parviainen and Pomeroy, 2000; Pomeroy et al., 2006; Pomeroy et al., 2002; Shamir and Georgakakos, 2006; Talbot et al., 2006; Williams et al., 1999; Woods et al., 2006; Zappa et al., 2003). Despite increasing social concerns, continental mountain basins at lower latitudes (i.e., the semiarid Southwest) have received little attention. Given their higher exposure to solar radiation, and the variable air temperature and relative humidity, snow cover in these regions is shallower and more transient than in other settings (Musselman, 2006; Rango, 2006). These regions also contain rugged mountain topography and variable vegetation that further complicate snow dynamics (Bales et al., 2006; Rango, 2006).

To help understand snow dynamics, mathematical models have been developed (Anderson, 1976; Hock, 2003). These mathematical models have proven able to perform reasonably in snow-dominated regions at high latitudes (Anderson, 1976; Gelfan et al., 2004; Hock, 2003; Lehning et al., 2006; Liston and Elder, 2006).

Currently developed and new models need to be applied to catchments in the semiarid Southwest and necessary adjustments made in order to capture the potentially important differences from previously studies settings (e.g., boreal forest, high latitude mountain forest, and high latitude prairie and tundra).

The following is an overview of snow processes, the implemented model and the remainder of the thesis. The summary focuses on the experimental design and scientific question presented in Chapter 2, but also includes an overview of ancillary results and discussion, concluding statements and recommendations for future work (Chapter 3), as well as a synopsis of the algorithm documentation (Appendix).

1.2 Review of Snow Processes

Before embarking into a study of the sensitivities of snow cover to variations in radiative fluxes, it is necessary to briefly review the processes that control snow dynamics. Figure 1.1 presents a schematic of the major fluxes, processes and states that dominate the snow-covered landscape. These variables group into processes that affect both snow in the canopy and snow on the ground (top-center of Fig. 1.1), processes limited strictly to snow in the canopy (right-hand side of Fig. 1.1), and processes related to the state of the snow pack, i.e., snow on the ground (left-hand side of Fig. 1.1). The following material was derived from Male and Gray (1981).

The three water and energy fluxes that affect both snow on the ground and in the canopy are incoming shortwave radiation, incoming longwave radiation and precipitation. Incoming shortwave radiation is solar radiation in the visible and ultraviolet bands. Geographic position, day of year, cloud cover, humidity, the fraction of sky visible from a point, the reflected radiation from the surrounding

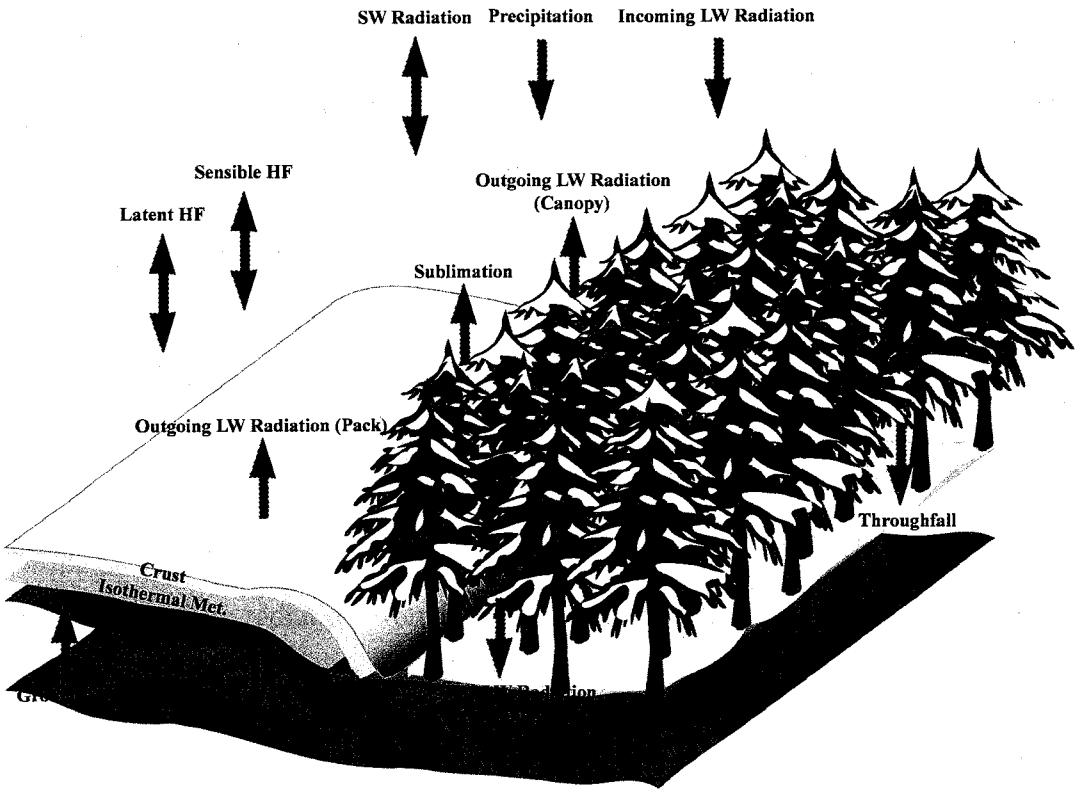

Figure 1.1 Schematic of dominant mass and energy fluxes in a snow-covered landscape. Fluxes over the entirety of schematic influence both dynamics in the canopy and snow pack. Fluxes on a given side only affect the canopy or snow pack, respectively.

landscape, scattering and extinction within a canopy, and the albedo (reflectivity) of the surface control the amount of radiation absorbed by at a point. These controls exit in all settings. In snow-covered settings, shortwave radiation behaves in specific ways that are generally considered unimportant in other settings. The high time-varying albedo of snow decreases the amount of absorbed shortwave radiation by a factor of 3 to 4. Because of the higher albedo, a greater amount of light is reflected from the surface, increasing the amount of incoming radiation at other points in the landscape. Absorbed shortwave radiation can penetrate fairly deep into the snow (~0.2 m), and, when snow is shallow, this radiation warms the surface beneath it. This can be especially important in areas of low albedo (i.e. rock outcrops) and in the vegetation

canopy. The warmed surface leads to lower viscosities and greater rates of mass movement (i.e., increased chances of avalanche and sloughing). For both the snow pack and snow in the canopy, greater incoming shortwave radiation increases the internal energy of the system, leading to higher snow temperatures, increased melt and, for snow in the canopy, greater sublimation.

Incoming longwave radiation is the radiation coming from the sky and landscape due to thermal emission. This is controlled by the temperature of the emitting media (i.e., air or surface temperature) and the emissivity of the media. Incoming longwave radiation from the surrounding land-surface can be significant enough to lead to preferential melt, especially in regions with steep, exposed, and dark bedrock. Even without these heterogeneities, incoming longwave radiation often forms a large portion of the incoming energy to snow throughout the landscape.

Processes related to precipitation in snow-covered environments are also primary drivers of snow dynamics. Snow- and rainfall are complicated in snow-covered environments by the multiple occurring forms of precipitation. These include not only rainfall and 'snow', but the many different forms of snow, freezing rain, sleet, hail, and mist. Each of form interacts differently with existing snow and initially forms different morphologies of snow cover. Rain-on-snow events can lead to the formation of horizontal ice layers within a snow pack, vertical channels from the snow surface down, among others. Rain-on-snow events can also cause large unloading events if snow is in the canopy. If precipitation is solid phase, then it can load the canopy with snow, and, if snow already exists in the canopy, cause both further accumulation of snow and unloading to occur. Snow-on-snow events lead to

new stratigraphic layers of snow, often burying previously formed surface crusts and changing the density, permeability and morphology of buried snow.

The dynamics of snow in the canopy are very complicated. They fall into three categories: loading the canopy with snow, transformations of snow in the canopy and unloading the canopy. The process of loading the canopy is complex. Individual snow flakes interact with other snow flakes, individual leaves and clusters of leaves, and branches. Once snow begins to settle into trees, then crystal to crystal interactions occur. If snow already is in the canopy, then the change in surface roughness from the bare branches and leaves may be significant. The orientation of individual branches may affect their ability to gain snow. In addition, vegetation varies considerably from plant to plant, stand to stand, forest to forest.

Once snow is established in the canopy, then wind, changes in air temperature, shortwave radiation, longwave radiation emitted from the sky, distant landscape and the tree itself, and additional precipitation all change the state of intercepted snow. Surface crusts can form, as well as weak fluid layers at the branch-snow interface. Sublimation is thought to be a large loss (up to 15% of the seasons snow pack). Traditionally, sublimation, or latent heat flux from solid to vapor phase, is strictly a function of relative humidity, atmospheric pressure, surface roughness and wind speed. Given the difficulties in calculating an exact energy balance in the canopy, sublimation from the canopy is conceptualized as a combination of the traditional form (vapor pressure gradients and turbulent mixing driving phase transitions) and available energy from shortwave radiation. Given the complexities of extinction and

absorption of shortwave radiation, as well as the complex micrometeorology of canopies, this basic conceptualization of 'available energy' appears reasonable.

Snow does not remain in the canopy for very long periods of time. After being captured by the vegetation, it is either sublimated or unloaded. The problem of unloading from the canopy is challenging. Individual branches are unique both in the physical characteristics, but also in their orientation in space with respect to both gravity and wind. High winds, rainfall, exposure to the sun, and aging of the snow all lead to branches sloughing off the intercepted snow.

Once the snow reaches the ground, a variety of processes occur that transform it until it eventually melts or sublimates. The internal energy, temperature and phase gradients, internal structure, mass and history all determine the state and response of the snow pack. For example, if there is a refrozen crust at the surface, this will limit air circulation and water infiltration from penetrating deeper into the pack. A buried or frozen ice layer in the pack can stop infiltration of rain water, but the ice layer itself is a manifestation of the history of the snow pack; either water infiltrated and froze or a surface ice crust (formed by melt or wind-packing) was buried by a large snow event.

Other states of the snow pack include are layers that have undergone either equi-temperature metamorphism or have metamorphosed to hoar. Equi-temperature metamorphism is the transformation of ice from pointed and edged crystals to nearly spherical and fairly uniformly sized crystals. This occurs as the ice surface minimizes surface area in the presence of air and water vapor. Hoar occurs in areas with persistent gradients in water vapor pressure. As water is sublimated from the ice, it is

passed down gradient (generally, upward from near the ground surface) 'hand-to-hand', i.e., from crystal to crystal. The loss of water leads to low density snow with individual crystals that have become faceted in a step-like pattern. In many snow packs in the Southwest, with depths of less than 2 m, the snow pack consists of hoar at the base of the pack, alternating and variably aged layers of ice and equi-temperature metamorphosed snow in the interior and a wind- and melt- hardened ice crust at the surface.

There are several sources of mass and energy for a snow pack. Neglecting avalanches, precipitation and unloading from a canopy are the primary sources of water. Snow is often is transported by the wind and can be very significant. Exposed ridgelines will generally have thinner snow packs, while sheltered areas downwind will have more snow, often with a looser, less dense structure than in snow pack formed strictly by precipitation. Vegetation serves to shelter snow from winds. Wind also forces turbulent heat exhange, both latent (from variation in relative humidity) and sensible (from variation in temperature). Turbulent heat exhange can either add or subtract heat from the snow pack, depending on the relative states of the atmosphere and the snow surface. Snow emits longwave thermal radiation and has a very high emmissivity. Outgoing longwave radiation is a major loss of energy for the snow pack, but is usually of the same order as incoming longwave radiation. Most energy exchange occurs within the top 10 cm of the snow pack, and melt water generally forms within the surface layer and percolates down. Ground heat flux driven by temperature gradients can be a large flux early in the season if the shallow

subsurface is very warm or cold, but is often assumed to be negligible after the snow pack is established.

Melt dynamics are complicated by the fact that melt water often refreezes deeper in the snow pack, leading to the formation of ice layers of low permeability to both air and water flow. This can cause perched flow and preferential flow into portions of the pack. Also, the formation of air columns also occurs, allowing preferential flow paths to form within the snow pack. Once melt reaches the land surface, it either infiltrates or runs off. Where frozen soils occur, permeability decreases as the pore spaces of the soil are filled with ice. In snow-dominated mountain settings, the soils often are shallow and the groundwater tables are often shallow, leading to saturated conditions.

1.3 Summary of Implemented Model

In order to examine the effects of radiation-topography-vegetation-snow interactions, a model is required that incorporates the controls of solar radiation. After a review of the current distributed and point snow cover models (see section 2.2), I have implemented a simple model. It consists of an energy balance snow pack model with a single layer adopted from Tarboton and Luce (1996) and Wigmosta et al. (1994). The model physics neglect blowing snow, bulk movement and shallow ground heat flux.

Vegetative controls on snow cover are accounted for in several aspects of the model. Vegetation is represented in the radiation scheme, where the algorithm used to compute scattering and absorption from the canopy is taken from Wilson and Gallant (2000). Vegetation is accounted for in the computation of wind speeds and turbulent

heat fluxes from Strack et al. (2004) and Wigmosta et al. (1994). The model also represents snow interception by the canopy, and the specific algorithm is taken from Liston and Elder (2006) and Pomeroy et al. (1998). Topographic shading from local topography (i.e., slope and aspect interacting with the position of the sun) is computed as in Wilson and Gallant (2000). Shading and scattering from distant surfaces is computed using the algorithm of Dozier and Frew (1990). Four representations of topographic controls on radiation are implemented in the model. The base case only considers local control. The other three cases incorporate shading and scattered radiation from distant features, but vary in the representation of the albedo of the distant surfaces used to calculate the scattered component. One case uses vegetation albedo as the distant albedo. The others use snow albedo, which changes with surface age, and a dynamic mixed vegetation-snow albedo that depends on the existence of snow in the canopy.

The snow model was added as a module of an existing distributed rainfall-runoff model, the TIN-based Real time Integrated Basin Simulator (tRIBS) (Ivanov et al., 2004; Vivoni et al., 2007). Snow melt is partitioned between infiltration and runoff by the existing tRIBS model, and subsequently routed along hillslopes, through streams and into the subsurface according to Ivanov et al. (2004).

1.4 Overview of Thesis

This thesis (1) demonstrates the importance of terrain scattered radiation and the significance of correctly representing the albedo of distant slopes; and (2) introduces and documents the developed distributed snow model (DSM).

The first chapter is this introduction, where a brief overview of the societal need for studies of snow cover in the semiarid Southwest and a description of the model are given. I also introduce the scientific question being addressed.

The second chapter has been written in paper format for submission to the **Ecohydrology** special issue *Mountain Ecohydrology: Quantifying the Role of Vegetation in the Water Balance of Montane Catchments*. The paper focuses on the relative controls of local and remote topographic sheltering from incoming radiation, and the effects of different representations of terrain-scattered radiation on the spatiotemporal distribution of snow in La Jara catchment. Given that this chapter has been submitted as a paper, I have changed from the singular first person suitable to theses to the plural first person used to acknowledge the co-authors. All other chapters are written in singular first person.

In the second chapter, I introduce the study area, La Jara catchment in the Valles Caldera of the Jemez Mountains, NM; review existing approaches to snow cover modeling; provide a detailed description of the implemented DSM; clarify the usefulness of the DSM through point comparison of simulated and measured snow water equivalent (SWE) at the Quemazon SNOTEL station; and describe the discretization and domain representation of the study area and period (1 November 2004 through 5 June 2005). I then present our results from four simulations. The first simulation, which is taken as the base case, considers only local topographic effects on incoming shortwave radiation. It does not account for shading or scattering of radiation from distant slopes. The latter three simulations all account for remote interactions of radiation, topography, snow and vegetation. All three treat shading

similarly. The difference between the three remotely sheltered cases is in the representation of the albedo of distant slopes, (i.e., effective hillslope or landscape albedo). The first case treats the effective landscape albedo as a static vegetation albedo. The second case uses snow albedo and the last case dynamically varies the landscape albedo, depending on the existence of snow in the canopy and the vegetative fraction.

The results of these simulations are presented examine (1) the distribution of diffuse, direct and total incoming radiation (Section 2.4.1); (2) the distribution of maximum SWE (Section 2.4.2); (3) the spatial distributions of the duration that points are snow-covered (Section 2.4.3); and (4) spatial distribution of the day of year in 2005 that peak SWE occurred (Section 2.4.3). These results are synthesized and discussed, focusing on the changes in the spatial and temporal snow dynamics in La Jara and the potential scientific implications (Section 2.5). Finally, the results are summarized (Section 2.6).

Ancillary results of a further sixteen (16) simulations where the radiation scheme is examined in greater detail are provided in Chapter 3. Here, the importance of controls of remote vegetation and topography on reflected shortwave radiation from distant slopes is emphasized. In addition, Chapter 3 presents a detailed summary of the work and recommendations for future studies.

The Appendix documents the numerical implementation of the DSM. Included in the appendix is explicit documentation of the new algorithms developed, adjustments made to the existing tRIBS code, additions to the user manual and

existing documentation, and enumeration of recommended changes to both the DSM module.

1.5 References

Anderson, E.A., 1976. Point energy and mass balance model of a snow cover. NOAA Technical Report NWS 19. 150 pp.

Bales, R.C. et al., 2006. Mountain hydrology of the western United States. Water Resources Research, **42**(8) DOI:10.1029/2005WR004387.

Baron, J.S. et al., 1998. Effects of land cover, water redistribution, and temperature on ecosystem processes in the South Platte Basin. Ecological Applications, **8**(4): 1037-1051.

Dozier, J., 1980. A clear-sky spectral solar radiation model for snow-covered mountainous terrain. Water Resources Research, **16**(4): 709-718.

Dozier, J. and Frew, J., 1990. Rapid calculation of terrain parameters for radiation modeling from digital elevations data. IEEE Transactions on Geoscience and Remote Sensing, **28**(5): 963-969.

Gelfan, A.N., Pomeroy, J.W. and Kuchment, L.S., 2004. Modeling forest cover influences on snow accumulation, sublimation, and melt. Journal of Hydrometeorology, **5**(5): 785-803.

Harding, R.J. and Pomeroy, J.W., 1996. Energy balance of the winter boreal landscape. Journal of Climate, **9**(11): 2778-2787.

Hardy, J.P. et al., 1997. Snow ablation modeling at the stand scale in a boreal jack pine forest. Journal of Geophysical Research-Atmospheres, **102**(D24): 29397-29405.

Hardy, J.P., Davis, R.E., Jordan, R., Ni, W. and Woodcock, C.E., 1998. Snow ablation modelling in a mature aspen stand of the boreal forest. Hydrological Processes, **12**(10-11): 1763-1778.

Hedstrom, N.R. and Pomeroy, J.W., 1998. Measurements and modelling of snow interception in the boreal forest. Hydrological Processes, **12**(10-11): 1611-1625.

Hiemstra, C.A., Liston, G.E. and Reiners, W.A., 2002. Snow redistribution by wind and interactions with vegetation at upper treeline in the Medicine Bow Mountains, Wyoming, USA. Arctic Antarctic and Alpine Research, **34**(3): 262-273.

Hock, R., 2003. Temperature index melt modelling in mountain areas. Journal of Hydrology, **282**(1-4): 104-115.

Harding, R.J. and Pomeroy, J.W., 1996. Energy balance of the winter boreal landscape. Journal of Climate, **9**(11): 2778-2787.

Hardy, J.P. et al., 1997. Snow ablation modeling at the stand scale in a boreal jack pine forest. Journal of Geophysical Research-Atmospheres, **102**(D24): 29397-29405.

Hardy, J.P., Davis, R.E., Jordan, R., Ni, W. and Woodcock, C.E., 1998. Snow ablation modelling in a mature aspen stand of the boreal forest. Hydrological Processes, **12**(10-11): 1763-1778.

Hedstrom, N.R. and Pomeroy, J.W., 1998. Measurements and modelling of snow interception in the boreal forest. Hydrological Processes, **12**(10-11): 1611-1625.

Hiemstra, C.A., Liston, G.E. and Reiners, W.A., 2002. Snow redistribution by wind and interactions with vegetation at upper treeline in the Medicine Bow Mountains, Wyoming, USA. Arctic Antarctic and Alpine Research, **34**(3): 262-273.

Hock, R., 2003. Temperature index melt modelling in mountain areas. Journal of Hydrology, **282**(1-4): 104-115.

Hubbart, J.A., Link, T.E., Gravelle, J.A. and Elliot, W.J., 2007. Timber harvest impacts on water yield in the continental/maritime hydroclimatic region of the United States. Forest Science, **53**(2): 169-180.

Ivanov, V.Y., Vivoni, E.R., Bras, R.L. and Entekhabi, D., 2004. Preserving high-resolution surface and rainfall data in operational-scale basin hydrology: a fully-distributed physically-based approach. Journal of Hydrology, **298**(1-4): 80-111.

Koivusalo, H. and Kokkonen, T., 2002. Snow processes in a forest clearing and in a coniferous forest. Journal of Hydrology, **262**(1-4): 145-164.

Lehning, M. et al., 2006. ALPINE3D: a detailed model of mountain surface processes and its application to snow hydrology. Hydrological Processes, **20**(10): 2111-2128.

Letsinger, S.L. and Olyphant, G.A., 2007. Distributed energy-balance modeling of snow-cover evolution and melt in rugged terrain: Tobacco Root Mountains, Montana, USA. Journal of Hydrology, **336**(1-2): 48-60.

Link, T.E., Marks, D. and Hardy, J.P., 2004. A deterministic method to characterize canopy radiative transfer properties. Hydrological Processes, **18**(18): 3583-3594.

Liston, G.E. and Elder, K., 2006. A distributed snow-evolution modeling system (SnowModel). Journal of Hydrometeorology, **7**(6): 1259-1276.

Liston, G.E., McFadden, J.P., Sturm, M. and Pielke, R.A., 2002. Modelled changes in arctic tundra snow, energy and moisture fluxes due to increased shrubs. Global Change Biology, **8**(1): 17-32.

Lundquist, J.D. and Flint, A.L., 2006. Onset of snowmelt and streamflow in 2004 in the western United States: How shading may affect spring streamflow timing in a warmer world. Journal of Hydrometeorology, **7**(6): 1199-1217.

Male, D.H. and Gray, D.M., 1981. Snowcover ablation and runoff. In: D.H. Male and D.M. Gray (Editors), Handbook of Snow: Principles, Processes, Management and Uses. Blackburn Press, Caldwell, NJ, pp. 360-430.

Marks, D. and Winstral, A., 2001. Comparison of snow deposition, the snow cover energy balance, and snowmelt at two sites in a semiarid mountain basin. Journal of Hydrometeorology, **2**(3): 213-227.

Marks, D., Winstral, A. and Seyfried, M., 2002. Simulation of terrain and forest shelter effects on patterns of snow deposition, snowmelt and runoff over a semi-arid mountain catchment. Hydrological Processes, **16**(18): 3605-3626.

Mote, P.W., Hamlet, A.F., Clark, M.P. and Lettenmaier, D.P., 2005. Declining mountain snowpack in western north America. Bulletin of the American Meteorological Society, **86**(1): 39-49.

Musselman, K., 2006. Quantifying the Effects of Forest Vegetation on Snow Accumulation, Ablation, and Potential Meltwater Inputs, Valles Caldera National Preserve, NM, USA, University of Arizona, Tucson, 127 pp.

Parviainen, J. and Pomeroy, J.W., 2000. Multiple-scale modelling of forest snow sublimation: initial findings. Hydrological Processes, 14(15): 2669-2681

Pomeroy, J.W. et al., 2006. Shrub tundra snowmelt. Hydrological Processes, **20**(4): 923-941.

Pomeroy, J.W. and Dion, K., 1996. Winter radiation extinction and reflection in a boreal pine canopy: Measurements and modelling. Hydrological Processes, **10**(12): 1591-1608.

Pomeroy, J.W., Gray, D.M., Hedstrom, N.R. and Janowicz, J.R., 2002. Prediction of seasonal snow accumulation in cold climate forests. Hydrological Processes, **16**(18): 3543-3558.

Pomeroy, J.W. et al., 1998a. An evaluation of snow accumulation and ablation processes for land surface modelling. Hydrological Processes, **12**(15): 2339-2367.

Pomeroy, J.W., Marsh, P. and Gray, D.M., 1997. Application of a distributed blowing snow model to the arctic. Hydrological Processes, **11**(11): 1451-1464.

Pomeroy, J.W., Parviainen, J., Hedstrom, N. and Gray, D.M., 1998b. Coupled modelling of forest snow interception and sublimation. Hydrological Processes, **12**(15): 2317-2337.

Rango, A., 2006. Snow: The real water supply of the Rio Grande basin. New Mexico Journal of Science, **44**: 99-118.

Shamir, E. and Georgakakos, K.P., 2006. Distributed snow accumulation and ablation modeling in the American River basin. Advances in Water Resources, **29**(4): 558-570.

Storck, P., Lettenmaier, D.P. and Bolton, S.M., 2002. Measurement of snow interception and canopy effects on snow accumulation and melt in a mountainous maritime climate, Oregon, United States. Water Resources Research, **38**(11).

Strack, J.E., Liston, G.E. and Pielke, R.A., 2004. Modeling snow depth for improved simulation of snow-vegetation-atmosphere interactions. Journal of Hydrometeorology, **5**(5): 723-734.

Talbot, J. et al., 2006. Relating snow dynamics and balsam fir stand characteristics, Montmorency Forest, Quebec. Hydrological Processes, **20**(5): 1187-1199.

Tarboton, D.G. and Luce, C.H., 1996. Utah Energy Balance Snow Accumulation and Melt Model (UEB), USFS. 64 pp.

Vivoni, E.R., Ivanov, V.Y., Bras, R.L. and Entekhabi, D., 2004. Generation of triangulated irregular networks based on hydrological similarity. Journal of Hydrologic Engineering, **9**(4): 288-302.

Wigmosta, M.S., Vail, L.W. and Lettenmaier, D.P., 1994. A Distributed Hydrology-Vegetation Model for Complex Terrain. Water Resources Research, **30**(6): 1665-1679.

Williams, K.S. and Tarboton, D.G., 1999. The ABC's of snowmelt: a topographically factorized energy component snowmelt model. Hydrological Processes, **13**(12-13): 1905-1920.

Wilson, J.P. and Gallant, J.C. (Editors), 2000. Terrain Analysis: Principles and Applications. John Wiley and Son, Inc., New York, 91-106 pp.

Zappa, M., Pos, F., Strasser, U., Warmerdam, P. and Gurtz, J., 2003. Seasonal water balance of an Alpine catchment as evaluated by different methods for spatially distributed snowmelt modelling. Nordic Hydrology, **34**(3): 179-202.

CHAPTER II: EFFECTS OF VEGETATATION, ALBEDO, AND RADIATION SHELTERING ON THE DISTRIBUTION OF SNOW IN THE VALLES CALDERA, NEW MEXICO

2.1 Abstract

The effects of radiation scattering and sheltering on snow distributions are poorly understood in montane regions of the southwestern United States. To examine this, we develop a single-layer distributed snow model that includes canopy interception and radiation scattering and sheltering. In our simulations, we distinguish between local and remote radiation controls. This allows us to vary the representation of the effective albedo of the surrounding terrain from a vegetated (< 0.2) to a snow-covered landscape (0.4-0.8), which will increase the amount of scattered shortwave radiation. The variation of the landscape albedo changes the amount of scattered shortwave radiation. We examine the impact this has on snow accumulation and melt. The distributed model is applied to La Jara catchment in the Valles Caldera, New Mexico, during the 2004 to 2005 winter season. Results indicate that when the landscape albedo is controlled by vegetation, little change is seen in observables (e.g., absorbed radiation, peak snow water equivalent (SWE)). This implies that increases from scattered light are nearly equal to the losses of absorbed shortwave radiation

from remote sheltering. In contrast, when the landscape albedo is controlled by snow, there are large deviations in the spatiotemporal distributions of shortwave radiation and SWE due to scattered radiation exceeding the sheltering effects of remote topography. To capture the temporal variation of the albedo of the surrounding landscape, we propose a dynamic method that accounts for snow interception in vegetation canopies. Our study results indicate that remote interactions of radiation, vegetation and topography are critical to consider in snow ecohydrological studies in regions with high solar flux and rugged topography.

2.2 Introduction

Spring snowmelt is the primary source of surface water for the western United States (Bales et al., 2006), where it is used for drinking water, agriculture and riparian ecosystems. Infiltrating snowmelt is also a major source of plant-available water for local ecosystems during the subsequent growing season. Extensive vegetation changes are occurring in the mountain headwaters of these regions with potential consequences on water availability (Allen and Breshears, 1998). At relatively low mid-latitudes of the region (~35°N), such as the semiarid Southwest, higher solar radiation fluxes and warmer temperatures lead to an ephemeral and sparse seasonal snow pack, as compared to mountainous regions further north (Rango, 2006). These factors underscore the need for improved understanding of snow-vegetation-topography interactions in mountainous areas. Radiation fluxes and their interaction with vegetation and snow cover in the surrounding landscape are important for determining the energy and water balance in mountain basins of the lower latitude regions in the western U.S.

The distribution of solar radiation during the snow season in mountainous environments is complicated by interaction with surrounding topography. In settings with low relief, topographic shading is primarily caused by local terrain features (Oke, 1987). When relief is high, radiation is both blocked by and scattered from distant slopes (Dozier, 1980). In areas with dense vegetation, scattered light is thought to be less important due to the low albedo of vegetative cover (Oke, 1987). Thus, the vegetation properties in a landscape may control the distribution of snow through both local and remote effects by altering the partitioning of incoming solar radiation. As vegetation has changed in montane basins (Breshears and Allen, 2002; Davenport et al., 1998; Stott et al., 2004; Wilcox et al., 2003), it is vital to understand the cold-season ecohydrological dynamics in these water-limited environments.

The interactions of vegetation with seasonal snow pack have been examined extensively in the boreal forest (Brundl et al., 1999; Gelfan et al., 2004; Harding and Pomeroy, 1996; Liston and Elder, 2006; Pomeroy and Dion, 1996; Pomeroy et al., 2002; Pomeroy et al., 1998a; Pomeroy et al., 1998b; Zhang et al., 2004), continental alpine forests (Baron et al., 1998; Brooks et al., 1997; Hiemstra et al., 2002; Hubbart et al., 2007; Koivusalo and Kokkonen, 2002; Liston and Elder, 2006; Marks and Winstral, 2001; Marks et al., 2002; Parviainen and Pomeroy, 2000; Pomeroy et al., 2006; Pomeroy et al., 2002; Shamir and Georgakakos, 2006; Talbot et al., 2006; Woods et al., 2006; Zappa et al., 2003), maritime alpine forests (Hubbart et al., 2007; Storck et al., 2002; Whitaker and Sugiyama, 2005), and in the North American cold prairie and tundra (Liston et al., 2002; Pomeroy et al., 2006; Pomeroy et al., 1997;

Strack et al., 2007; Sturm et al., 2005a; Sturm et al., 2001; Sturm et al., 2005b; Tape et al., 2006).

These studies examine the controls of interception of snow in the canopy and the sheltering of snow from the wind by tall vegetation. In addition, detailed theoretical investigations have been conducted on the reflection of light within a snow-filled canopy (Chen et al., 2003; Link et al., 2004). To our knowledge, however, few studies have been conducted in lower mid-latitudinal (~35°N) alpine and subalpine regions. Existing work in these regions consists of field studies in the southern Sierra Nevada of California that examine topographic controls on the spatial dynamics of snow and timing of melt (Lundquist and Flint, 2006), and the effects of shading and interception by vegetation on the distribution of snow depth at short length scales (1 to 10s of meters) (Musselman, 2006).

In the southern portions of the western U.S., high solar fluxes increase the impact of shading and scattering of light by terrain. The amount and partitioning of radiation exerts both local and remote controls on snow processes through aspect controlled shading (local control), terrain blocking the sun (remote control), terrain limiting the amount of visible sky (remote control), and radiation being reflected, or scattered, from distant slopes (remote control). Local controls decrease the intensity of incoming radiation, and consist of slope and aspect effects on visibility of the sun and sky as well as vegetation absorption and scattering of radiation (Dozier, 1980; Essery et al., 2003b; Oke, 1987). Remote controls on incoming shortwave radiation are slightly more complex, since surrounding topography can, at a given time, shield a location in the landscape from direct exposure to the sun (Dozier, 1980; Essery et

al., 2003b; Oke, 1987). Furthermore, remote topography also limits the proportion of the sky that is visible and, thus, how much diffuse radiation can reach a particular point (Dozier, 1980; Essery et al., 2003b; Oke, 1987). Neighboring visible topography also reflects light, which, when snow is present, can lead to large quantities of scattered radiation (Dozier, 1980; Essery et al., 2003b; Oke, 1987). Scattered light is generally thought to be negligible if the surrounding landscape is heavily vegetated or has limited snow cover, but the degree to which changes in vegetation cover will affect scattered light is unclear.

In this study, we describe a new distributed snow model (DSM) based on a surface energy balance that is similar to Tarboton and Luce (1996) but with the advantage of four representations of sheltering from and scattering of shortwave radiation by the terrain. The model considers: (a) accumulation and ablation of the snow pack in forested and unforested areas, (b) snow interception in the vegetation canopy, (c) shading by the canopy, (d) effects of local topography on incoming solar radiation, and (e) effects of distant topography on incoming solar radiation. We utilize three representations of the landscape or hillslope albedo based on amount of vegetation cover to determine the scattering of radiation from the surrounding terrain. The DSM has been incorporated into the TIN-based Real-time Integrated Basin Simulator (tRIBS), a distributed rainfall-runoff model based on a triangulated irregular network (TIN) (Ivanov et al., 2004; Vivoni et al., 2007).

We apply the DSM to a small forested catchment in the Valles Caldera National Preserve (VCNP) of north-central New Mexico. In section 2.3, we summarize the model physics and present a description of the basin and its representation in the

DSM. Section 2.4 presents modeling results that examine the controls of remote vegetation and topography on the distribution of snow. We consider four representations: (1) only local vegetative and terrain controls that neglect scattered radiation from surrounding areas; (2) remote controls with a vegetation-covered surrounding landscape; (3) remote controls with a snow-covered surrounding landscape; and (4) remote controls with a dynamically updated snow-vegetation cover. Based on these simulations, we analyze the differences in incoming shortwave radiation and the control that shading and scattered light has on the snow distribution. In section 2.5, we discuss the implications of this work on the use of DSMs in rugged terrain. Study conclusions are presented in section 2.6.

2.3 Methods

2.3.1 Site and Study Period Description

The study basin, La Jara catchment, is located on Redondo Peak in the Valles Caldera, NM (35.858°N, 106.521°W). The Valles Caldera is a collapsed, rhyolitic, geothermally active caldera dated to 1.4 Ma (Goff et al., 1989; Goff et al., 1996). It is the dominant feature of the Jemez Mountains (Fig. 2.1). The caldera empties through the San Diego Canyon into the Jemez River (12,190 km^2 above the USGS gauge at Jemez, NM 08324000) and then flows into the Río Grande. The caldera has a classic morphology with multiple resurgent domes and extensive lacustrine deposits in the valley bottoms. The lithology consists primarily of rhyolites and tuffs with various intermingled sedimentary rocks (Goff et al., 1989). The largest features of the caldera are the primary resurgent dome, Redondo Peak, and the largest valley, Valle Grande.

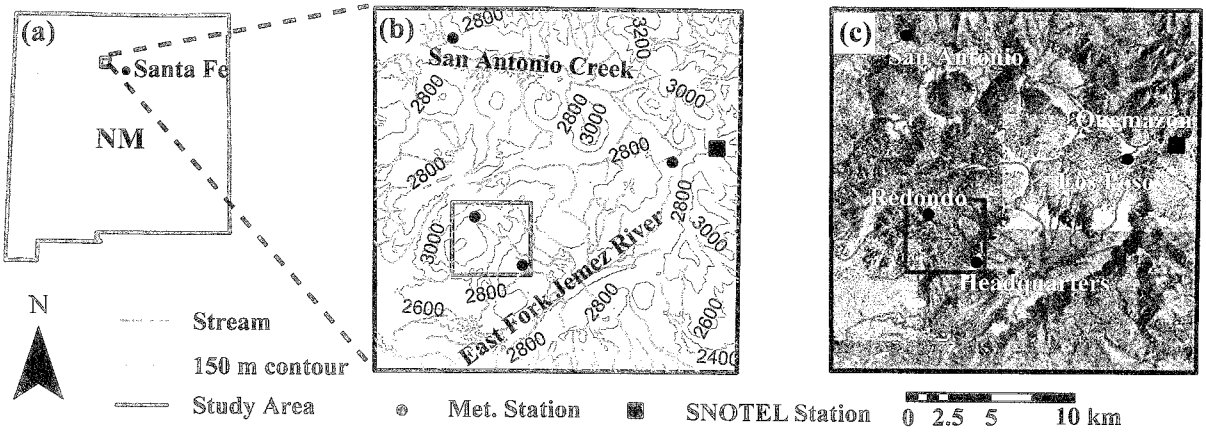

Figure 2.1. Map (a) and orthophoto mosaic (b) of the VCNP, including the Quemazon SNOTEL station and weather stations. The small box outlines the La Jara catchment.

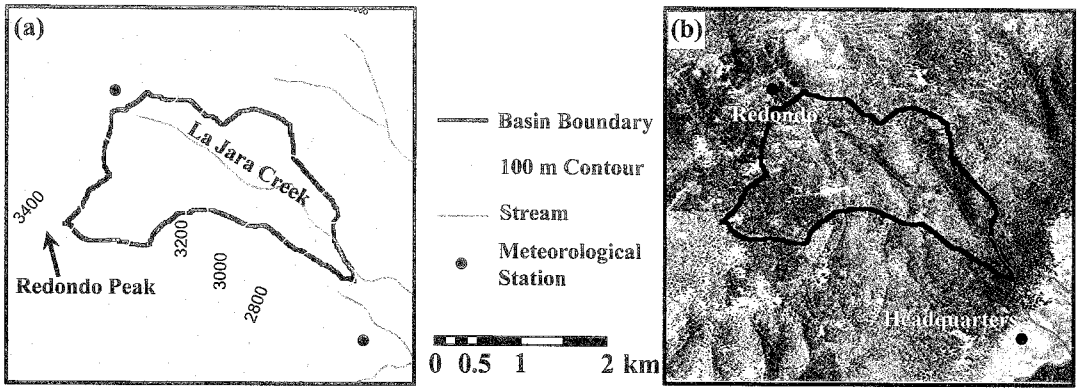

Figure 2.2. Map (a) and orthophoto mosaic (b) of La Jara catchment (3.4 km^2). Note the two nearby meteorological stations. The catchment is dominantly forested by subalpine fir (*Abies lasiocarpa)*, with some open meadows and talus slopes. The open linear contours in (b) are the result of historical logging in the region.

Given the large range of elevation (1625 m to 3526 m), a wide variety of vegetation and soil conditions exist in the Valles Caldera. Vegetation on the resurgent domes consists primarily of spruce fringe and fir forest, intermingled stands of quaking aspen, montane wetlands and grassy meadows with unvegetated active talus slopes at high elevations (Coop and Givnish, 2007). The broad valley bottoms are large homogeneous grasslands with small riparian wetlands and bogs. Ponderosa pine

forest lies along the rim of the valleys and in the drier and warmer areas of the domes. The soils on the resurgent domes are variable in depth, frigid, well-drained sandy loams with high permeability. In the valleys, the soils vary more dramatically, ranging from deep well-drained sandy loams, to poorly drained silty clay loams near the streams (NRCS, 2007a).

La Jara catchment (3.5 km^2) drains the southwest section of Redondo Peak into Valle Grande (Fig. 2.2). Vegetation is primarily subalpine fir (*Abies lasiocarpa*) forest with grassy meadows (Coop and Givnish, 2007). The combination of mountain topography and homogeneous forests facilitates analysis of the effects of the different representations of radiation scattering and sheltering. Furthermore, the basin was the site of an intensive snow measurement campaign during March 2005 that we have used to ensure that our simulation results are reasonable (Musselman, 2006). The catchment has an elevation range from 2700 m to 3425 m. Streams are located in small steep valleys (slopes between 0° and 45°) that rise up to broad, slightly rounded ridges (slopes between 0° and 10°). La Jara also contains Redondo Peak (3431 m) and its steep southeastern flank as well as a range of slope aspects, but on average faces east-southeast. Additional descriptions of the study site and its representation in the model will be discussed in section 2.4.

A number of weather and snow stations are close to La Jara catchment. Average conditions at the Quemazon SNOTEL station (2895 m), located just outside the VCNP, are mean snow season temperature of -2°C, a mean minimum temperature of -20°C, an annual precipitation of 72.3 cm and a maximal snow water equivalent (SWE) of 25.7 cm (Fig. 2.1) (NRCS, 2007b). The measurements taken at this location

Measurement Type	Sensor
Precipitation	TE Rain Gauge, TE525WS-L, CS705 snowfall adaptor
Air Temperature	Vaisala Temperature Probe HMP45C-L
Relative Humidity	Vaisala Relative Humidity Probe HMP45C-L
Wind Speed	Met One Wind Set 03B-L, Part # 15797

Table 2.1. Continuous instrumentation at the Redondo meteorological station operated by the Valles Caldera National Preserve.

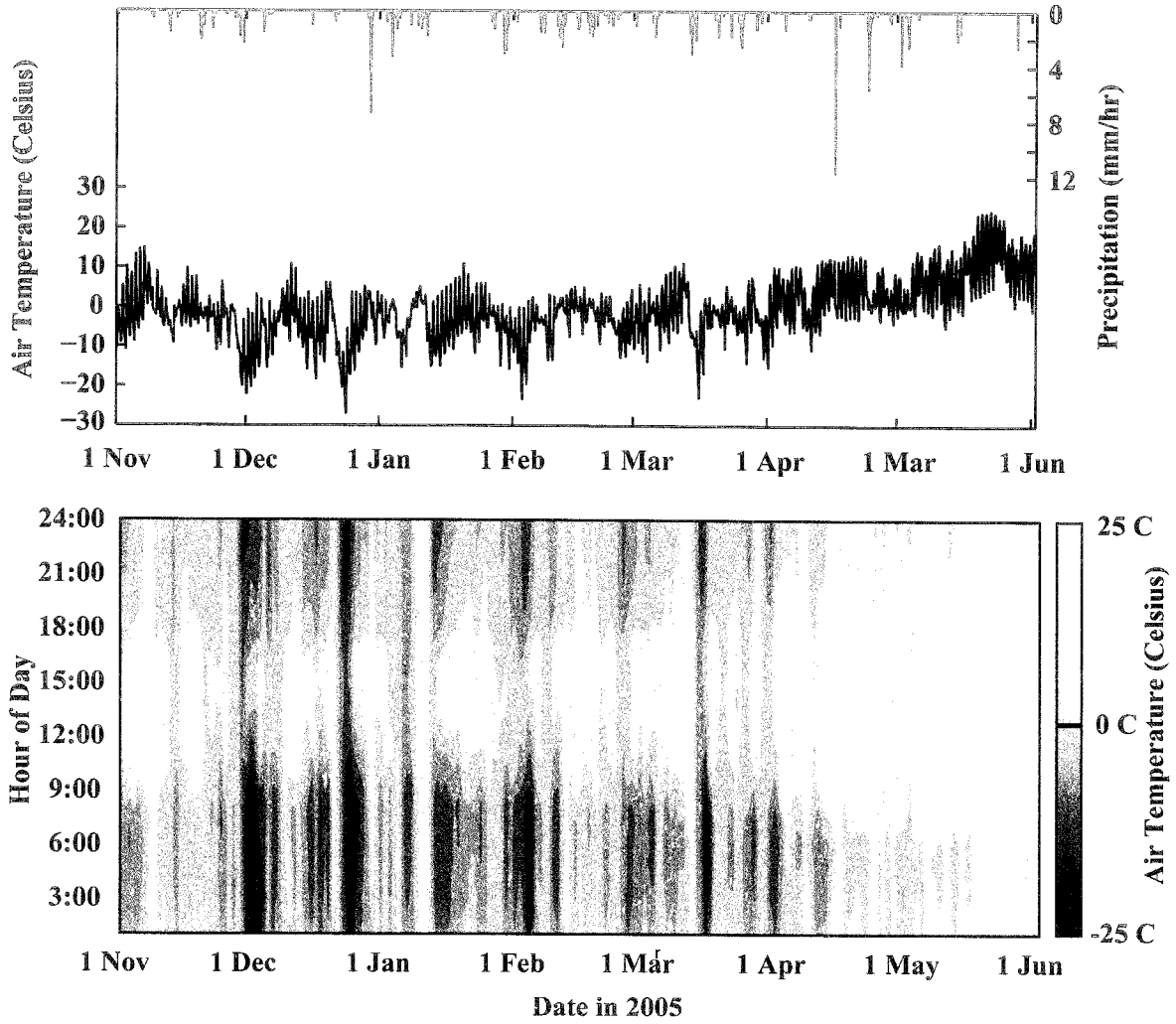

Figure 2.3. Meteorological record from VCNP Redondo station from November 1, 2004 to June 5, 2005. (a) Hourly precipitation accumulation (mm/hr) and temperature (°C). (b) Diurnal cycle of air temperature, showing the average time of maximum and minimum daily temperature, and periods of correlated temperature throughout the season.

provide representative values for our study region, but local topographic gradients lead to differences in climate throughout the VCNP. The Redondo station, located on the northwestern border of the La Jara basin, is the most representative to the conditions in La Jara catchment, in terms of elevation, vegetation and topography. Figure 2.3 presents the air temperature and precipitation records of the Redondo station during the study period. Table 2.1 presents a list of the relevant instruments for the station.

Our study is focused on the period between November 1, 2004 and June 5, 2005, one of the wettest snow seasons on record in the region, with a peak SWE of 38 cm at the Quemazon SNOTEL station. These winter and spring seasons are uniquely suitable for this study based on the availability of Redondo station data and the concurrent distributed field study carried out in March 2005. The next winter season (2005-2006) was an unusually warm and dry year with low snow packs in the VCNP, limiting our capacity to carry out snow-based simulations during this period.

2.3.2 Model Description

2.3.2.1 Review of Snow Models

A variety of approaches, each with advantages and disadvantages, are used to simulate snow processes either at a point or distributed in space. These range from empirical degree-day or melt-factor methods that assume snow melt is directly proportional to a normalized air temperature; restricted degree-day methods that account for the effects of solar radiation; and a range of energy-balance models (Anderson, 1976; Bloschl et al., 1991; Gelfan et al., 2004; Jordan, 1991; Lehning et al., 2006; Letsinger and Olyphant, 2007; Liston and Elder, 2006; Marks et al., 1999;

Tarboton and Luce, 1996). Degree-day models operate quickly using widely available meteorological forcing and perform successfully in low relief regions sheltered by vegetation. Restricted degree-day models capture the development and melt of snow in regions with higher and more variable radiative fluxes. Both approaches, however, lump processes such as sublimation and snow interception into a single, region-specific calibration factor.

Energy-balance models perform significantly better in regions of complex terrain and high exposure to the wind and sun (Anderson, 1976; Hock, 2003; Marks et al., 1999; Tarboton et al., 2001). These models capture individual fluxes in the snow pack with a limited set of parameters. Most energy-balance models vary in their representation of: (1) internal snow pack physics; and (2) boundary and initial conditions. The most complex models operate at the point-scale, include the effects of boundary conditions and simulate snow microphysics, including the internal metamorphism of snow pack properties (Anderson, 1976; Gelfan et al., 2004; Jordan, 1991; Lehning et al., 2006; Liston and Elder, 2006; Tuteja and Cunnane, 1997). A class of simplified models considers only a thin active top layer and a less sensitive inactive layer, neglecting the complex internal snow microphysics (Marks et al., 1999). The simplest models utilize a single snow layer and account for the densification of snow with time and changes in albedo with surface age (Anderson, 1976; Tarboton and Luce, 1996; Wigmosta et al., 1994).

Single-layer models emphasize the importance of climatic forcing (e.g. incoming shortwave radiation, air temperature, relative humidity) in determining the state of the snow pack. Consequently, these models represent the first-order controls

Parameter	Symbol	Value			Reference
		Forest	*Shrub*	*Grass*	
Vegetative Fraction [-]	v	0.60	0.45	0.65	(Bras, 1989)
Albedo [-]	a_{veg}	0.16	0.30	0.20	(Bras, 1989)
Leaf Area Index [-]	LAI	3.8	2.0	2.0	–
Optical Transmission Coef. [-]	K_t	60	50	40	(Ivanov et al., 2004)
Height [m]	z_{veg}	12.0	1.0	0.7	(Bras, 1989)
Minimum Snow Temperature [°C]	T_{min}	-27			–
Snow Roughness Height [m]	z_{snow}	0.1			(Anderson, 1976)
Minimum Prec. Partition Temp. [°C]	T_{sol}	-1.1			(Tuteja and Cunnane, 1997)
Maximum Prec. Partition Temp. [°C]	T_{liq}	3.3			(Tuteja and Cunnane, 1997)
Snow Emmissivity [-]	ε	0.95			(Tuteja and Cunnane, 1997)

Table 2.2. Simulation parameters used in this study based on estimates provided in the cited references for different vegetation types, where appropriate. The leaf area index for the different vegetation classification obtained from site measurements, while the minimum snow temperature was estimated from data at the Quemazon SNOTEL station.

on snow distribution, while remaining very sensitive to variations in radiation and temperature (Marks et al., 1999; Tarboton and Luce, 1996). These characteristics make a single-layer energy-balance model appropriate for our effort to quantify the controls that terrain shading and scattered light from distant vegetated or snow-covered hillslopes have on the distribution of snow. Previous work has included combined local and remote sheltering effects in distributed snow models (Lehning et al., 2006; Letsinger and Olyphant, 2007; Tarboton and Luce, 1996), though some consider only local controls (Gelfan et al., 2004; Liston and Elder, 2006; Wigmosta et al., 1994). To our knowledge, however, the effect of the albedo of the surrounding landscape on absorbed radiation and the distribution of snow as influenced by vegetation, snow cover and snow interception, has not been previously treated.

2.3.2.2 Governing Equations

The complexity of our model lies between those of Tarboton and Luce (1996) and Wigmosta et al. (1994). We begin with an overview of the state equations. We assume that the internal energy of the snow pack develops as:

$$\frac{dU}{dt} = L + H + G + P + R_S + R_L^{in} + R_L^{out}, \qquad (1)$$

where U is the internal energy (J/m^2), L is the latent heat flux (W/m^2), H is the sensible heat flux (W/m^2), G is the ground heat flux (W/m^2), P is the precipitation heat flux (W/m^2), R_S is the incoming shortwave radiation (W/m^2), R_L^{in} is the incoming longwave radiation (W/m^2), and R_L^{out} is the outgoing longwave radiation (W/m^2). The mass balance equation is:

$$\frac{dW_i}{dt} = P_i + \frac{1}{\rho_{liq}\lambda_i} L_i + M_{ji} - R_i \delta_{liquid,i}, \qquad (2)$$

where i and j = ice and liquid, W_i is the water equivalent in the i^{th} phase (m), P_i is the precipitation in the i^{th} phase (m), λ_i is the latent heat of freezing or vaporization for i and j respectively, L_i is the mass deposited or sublimated in the i phase by turbulent exchange (J/m^2), M_{ji} is amount of water that internally changes from the j phase to the i phase (m), R_i is the melt water equivalent that leaves the pack in the i^{th} phase (m), and $\delta_{liquid,i}$ is a Kroenecker delta to ensure that only liquid water is routed out of the pack.

Letting U = 0 J/m^2 when the T_{sn} = 0° C with no liquid water content (i.e., an isothermal dry pack at 0° C), then, if $U < 0$ J/m^2, then $T_{sn} = U / c_P \rho_{ice} W_{sn}$, otherwise $W_{liq} = U / \lambda_f \rho_{liq}$, where T_{sn} is the temperature of the snow pack, c_P is the heat capacity of water, ρ_{ice} is the density of ice, ρ_{liq} is the density of liquid water, and λ_f is the latent

heat of freezing for water (Tarboton and Luce, 1996). If $W_{liq} > 0.4W_{ice}$, then $R_{liq} = W_{liq} - W_{ice}$ (Wigmosta et al., 1994). This relationship to route water out of the pack is a simplification that can cause rapid melt to occur with small perturbations. With single-layer models that neglect ground heat flux (G), T_{sn} can also quickly drop to unrealistic values (Marks et al., 1999). To control this nonlinear behavior, we fixed a minimum snow temperature, T_{min}, according to the method recommended by Anderson (1976). Table 2.2 presents parameter values assumed in this study for the DSM.

2.3.2.3 Forcing and Boundary Conditions

The forcing terms in equations (1) and (2) are defined using standard methods. Latent (L) and sensible (H) heat fluxes are described in Wigmosta et al. (1994). The roughness height of the vegetation is adjusted to compensate for snow depth as:

$$z_{height} = \begin{Bmatrix} z_{veg} - z_{depth} \text{ if } z_{veg} > z_{depth} \\ z_{snow} \text{ otherwise} \end{Bmatrix}, \quad (3)$$

where z_{veg} is the height of the vegetation, z_{depth} is the snow depth, z_{snow} is the effective roughness height of snow (z_{snow} = 0.1 m), and z_{height} is the effective height used to compute the aerodynamic resistance (Strack et al., 2004). In the DSM, we neglect ground heat flux (G) due to its small value averaged over a snow season. We recognize that G can be significant early in the snow season and can affect our results (Anderson, 1976; Tarboton and Luce, 1996). In this study, though, we focus on the effects of radiation and vegetation, which are considered independent of G.

Precipitation (P) is linearly partitioned between liquid and solid phases according to air temperature (T_a in °C) by:

$$\phi_{sn} = \begin{Bmatrix} 1, \text{ if } T_a < T_{sol} \\ 0, \text{ if } T_a > T_{liq} \\ \dfrac{T_a - T_{sol}}{T_{liq} - T_{sol}} \text{ otherwise} \end{Bmatrix}, \quad (4)$$

where ϕ_{sn} is the fraction of precipitation that is solid, and T_{sol} (°C) and T_{liq} (°C) are the temperature at which all of the precipitation is solid or liquid, respectively (Wigmosta et al., 1994). Due to the importance of orographic controls on precipitation and air temperature (Brooks et al., 1997; Tarboton et al., 2001), linear lapse rates have been used in the DSM. A seasonal precipitation lapse rate was derived from VCNP station data. Temperature is adjusted according to the pseudo-adiabatic lapse rate (~6.5 °K/km), which was found compatible with regional temperature gradients (Kleissl, personal communication, 2007). For simplicity, we have neglected changes of vapor pressure with elevation.

The calculation of incoming shortwave radiation (R_S) is taken from Wilson and Gallant (2000), as implemented in Ivanov et al. (2004), with sheltering and reflection by topography from Dozier and Frew (1990). The computation of R_S accounts for atmospheric turbidity, cloud cover, atmospheric incident angle, light extinction in the vegetation canopy, surface albedo, and shading and scattering of radiation from the surrounding landscape (Wilson and Gallant, 2000). The algorithm disaggregates R_S into diffuse and direct components (see further details in section 2.3.2.4).

Incoming longwave radiation (R_{Lin}) is calculated from an adjusted gray-body Stefan-Boltzmann equation:

$$R_{Lin} = \sigma K_{cloud} \varepsilon_{sky}(e) T_a^4, \quad (5)$$

where σ is the Stefan-Boltzmann constant, K_{cloud} adjusts for radiation absorption by clouds, and ε_{sky} is the atmospheric emissivity as a function of vapor pressure, e (Bras, 1989). Outgoing longwave radiation (R_{Lout}) is computed as a function of snow emissivity ($\varepsilon_{snow} = 0.95$) and temperature (Tarboton and Luce, 1996; Wigmosta et al., 1994).

The interception of snow by vegetation and its subsequent sublimation or unloading has a significant effect on the distribution of snow (Bayard et al., 2005; Essery et al., 2003a; Gelfan et al., 2004; Hardy et al., 1997; Hardy et al., 1998; Hedstrom and Pomeroy, 1998; Liston and Elder, 2006; Montesi et al., 2004; Parviainen and Pomeroy, 2000; Pomeroy et al., 2006; Pomeroy et al., 2002; Pomeroy et al., 1998b; Storck et al., 2002). A number of approaches have been developed to model snow interception. These including applying rainfall interception schemes to snowfall (Wigmosta et al., 1994) and more complex physically-based algorithms (Gelfan et al., 2004; Parviainen and Pomeroy, 2000; Pomeroy et al., 2002; Pomeroy et al., 1998b). Multiple approaches have also been used for snow sublimation (Pomeroy et al., 1998b; Wigmosta et al., 1994) and unloading from the canopy (Liston and Elder, 2006; Pomeroy et al., 1998b). We have implemented the hybrid approach of Liston and Elder (2006), which is derived from Pomeroy et al. (1998b) for interception and sublimation, but uses a temperature index model for unloading. When snow is captured in the canopy, sublimation is proportional to the incoming shortwave radiation and relative humidity.

2.3.2.4 Shading and Reflectance Parameterization

Topographic controls on net absorbed shortwave radiation are conceptualized in two ways: (1) the local controls of slope, aspect and vegetation; and (2) shading and reflected light from the surrounding landscape. For both cases, there are separate controls on diffuse (R_{Sdif}), direct (R_{Sdir}) and total shortwave radiation (R_S). To account for local vegetative shading, R_S is multiplied by

$$K_t\gamma+(1-\gamma), \tag{6}$$

where K_t is the canopy extinction coefficient and γ is the canopy fraction in the model element (Ivanov et al., 2004). To account for local terrain limiting the amount of visible sky, R_{Sdif} is multiplied by the local sky-view factor:

$$v_{local} = 0.5(1+\cos(S)), \tag{7}$$

where S is element slope (Dozier and Frew, 1990). For the most regions, $v_{local} > 0.9$, due to the relatively low slopes (<36°) generally found (Wilson and Gallant, 2000). Local shading also accounts for the incidence angle of direct shortwave radiation with the model element. This is captured by multiplying R_{Sdir} by $\xi = \max(\cos(S)\sin(\delta)+\sin(S)\cos(\delta)\cos(\alpha-A),0)$, where ξ adjusts for the angle of incidence at the surface, assuming it is locally visible; δ is solar altitude; α is the sun's azimuth; and A is aspect (Wilson and Gallant, 2000).

The effects of the surrounding landscape on shortwave radiation at a specific location are more complicated to represent. In order to represent these affects, the geometry of the landscape surrounding a point of interest (POI) must be defined. This is done by measuring the angle from vertical to the steepest point in a given horizontal direction, for all horizontal directions. These measurements yield horizon angles, which can then be used to determine how much sky is visible (i.e., the sky-

view factor), how much land is visible (i.e., the land-view factor), and whether or not the sun at a given time can be seen at the POI.

The algorithm used to calculate horizon angles follows algorithm of Dozier and Frew (1990). A grid digital elevation model (DEM) was selected that included La Jara and the major topographic features surrounding La Jara. Horizon angles were found in 16 directions ($\Delta\theta = \pi/8$) for every grid point. Dozier and Frew (1990) found that this fairly coarse representation of horizon angles is sufficient to represent horizon angles for calculations of sky-view and land-view factors as well as deciding if the sun is visible at a given time at the POI. Once horizon angles for the entire grid were defined, the horizon angles were resampled from the grid to the Voronoi polygon mesh used in the model (see section 2.3.3.1). The resampling scheme uses an areally-weighted average to find the representative horizon angle of a given polygon.

Once the 16 horizon angles are assigned, it is possible to calculate the remote controls on absorbed shortwave radiation. The remote sky-view factor, v_{remote}, is calculated from the horizon angles as:

$$v_{remote} \cong \sum_{m=1}^{16} \cos(S)\sin^2(HA_m) + 0.5\sin(S)\cos(\theta_m - A)(HA_m - \sin(2HA_m))\Delta\theta_m , \qquad (8)$$

and the land-view factor, ζ, as:

$$\zeta \cong v_{local} - v_{remote} , \qquad (9)$$

where HA_m is the horizon angle measured from vertical with $HA_m = HA(\theta_m)$, θ_m is a azimuthal angle, $\Delta\theta_m = \pi/8$ is change in azimuthal angle for each step of the summation, m is the summation index, going counterclockwise from $m=1$ at north and $m=16$ at north-northeast. The shortwave diffuse radiation is multiplied by v_{remote}.

In order to calculate if the sun is visible at a POI, first the location of the Sun (δ and α) is calculated at each time step during the simulation. If $HA(\alpha) \geq \delta$, then $R_{Sdir} \neq 0$; otherwise $R_{Sdir} = 0$. The direct shortwave radiation is multiplied by ξ to account for the angle of incidence at the computational node.

To account for reflected shortwave radiation from the surrounding hillslopes,

$$a_{hill}\zeta(R_{Sdir} + R_{Sdir}) \tag{9}$$

is added to the total incoming radiation as part of the diffuse radiation component, where a_{hill} is the hillslope or landscape albedo. In order to exactly calculate the effects of scattered light, it would be necessary find the distribution of surface conditions and topography visible from the point of interest. We use the state of the surface at the POI to approximate the albedo of the surrounding hillslopes (a_{hill}). Local slopes and aspects are computed from the TIN using the steepest downward TIN edge (see section 2.3.3.1).

The representation of albedo forms the final part of modeling the shortwave radiative flux. Vegetation albedo (a_{veg}) is taken as a constant value for distinct vegetation types (see Table 2.2). Snow albedo (a_{sn}) ages according to:

$$a_{sn} = \begin{Bmatrix} 0.85(0.94)^{N^{0.58}} & \text{if } W_{liq} = 0 \\ 0.85(0.82)^{N^{0.46}} & \text{otherwise} \end{Bmatrix}, \tag{10}$$

where N is the age of the snow surface in days (Wigmosta et al., 1994). We consider the hillslope albedo in three distinct manners. We treat it as: (1) the vegetation albedo at the point of interest:

$$a_{hill} = a_{veg}; \tag{11}$$

(2) the snow albedo at the point of interest:

$$a_{hill} = a_{sn}; \tag{12}$$

or (3) a mixed snow-vegetation albedo model:

$$a_{hill} = \begin{pmatrix} a_{sn} \text{ if there is snow in the canopy} \\ \gamma a_{veg} + (1-\gamma) a_{sn} \text{ otherwise} \end{pmatrix}. \tag{13}$$

If there is no snow cover at the point, then vegetation albedo is used. By using the different albedo schemes, it is possible to test the effect of different representations of distant surfaces on the development and melt of snow.

2.3.2.5 Model Confidence

To build confidence in the model physics, we have compared simulation results to measurements at the Quemazon SNOTEL station located on the eastern rim of the caldera. The station is in a small meadow surrounded by mixed-fir forest and lies on a saddle between two high ridges at an elevation of 2896 m. For the 2005 water year (October 1, 2004 to September 31, 2005), the maximum recorded SWE was 38 cm, as measured by the snow pillow. We forced the model at an hourly time step with three-hourly precipitation and air temperature data from the station. To disaggregate to the hourly model time step, we assumed air temperature remained constant and precipitation occurred over the first hour of each three-hour interval. As the Quemazon station is sheltered from wind and in a clearing, it was not necessary to correct for wind-induced undercatch or to include the canopy interception processes. Because of limited instrumentation at the station, wind speed and relative humidity data from the Headquarters station were used (6-km distant).

Considering these forcing uncertainties, Figure 2.4 presents a promising comparison of the SWE at the Quemazon station to the model predictions at the

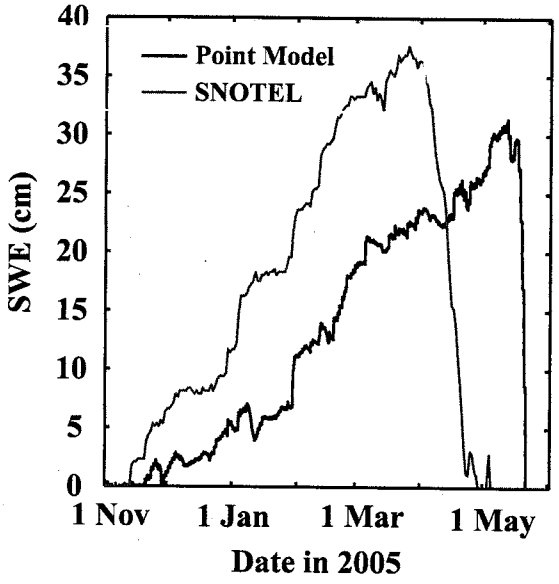

Figure 2.4. Comparison of snow water equivalent (SWE) measurements at the Quemazon station with predictions from the point snow model applied to the site.

coincident element. For this season, the simulated SWE consistently lags behind the measured SWE. At the time of measured maximum SWE (38 cm), the simulated SWE was 24 cm. Further, the simulated SWE persists for too long and exhibit a precipitous late fall. Most simulation errors are accrued during the accumulation of SWE early in the season (Nov. to Jan.), where a slight underestimation of SWE was exacerbated by an overestimation of snowmelt. Interactions between the ground surface and snow pack, neglected in the model, are most important early in the season. Moreover, buffering of temperature changes in a snow pack by a top active layer (Marks et al., 1999) is missing from the single layer model.

Despite these problems with the model performance, the qualitative behavior of the model agrees with the measurements. The model accumulates snow at the same times and, except for the final melt, melts snow at the same times as the

measurement. The errors are primarily in terms of magnitudes. The model does not accumulate enough snow and melts too much snow during most events. This is seen in the jagged shape of the modeled SWE in Figure 2.4 as compared to the measured SWE. Nonetheless, if we examine the response of the model in terms of seasonal behavior (e.g., time snow-covered, seasonal average incoming radiation, modeled peak SWE and date of modeled peak SWE), the model should perform with reasonable accuracy for the proposed sensitivity analysis.

2.3.3 Model Topographic and Vegetation Representations

2.3.3.1 Computational Mesh

The DSM was developed in the framework of the tRIBS model that uses a triangulated irregular network (TIN) as a computational mesh. Vivoni et al. (2004) and Tucker et al. (2001) described the development of the model domain in the following manner: (a) resample a DEM with embedded hydrologic features into a list of nodes, according to an elevation error minimizing criteria; (b) develop a constrained Delaunay triangulation of the set of nodes; and (c) compute the complementary Voronoi polygons from the TIN. The resampling of the DEM effectively leads to higher node density in regions of high topographic variability (Kumler, 1994; Vivoni et al., 2004). The Delaunay criterion yields a nearly maximal angle between all edges in the triangulation (Tucker et al., 2001). As a result, the nodes closest to one another are connected, while ensuring relatively uniform triangle geometry (Vivoni et al., 2004). From the TIN, Voronoi polygons are derived for each computation node, and assumed as a representative area for the point.

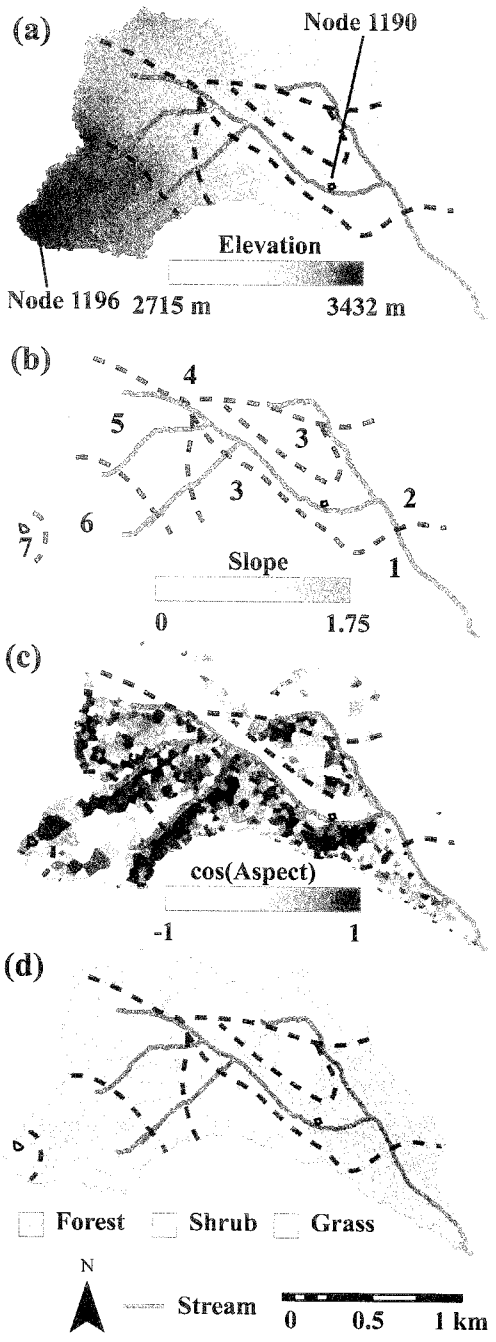

Figure 2.5. Distribution of topographic characteristics and vegetation in La Jara catchment as represented by Voronoi polygons. (a) Elevation (m). (b) Slope (ratio of y/x). (c) Cosine of the aspect (-). (d) Vegetation. In (c), south facing polygons ($\cos(A) < 0$) have light colors, depicting higher solar exposure, while north facing areas ($\cos(A) > 0$) have dark colors. East and west aspects are equivalent in color, but can be discerned relative to the streams derived from the DEM using a 500 m^2 constant area threshold. Zones with different responses to shortwave radiation have been delineated 1 through 7.

The computational mesh used for this study was derived from a 10-m DEM constructed from orthophotos of the VCNP. An error in elevation of 2 m was found to be a nearly optimum criterion, simultaneously limiting the number of nodes and the error in elevation when comparing a polygon's elevation to the original DEM. The topographic properties of the domain are summarized in Figures 2.5a-c. The mesh ranges in elevation from 2715 m to 3432 m, in slopes from 0 to 1.75, and contains all possible aspects.

The lowest portion of the domain forms part of the broad pediment emptying into Valle Grande and is thus relatively uniform in slope (Zone 1). The middle elevations are more rugged, with steep narrow valleys preserved at high resolution (Zone 2) and valley-side tops where the topographic curvature is high (Zone 3). Generally, valley sides either face mostly south or north, with only small area facing east or west. High elevations occur into three regimes: (a) the eastern side slope of Redondo, where the ridge tops are gentle, low slope features with south-facing aspects (Zones 4 and 5); (b) the northeast slope of Redondo with slight incision from the stream at lower elevations (Zone 6); and (c) the peak of Redondo (Zone 7).

Redondo Peak, the deeply incised rivers and the open valley to the south lead to La Jara having a wide range of horizon angles. This, in turn, causes a variety of regimes of sheltering and scattering of shortwave radiation from distant slopes to occur. We have parsed the catchment into topographic zones that have distinct radiative behavior (see Section 2.4.1 for details), which range from dominantly locally controlled by slope and aspect (Zones 1, 6, and 7), to primarily shaded by

nearby topography (Zone 2), to shaded strongly by Redondo (Zone 5), to shaded mildly by nearby topography (Zone 4) or by Redondo (Zone 3).

2.3.3.2 Vegetation Parameterization

The 30-m National Land Cover Data (NLCD) map (2001) overlapping the La Jara catchment was simplified into three classifications (forest, shrub and grassland) and resampled to the computational mesh (Fig. 2.5d and Table 2.2). In light of the limited parameter values available for vegetation in the area, we treat the forest cover as a single classification. Similar simplifications have been made for the grassland and shrub classifications. Each computational node is represented by the dominant vegetation type (Ivanov et al., 2004). Model parameters used in the study are summarized in Table 2.2.

2.3.4 Numerical Experiments

We examine four representations of snow-vegetation-topography interactions in La Jara catchment. The first only considers local effects (i.e. slope, aspect and snow interception and shading by vegetation). The latter three represent landscape or hillslope albedo (a_{hill}) according to equations (12) to (14), and also incorporate the local effects as in the first representation. We use the local sheltering as our base case in order to examine the relative importance of scattered shortwave radiation on the spatial and temporal distribution of snow.

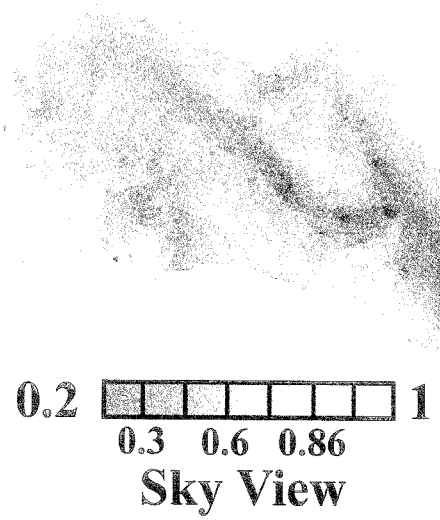

Figure 2.6. Sky-view factor distribution for cases with remote shading. Land view factors are roughly reciprocal to sky view, but adjusted for local shading (slope and aspect).

2.4 Results

The distributed snow model calculates the incoming shortwave radiation and the topographic interactions with radiation, as well as represents the dynamics of the snow pack in time and space. A number of integrated metrics of the radiation forcing and the model states are presented to identify the effect of changing the albedo of the surrounding terrain. These metrics fall into three categories: (1) measures of sheltering and exposure to shortwave radiation; (2) peak SWE; and (3) temporal characteristics of the snow pack dynamics. We also compare the four simulations and the basin-average SWE measured in March 2005 during an intensive field campaign.

2.4.1 Degrees of Sheltering and Exposure

The distant landscape controls the amount of incoming radiation by (a) changing the proportion of the sky emitting diffuse shortwave radiation, as represented by the sky view factor; (b) determining whether the sun is visible or hidden behind distant topography; and (c) calculating how much light is scattered

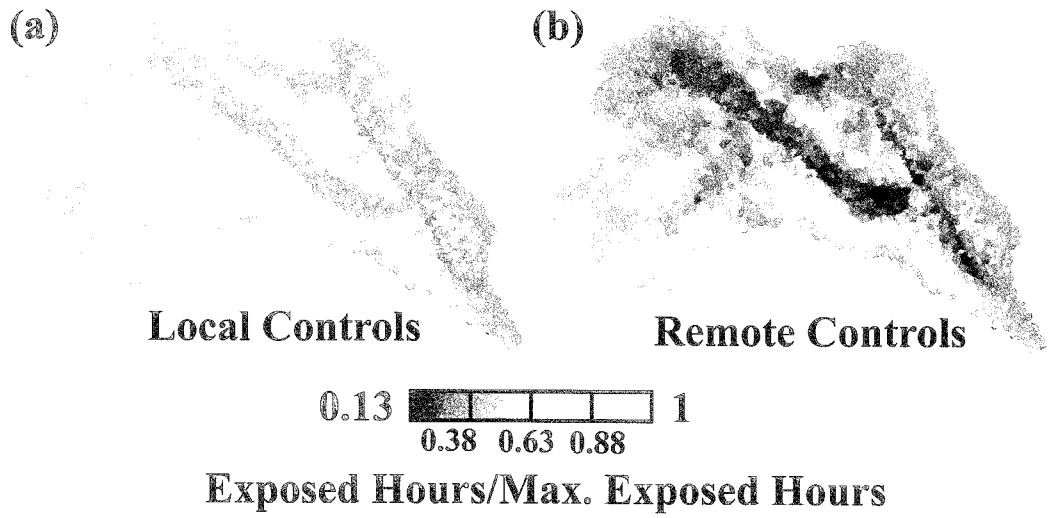

Figure 2.7. Spatial distribution of the proportion of time directly exposed to the sun during the study period. (a) Slope and aspect controls on amount of direct exposure. (b) Local and remote controls on amount of direct exposure.

from distant topography, as controlled by the land view factor and the hillslope albedo. We first present the distribution of sky- and land-view factors in the basin to delineate zones that will aid in the interpretation of the simulation results.

Figure 2.6 shows the sky-view factors derived from remote controls. Each zone outlined in Figure 2.5 has a range of sky-view factors consistent with the topography and position of the zone. Zone 1 has higher sky view factors with some moderate values in its higher elevations. This is consistent with the broad shallow slopes of the lower pediment and the abrupt rise of the mountain at the boundary of the zone. Zone 2, which consists of steep narrow streams, has the lowest sky-view factors in the basin with values down to 0.2. Zone 3 has broad ridge tops but is sheltered by rugged topography within the zone. This combination yields moderate to high sky-view factors of 0.7 to 0.9. Zone 4 is shaded by Redondo Peak to its south and correspondingly has low to moderate sky-view factors (0.4-0.8). Zone 5 is closer to

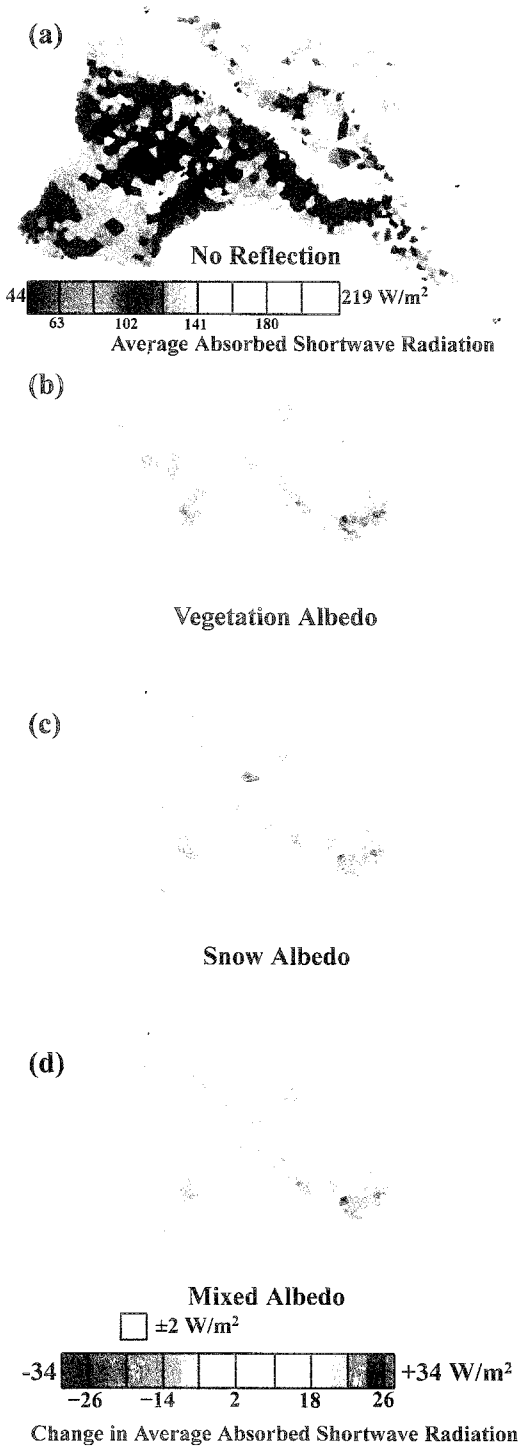

Figure 2.8. Spatial distribution of (a) the distribution of absorbed shortwave radiation at a point (W/m^2) when only local topographic controls are considered (base case), and the deviations in incoming shortwave radiation when remote shading and hillslope albedo are modeled by (b) vegetation albedo, (c) snow albedo and (d) dynamic snow-vegetation albedo. Greens correspond to little or no change.

Redondo Peak and has slightly lower sky-view factors that Zone 4. Most importantly, at the base of Redondo Peak in Zone 4, sky-view factors are as low as 0.3. Zones 6 and 7 have high sky view factors (> 0.9), as they are among the highest topography in the catchment and cannot be shaded from a distance.

Figure 2.7 shows the fraction of days exposed to direct sunlight (maximum of 100 exposed days) over the study period. We represent shading of direct shortwave radiation by: (a) considering only slope and aspect controls (Fig. 2.7a); and (b) accounting for both the local and remote controls (Fig. 2.7b). In the locally controlled case, polygons with north aspects or very high slopes receive the lowest amount of direct exposure (Fig. 2.7a). Low exposure occurs predominantly in Zones 2 and 4, which is consistent with the zones' rugged topography. In the remotely shaded case (Fig. 2.7b), a pattern consistent with the sky-view maps is seen. Zones 2, 5 and 4 are directly exposed the least, consistent with the rugged topography both within and immediately neighboring the zones. Zone 3, with its broad ridges, and Zones 6 and 7, with their broad high elevation surfaces, have the highest exposure rates, differing slightly from the locally shaded case.

Topographic attributes and the sky- and land-view factors are reflected in the spatial patterns of the average amount of absorbed shortwave radiation (W/m^2) received at a site over the entire simulation period (November 1, 2004 through June 5, 2005), as seen in Figure 2.8. Four cases are presented in this analysis (and subsequent figures as well). We first present the locally controlled or base case as a map of average absorbed shortwave radiation (Fig. 2.8a) and then indicate the differences between the remote cases and the base case. The only variation among the remote

cases is the representation of the effective hillslope albedo: vegetation (Fig. 2.8b), snow (Fig. 2.8c) and mixed snow-vegetation (Fig. 2.8d).

The absorbed solar radiation in the base case has no scattered component, or effects of remotely restricted sky-view and exposure time. When the albedo of the local vegetation is used to represent hillslope albedo, little change is evident. Small areas of increased incoming shortwave radiation (+6 to +10 W/m^2) are found in the Zone 4. Some south-facing slopes in Zone 2 showing large decreases (~ -10 W/m^2) due to the large amount of sheltering. The rest of the catchment shows little to no change in the amount of absorbed radiation. When snow albedo is used as the hillslope albedo, deviations from the base case become widespread. Increases in incoming shortwave radiation occur in regions with moderate to high land-view factors (Fig. 2.6) and moderate to high amounts of direct solar exposure (Fig. 2.7). These areas encompass portions of Zone 2, and Zones 3 and 4. The majority of the decreases in shortwave radiation occur in Zones 2 and 5. When a mixed snow-vegetation albedo is used, the pattern of deviation from the base case resembles the snow albedo case. The increases in average absorbed solar radiation, however, are slightly smaller. In all cases considering remote effects, Zones 1, 6 and 7 have little change (±8 W/m^2) in absorbed shortwave radiation.

2.4.2 Spatial Distribution of Peak SWE

The pattern of peak SWE in La Jara catchment is complex (Fig. 2.9). In the base case, where only local controls are considered, there are three distinct regions, similar to those found for the radiation exposure (Fig. 2.9a). There is a homogeneous swath of peak SWE of ~30 cm in Zones 1 and 2, and the eastern half of Zone 4 (i.e., the

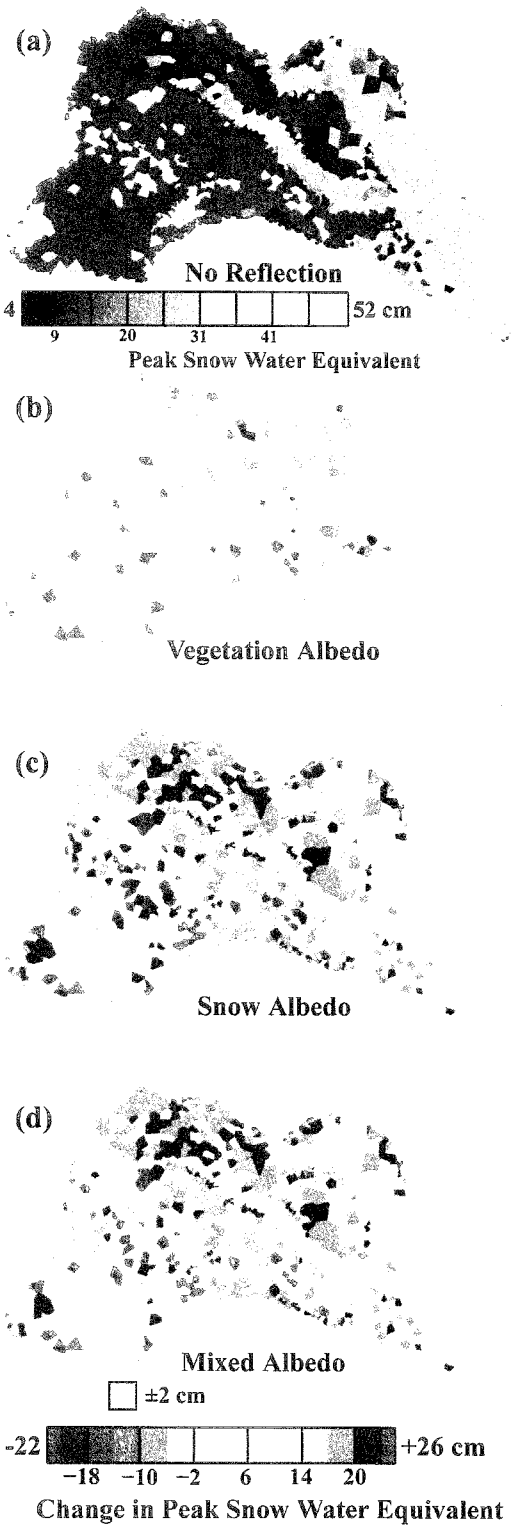

Figure 2.9. Spatial distribution of (a) the distribution of maximum SWE (cm) for the base case, and the deviations when remote shading and hillslope albedo is modeled by (b) vegetation albedo, (c) snow albedo and (d) dynamic snow-vegetation albedo.

steep valley bottoms). The ridge tops in the middle elevations (Zone 3) and the flank of Redondo (Zone 6) form another fairly distinct unit with peak SWE of ~20 cm with some observed variations. Zone 5, with its high slopes and north-aspects, forms another distinct zone of peak SWE, with high, fairly uniform peak SWE (~20 cm). The top of Redondo Peak accumulates the largest amount of snow with peak SWE of 49 cm. In the remote case using vegetation albedo, few deviations from the base case are observed with differences between –5 cm and +5 cm (Fig. 2.9b). In contrast, when snow is the effective hillslope albedo (Fig. 2.9c), large deviations appear. In particular, Zones 3 and 4 (middle elevation ridge tops) show large increases in peak SWE (20 – 26 cm). Zones 1 and 2 (valley bottoms and pediment), which in the base case have a peak SWE of ~30 cm, show a slight increase in maximum SWE (from 2 to 6 cm). The north facing flank of Redondo Peak (Zone 6), the ridge tops at the break in the flank (Zone 5) and the peak of Redondo (Zone 7) show marked decreases in peak SWE, with some decreasing by ~20 cm. When a mixed albedo is used (Fig. 2.9d), the results are nearly identical to those using the snow albedo (Fig. 2.9c).

2.4.3 Spatial Patterns of Temporal Snow Variability

Spatial patterns of temporal snow metrics permit close inspection of the differences between the simulation cases during the entire period. We present the spatial distribution of the total number of days that a particular node is snow-covered (Fig. 2.10) and the day of year of the peak SWE (DOYP) (Fig. 2.11).

The spatial pattern of the number of snow-covered days fall into similar regions as those observed for peak SWE (Fig. 2.9). In the base case (Fig. 2.10a), the response within the catchment can be grouped: (1) Zones 1 and 2 (the narrow valleys and the

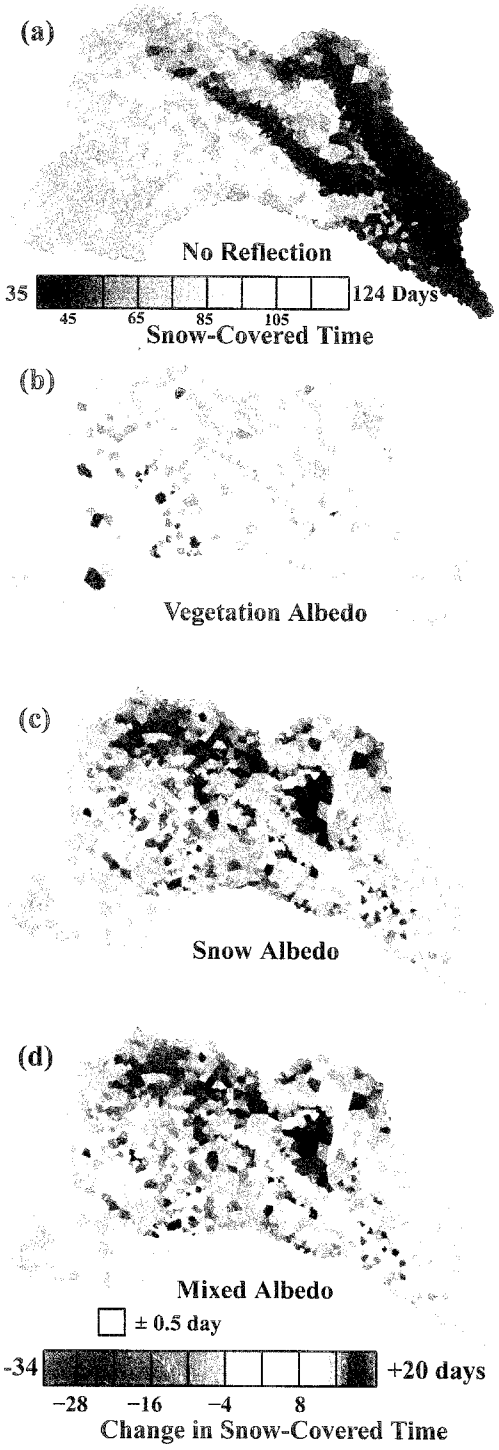

Figure 2.10. Spatial distribution of (a) the number of snow cover days for the base case, and the deviations when remote shading and hillslope albedo is modeled by (b) vegetation albedo, (c) snow albedo and (d) dynamic snow-vegetation albedo.
low elevations) of the catchment spend little time with snow cover (33-40 days);

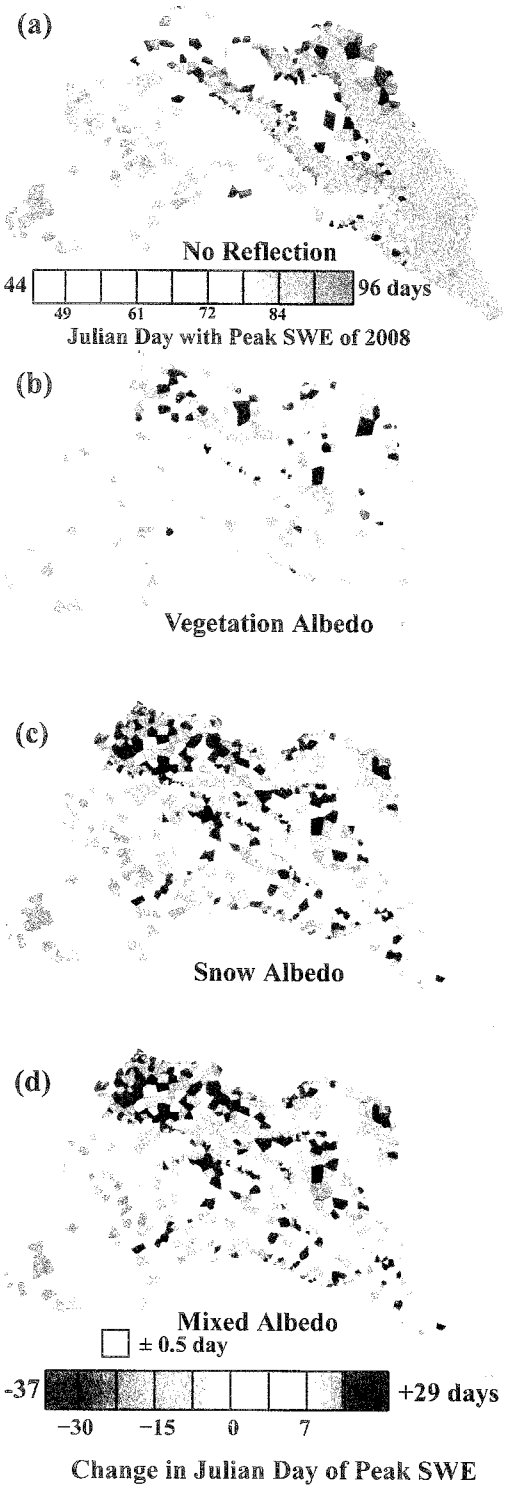

Figure 2.11. Spatial distribution of (a) the date of maximum SWE for the base case, and deviations when remote shading and hillslope albedo is modeled by (b) vegetation albedo, (c) snow albedo and (d) dynamic snow-vegetation albedo.

(2) Zones 6 and 7 (the flank of Redondo Peak) is fairly homogeneous with some very persistent snow patches (60-125 days); (3) Zone 5 is snow-covered for much of the season; (4) Zones 3 and 4 are heterogeneous, with the south-facing slopes being less persistent (40-60 days), than the north facing slopes (40-120 days).

When vegetation is used as the effective hillslope albedo (Fig. 2.10b), there is a small decrease in the number of snow-covered days (~ -5 days) in the northern regions of the catchment (Zones 3 and 4), where the flank of Redondo Peak is visible and to the southwest. In Zones 5 and 6, there are some areas of large increases in the number of snow-covered days (+10 to +23 days), though generally the increases are small (~ +5 days). The spatial patterns, however, largely do not change with respect to the base case and the majority of the catchment exhibits little change. When snow albedo (Fig. 2.10c) or mixed snow-vegetation albedo (Fig. 2.10d) is used, a large area of the catchment decreases in the number of snow covered days. This is occurs in all of Zones 3 and 4, with deviations ranging from –10 to –40 days. Only minor deviations are observed between the snow and mixed snow-vegetation albedo cases.

The spatial distributions of the DOYP (Fig. 2.11) is similar to those of snow-covered days. In the base case, Zones 1 and 2 have a more or less uniform DOYP value (~80 DOY). Zones 3 and 4 have a heterogeneous pattern, with some peak days occurring earlier (43 to 50 DOY), at an intermediate time (60 to 70 DOY), at values commensurate with those in the valleys (~80 DOY) and later in the season (~90 DOY). Zones 6 and 7 are fairly uniform with a low DOYP value (60 to 70 DOY), with very late peaks at high elevation (>90 DOY). High values of DOYP are found in Zone 5. Deviations from the base case when applying the vegetation albedo are

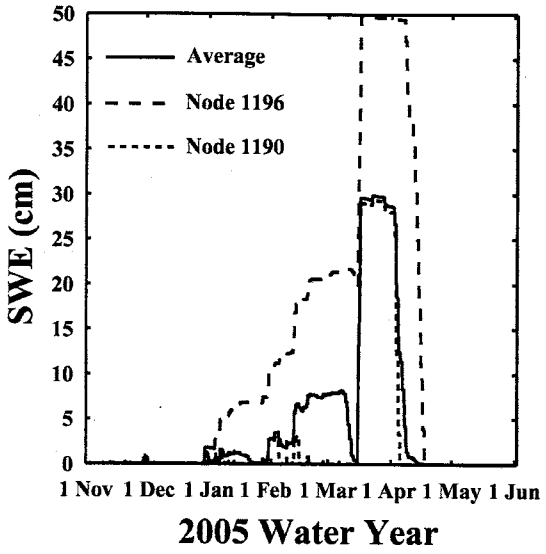

Figure 2.12. Temporal distribution of the average SWE (solid line), SWE at node 1190 (dotted line) and at node 1196 (dashed line) when only local controls are considered.

generally small (Fig. 2.11b), though differences are found in the northern portions of La Jara (Zone 4). Here, some areas have SWE peaks that occur much later (~40 days), while others peaks occur earlier (10 to 20 days). The majority of the basin shows relatively little change in the time of the peak SWE. On the other hand, when snow albedo (Fig. 2.11c) or mixed snow-vegetation albedo (Fig. 2.11d) are used, deviations in the peak SWE time are widespread with Zone 4 having later peaks (30 to 41 days) and Zones 3, 5 and 6 having earlier DOYP (10 - 20 days).

2.5 Discussion

2.5.1 Synthesis of Site-Specific Results

The study results are internally consistent and, when taken together, provide an indication of the importance of incorporating the scattering of radiation from the surrounding landscape and the representation of landscape albedo during the snow-covered season. The characteristics of the average absorbed shortwave radiation and

the spatiotemporal variations of the snow pack are manifestations of the topographic, vegetative and meteorological properties captured in the simulations. For example, the net behavior at different basin locations and the averaged conditions can be observed in Figure 2.12. Here, the temporal variations in SWE are shown for the base case, where only local controls on radiation are considered. Note that this depicts conditions at two node locations (mapped in Fig. 2.5), as well as the catchment spatial average. Node 1190 is a middle elevation valley bottom that faces south, while node 1196 is a steep, high elevation north-facing site. Clearly, the simulated snow pack in the catchment can be very ephemeral, with some areas exhibiting multiple small peaks and short ablation limbs (node 1190), while other sites have a deep and consistent snow pack (node 1196). The average catchment dynamics lie in between those observed at the two individual nodes.

The differences between the two sites and across the catchment are caused by the controls of snow in the canopy and the relative exposure. Snow that is captured in the plant canopy is held for long periods until it is sublimated or unloaded. Given the cold temperatures of the simulation (time-averaged T_a = -1.8 $^{\circ}C$) and the temperature lapse rate, areas in the higher elevations will generally hold snow for longer periods, increasing its exposure to sublimation but also increasing the time it takes to unload snow. This causes a change in behavior between the low and high elevations in the basin. Snow is released more quickly in the lower elevations by the temperature-index unloading model and is sublimated more slowly, due to lower amounts of incoming radiation and higher relative humidity. In forested middle and upper elevations, snow is released very slowly and is incrementally exposed to radiation,

causing a lower peak with longer accumulation periods from throughfall. The remaining variations of maximum SWE and temporal metrics are primarily explained by the variability of absorbed shortwave radiation due to local aspect and slope and effects of the temperature lapse rate.

When vegetation is used as the hillslope albedo, there is little change through the catchment in the integrated metrics of shortwave radiation, maximum SWE, total amount of snow-covered days and DOYP. This suggests the important role that vegetation plays in the radiation budget during the cold season. In particular, the incoming shortwave radiation that has been scattered by distant vegetation appears to almost perfectly compensate for the decrease in radiation from topographic shading.

For the snow hillslope albedo, the scattered incoming shortwave radiation often more than compensates for losses from topographic shading. This results in catchment areas with high land-view factors having a greater average incoming shortwave radiation, and a more intense snow melt, leading to fewer snow-covered days. Regions with moderate to high sky-view factors and a small proportion of directly exposed hours (i.e., near or at the base of the flank of Redondo), show a decrease in incoming radiation as there is not enough scattered light from the land view factor to compensate for losses from direct radiation. Regions with high sky view factors that are also exposed show little change from the base case.

In the mixed snow-vegetation albedo, the deviations from the base case are almost exactly the same as the snow albedo case. This is primarily due to the use of the snow albedo during periods of snow interception, which last for extended periods of time during the simulation. In meadows and shrub vegetation, where interception is

minor, the vegetative fraction is also low. This leads to the dominant control of the snow albedo on the mixed snow-vegetation case in these regions. Overall, this correspondence yields similar distributions to the snow albedo case in incoming shortwave radiation and, thus, leads to a similar spatial and temporal evolution of the snow pack over the winter season.

These simulated spatiotemporal changes for the snow albedo and mixed snow-vegetation albedos are significant in terms of the reflectance of the land surface, as well as the amount of snow at any given time. The effects of hillslope albedo can delay the day of peak SWE by more than a month, as well as change the peak SWE by more than 50%. The decrease in the number of snow covered days is also marked, reducing these by at most 40 days. As a result, varying the albedo of the surrounding terrain alters land surface conditions throughout the season.

2.5.2 General Implications

Our results have potentially important implications for the use of distributed snow models, especially in regions of rugged terrain or high solar fluxes. We have presented two end members for depicting the albedo of the surrounding terrain (i.e. vegetation and snow albedos) and a possible intermediate model (dynamic or mixed snow-vegetation model). Differences from the base case, which only captures local controls, are significant. Despite this, without field studies designed to evaluate this particular set of processes, it is unclear which of the simulations is closest to reality. To our knowledge, field observations that focus on both the distribution of snow and the partitioning of the radiation budget, specifically scattered radiation, have not

taken place. This is complicated by the lack of robust snow-interception models that have been tested for wide ranges of conditions.

If the vegetative case were closest to actuality, then the temporal variations of vegetation albedo could be significant in determining the dynamics of snow accumulation and ablation. On the other hand, if the vegetation albedo varies little and occupies a large fraction of the landscape, it may be possible to neglect remote topographic effects in distributed snow models for regions of dense vegetation. If the snow albedo case is more appropriate, accurate representations of the evolution of distant snow packs may be a key element. For instance, in glaciated environments, the lower albedo of ice, when exposed, may alter the distribution of snow in surrounding areas. In areas of ephemeral snow packs, accumulation of snow in unvegetated valleys may also produce changes in the snow melt and its distribution.

A subtle, but possibly important point, raised by these results is how different conditions may affect the distribution of vegetation in snow-dominated environments. We have focused on the coupling in the opposite direction, i.e. how the distribution of vegetation affects snow. By increasing the amount of incoming radiation and compensating for remote shading, radiation scattering from the vegetated landscape changes both water availability, through changes in snow melt, and the amount of shortwave radiation available for uptake by plants. Then, does vegetation arrange itself to exploit these possibly significant factors? At this point, we can only say that the state of the surrounding landscape affects the overall character of the snow season at a point.

Our results are based on the distributed snow model presented in this study with its limitation and assumptions. Given these, however, we have identified the large effects of radiation scattering on the snow distribution in mountainous, lower mid-latitude settings. We believe this question needs to be investigated further through field studies that focus on the effects of remote vegetation on the distribution of snow and shortwave radiation. Also, the results of this study could be further pursued by using DSMs with more detailed implementations of remote and local vegetation and snow pack interactions, including a temporally varying implementation of land-view factors and landscape albedo.

2.6 Conclusions

Based on the proposed distributed snow model, we have shown that the albedo of the surrounding landscape exerts control on the spatiotemporal distribution of snow water equivalent and incoming shortwave radiation in La Jara catchment. The simulated interactions of vegetation, snow and topography provide the following insights:

(1) When vegetation albedo is used to represent the surrounding landscape, increases in incoming shortwave radiation compensate almost perfectly for the decreases in incoming shortwave radiation from topographic sheltering;

(2) When snow albedo is used, large deviations occur in the amount of maximum SWE and in the date that the maximum SWE occurs. A large decrease in the number of snow-covered days in the catchment is also observed;

(3) A mixed snow-vegetation albedo for the surrounding landscape produces patterns nearly identical to those simulated with the snow albedo; and

(4) A complicated balance exists between local vegetation controls (i.e. snow interception) and remote snow-vegetation-topographic controls that yields complex, but interpretable, patterns of integrated metrics of shortwave radiation and snow dynamics.

Given the potential for land-use changes in much of the western United States, a better understanding of snow-vegetation-topographic interactions is desirable. As revealed in this study, the relatively easy to characterize local conditions, such as slope, aspect and nearby vegetation, are not the only controls on snow-cover. The condition and relative position of distant slopes matters to snow cover, increasing the range of impact of vegetation change by the corresponding changes in scattered light.

2.7 Acknowledgements

This material is based upon work supported under the National Science Foundation Graduate Research Fellowship, NSF Grant EAR 0342526, and New Mexico Water Resources Research Institute – Student Grant Program. We thank John L. Wilson, Fred M. Phillips, Keith Musselman, Robert Wyckoff, Ricardo Mantilla and Soni Yatheendradas for helpful conversations and advice during the development of the study. Robert Parmenter from the VCNP gave access to the meteorological data from VCNP stations.

2.8 References

Anderson, E.A., 1976. Point energy and mass balance model of a snow cover. NOAA Technical Report NWS 19. 150 pp.

Bales, R.C. et al., 2006. Mountain hydrology of the western United States. Water Resources Research, 42(8).

Baron, J.S. et al., 1998. Effects of land cover, water redistribution, and temperature on ecosystem processes in the South Platte Basin. Ecological Applications, 8(4): 1037-1051.

Bayard, D., Stahli, M., Parriaux, A. and Fluhler, H., 2005. The influence of seasonally frozen soil on the snowmelt runoff at two Alpine sites in southern Switzerland. Journal of Hydrology, 309(1-4): 66-84.

Bloschl, G., Kirnbauer, R. and Gutknecht, D., 1991. Distributed Snowmelt Simulations in an Alpine Catchment .1. Model Evaluation on the Basis of Snow Cover Patterns. Water Resources Research, 27(12): 3171-3179.

Bras, R.L., 1989. Hydrology: an Introduction to Hydrologic Science. Addison-Wesley, Inc., New York, 660 pp.

Breshears, D.D. and Allen, C.D., 2002. The importance of rapid, disturbance-induced losses in carbon management and sequestration. Global Ecology and Biogeography, 11(1): 1-5.

Brooks, P.D., Schmidt, S.K. and Williams, M.W., 1997. Winter production of CO2 and N2O from Alpine tundra: Environmental controls and relationship to inter-system C and N fluxes. Oecologia, 110(3): 403-413.

Brundl, M., Bartelt, P., Schneebeli, M. and Fluhler, H., 1999. Measuring branch defection of spruce branches caused by intercepted snow load. Hydrological Processes, 13(14-15): 2357-2369.

Chen, J.M. et al., 2003. Spatial distribution of carbon sources and sinks in Canada's forests. Tellus Series B-Chemical and Physical Meteorology, 55(2): 622-641.

Coop, J.D. and Givnish, T.J., 2007. Gradient analysis of reversed treelines and grasslands of the Valles Caldera, New Mexico. Journal of Vegetation Science, 18(1): 43-54.

Davenport, D.W., Breshears, D.D., Wilcox, B.P. and Allen, C.D., 1998. Viewpoint: Sustainability of pinon-juniper ecosystems - a unifying perspective of soil erosion thresholds. Journal of Range Management, 51(2): 231-240.

Dozier, J., 1980. A clear-sky spectral solar radiation model for snow-covered mountainous terrain. Water Resources Research, 16(4): 709-718.

Dozier, J. and Frew, J., 1990. Rapid calculation of terrain parameters for radiation modeling from digital elevations data. IEEE Transactions on Geoscience and Remote Sensing, 28(5): 963-969.

Essery, R., Pomeroy, J., Parviainen, J. and Storck, P., 2003a. Sublimation of snow from coniferous forests in a climate model. Journal of Climate, 16(11): 1855-1864.

Essery, R.L.H., Best, M.J., Betts, R.A., Cox, P.M. and Taylor, C.M., 2003b. Explicit representation of subgrid heterogeneity in a GCM land surface scheme. Journal of Hydrometeorology, 4(3): 530-543.

Gelfan, A.N., Pomeroy, J.W. and Kuchment, L.S., 2004. Modeling forest cover influences on snow accumulation, sublimation, and melt. Journal of Hydrometeorology, 5(5): 785-803.

Goff, F. et al., 1989. Volcanic and hydrothermal evolution of Pleistocene Valles caldera and Jemez volcanic field in Field Excursions to Volcanic Terranes in the Western United States, Volume I: Southern Rock Mountain Region, ed. C.E. Chapin and J. Zidek. N.M.Bureau of Mining and Mineral Resources Memoir 46. University of New Mexico Printing Services, pp. 381-431.

Goff, F., Kues, B.S., Roger, M.A., McFadden, L. and Garnder, J.N., 1996. The Jemez Mountain Region, New Mexico Geological Society 47th Annual Field Conference. New Mexico Geological Society, Jemez Mountains, NM, pp. 1-484.

Harding, R.J. and Pomeroy, J.W., 1996. Energy balance of the winter boreal landscape. Journal of Climate, 9(11): 2778-2787.

Hardy, J.P. et al., 1997. Snow ablation modeling at the stand scale in a boreal jack pine forest. Journal of Geophysical Research-Atmospheres, 102(D24): 29397-29405.

Hardy, J.P., Davis, R.E., Jordan, R., Ni, W. and Woodcock, C.E., 1998. Snow ablation modelling in a mature aspen stand of the boreal forest. Hydrological Processes, 12(10-11): 1763-1778.

Hedstrom, N.R. and Pomeroy, J.W., 1998. Measurements and modelling of snow interception in the boreal forest. Hydrological Processes, 12(10-11): 1611-1625.

Hiemstra, C.A., Liston, G.E. and Reiners, W.A., 2002. Snow redistribution by wind and interactions with vegetation at upper treeline in the Medicine Bow Mountains, Wyoming, USA. Arctic Antarctic and Alpine Research, 34(3): 262-273.

Hock, R., 2003. Temperature index melt modelling in mountain areas. Journal of Hydrology, 282(1-4): 104-115.

Hubbart, J.A., Link, T.E., Gravelle, J.A. and Elliot, W.J., 2007. Timber harvest impacts on water yield in the continental/maritime hydroclimatic region of the United States. Forest Science, 53(2): 169-180.

Ivanov, V.Y., Vivoni, E.R., Bras, R.L. and Entekhabi, D., 2004. Preserving high-resolution surface and rainfall data in operational-scale basin hydrology: a fully-distributed physically-based approach. Journal of Hydrology, 298(1-4): 80-111.

Jordan, R., 1991. One-dimensional temperature model for a snow cover: Technical documentation for SNTHRM.89. U.S. Army Corp of Engineers, Cold Regions Research and Engineering Laboratory Special Report 91-16, pp. 1-45.

Koivusalo, H. and Kokkonen, T., 2002. Snow processes in a forest clearing and in a coniferous forest. Journal of Hydrology, 262(1-4): 145-164.

Kumler, M.P., 1994. An Intensive Comparison of Triangulated Irregular Networks (TINs) and Digital Elevation Models (DEMs). Cartographica Monograph 45, 31. University of Toronto Press, Toronto, 47 pp.

Lehning, M. et al., 2006. ALPINE3D: a detailed model of mountain surface processes and its application to snow hydrology. Hydrological Processes, 20(10): 2111-2128.

Letsinger, S.L. and Olyphant, G.A., 2007. Distributed energy-balance modeling of snow-cover evolution and melt in rugged terrain: Tobacco Root Mountains, Montana, USA. Journal of Hydrology, 336(1-2): 48-60.

Link, T.E., Marks, D. and Hardy, J.P., 2004. A deterministic method to characterize canopy radiative transfer properties. Hydrological Processes, 18(18): 3583-3594.

Liston, G.E. and Elder, K., 2006. A distributed snow-evolution modeling system (SnowModel). Journal of Hydrometeorology, 7(6): 1259-1276.

Liston, G.E., McFadden, J.P., Sturm, M. and Pielke, R.A., 2002. Modelled changes in arctic tundra snow, energy and moisture fluxes due to increased shrubs. Global Change Biology, 8(1): 17-32.

Ludwig, J.A., Wilcox, B.P., Breshears, D.D., Tongway, D.J. and Imeson, A.C., 2005. Vegetation patches and runoff-erosion as interacting ecohydrological processes in semiarid landscapes. Ecology, 86(2): 288-297.

Lundquist, J.D. and Flint, A.L., 2006. Onset of snowmelt and streamflow in 2004 in the western United States: How shading may affect spring streamflow timing in a warmer world. Journal of Hydrometeorology, 7(6): 1199-1217.

Marks, D., Domingo, J., Susong, D., Link, T. and Garen, D., 1999. A spatially distributed energy balance snowmelt model for application in mountain basins. Hydrological Processes, 13(12-13): 1935-1959.

Marks, D. and Winstral, A., 2001. Comparison of snow deposition, the snow cover energy balance, and snowmelt at two sites in a semiarid mountain basin. Journal of Hydrometeorology, 2(3): 213-227.

Marks, D., Winstral, A. and Seyfried, M., 2002. Simulation of terrain and forest shelter effects on patterns of snow deposition, snowmelt and runoff over a semi-arid mountain catchment. Hydrological Processes, 16(18): 3605-3626.

Montesi, J., Elder, K., Schmidt, R.A. and Davis, R.E., 2004. Sublimation of intercepted snow within a subalpine forest canopy at two elevations. Journal of Hydrometeorology, 5(5): 763-773.

Musselman, K., 2006. Quantifying the Effects of Forest Vegetation on Snow Accumulation, Ablation, and Potential Meltwater Inputs, Valles Caldera National Preserve, NM, USA, University of Arizona, Tucson, 127 pp.

NRCS, 2007a. http://soils.usda.gov.

NRCS, 2007b. http://www.nrcs.usda.gov/snow.

Oke, T.R., 1987. Boundary Layer Climates. Methuen and Co. Ltd., New York, 435 pp.

Parviainen, J. and Pomeroy, J.W., 2000. Multiple-scale modelling of forest snow sublimation: initial findings. Hydrological Processes, 14(15): 2669-2681.

Pomeroy, J.W. et al., 2006. Shrub tundra snowmelt. Hydrological Processes, 20(4): 923-941.

Pomeroy, J.W. and Dion, K., 1996. Winter radiation extinction and reflection in a boreal pine canopy: Measurements and modelling. Hydrological Processes, 10(12): 1591-1608.

Pomeroy, J.W., Gray, D.M., Hedstrom, N.R. and Janowicz, J.R., 2002. Prediction of seasonal snow accumulation in cold climate forests. Hydrological Processes, 16(18): 3543-3558.

Pomeroy, J.W. et al., 1998a. An evaluation of snow accumulation and ablation processes for land surface modelling. Hydrological Processes, 12(15): 2339-2367.

Pomeroy, J.W., Marsh, P. and Gray, D.M., 1997. Application of a distributed blowing snow model to the arctic. Hydrological Processes, 11(11): 1451-1464.

Pomeroy, J.W., Parviainen, J., Hedstrom, N. and Gray, D.M., 1998b. Coupled modelling of forest snow interception and sublimation. Hydrological Processes, 12(15): 2317-2337.

Rango, A., 2006. Snow: The real water supply of the Rio Grande basin. New Mexico Journal of Science, 44: 99-118.

Shamir, E. and Georgakakos, K.P., 2006. Distributed snow accumulation and ablation modeling in the American River basin. Advances in Water Resources, 29(4): 558-570.

Storck, P., Lettenmaier, D.P. and Bolton, S.M., 2002. Measurement of snow interception and canopy effects on snow accumulation and melt in a mountainous maritime climate, Oregon, United States. Water Resources Research, 38(11): 1-16.

Stott, P.A., Stone, D.A. and Allen, M.R., 2004. Human contribution to the European heatwave of 2003. Nature, 432(7017): 610-614.

Strack, J.E., Liston, G.E. and Pielke, R.A., 2004. Modeling snow depth for improved simulation of snow-vegetation-atmosphere interactions. Journal of Hydrometeorology, 5(5): 723-734.

Strack, J.E., Pielke, R.A. and Liston, G.E., 2007. Arctic tundra shrub invasion and soot deposition: Consequences for spring snowmelt and near-surface air temperatures. Journal of Geophysical Research-Biogeosciences, 112(G4): 1-12.

Sturm, M., Douglas, T., Racine, C. and Liston, G.E., 2005a. Changing snow and shrub conditions affect albedo with global implications. Journal of Geophysical Research-Biogeosciences, 110(G1): 1-13.

Sturm, M. et al., 2001. Snow-shrub interactions in Arctic tundra: A hypothesis with climatic implications. Journal of Climate, 14(3): 336-344.

Sturm, M. et al., 2005b. Winter biological processes could help convert arctic tundra to shrubland. Bioscience, 55(1): 17-26.

Talbot, J. et al., 2006. Relating snow dynamics and balsam fir stand characteristics, Montmorency Forest, Quebec. Hydrological Processes, 20(5): 1187-1199.

Tape, K., Sturm, M. and Racine, C., 2006. The evidence for shrub expansion in Northern Alaska and the Pan-Arctic. Global Change Biology, 12(4): 686-702.

Tarboton, D.G., Bloschl, G., Cooley, K.R., Kimbauer, R. and Luce, C.H., 2001. Spatial snow cover processes at Kuhtai and Reynolds Creek. In: R. Grayson and G. Bloschl (Editors), Spatial Patterns in Catchment Hydrology. Cambridge University Press, Cambridge, pp. 158-186.

Tarboton, D.G. and Luce, C.H., 1996. Utah Energy Balance Snow Accumulation and Melt Model (UEB). USDA Forest Service--Intermountain Research Station. 64 pp.

Tucker, G.E., Lancaster, S.T., Gasparini, N.M., Bras, R.L. and Rybarczyk, S.M., 2001. An object-oriented framework for distributed hydrologic and geomorphic modeling using triangulated irregular networks. Computers & Geosciences, 27(8): 959-973.

Tuteja, N.K. and Cunnane, C., 1997. Modelling coupled transport of mass and energy into the snowpack--model development, validations and sensitivity analysis. Journal of Hydrology, 195: 232-255.

Vivoni, E.R., Ivanov, V.Y., Bras, R.L. and Entekhabi, D., 2004. Generation of triangulated irregular networks based on hydrological similarity. Journal of Hydrologic Engineering, 9(4): 288-302.

Vivoni, E.R., Entekhabi, D., Bras R.L., and Ivanov, V.Y., 2007. Controls on runoff generation and scale dependence in a distributed hydrologic model. Hydrology and Earth Systems Science, 11: 1683-1701.

Whitaker, A.C. and Sugiyama, H., 2005. Seasonal snowpack dynamics and runoff in a cool temperate forest: lysimeter experiment in Niigata, Japan. Hydrological Processes, 19(20): 4179-4200.

Wigmosta, M.S., Vail, L.W. and Lettenmaier, D.P., 1994. A Distributed Hydrology-Vegetation Model for Complex Terrain. Water Resources Research, 30(6): 1665-1679.

Wilcox, B.P., Breshears, D.D. and Allen, C.D., 2003. Ecohydrology of a resource-conserving semiarid woodland: Effects of scale and disturbance. Ecological Monographs, 73(2): 223-239.

Wilson, J.P. and Gallant, J.C. (Editors), 2000. Terrain Analysis: Principles and Applications. John Wiley and Son, Inc., New York, 91-106 pp.

Woods, S.W., Ahl, R., Sappington, J. and McCaughey, W., 2006. Snow accumulation in thinned lodgepole pine stands, Montana, USA. Forest Ecology and Management, 235(1-3): 202-211.

Zappa, M., Pos, F., Strasser, U., Warmerdam, P. and Gurtz, J., 2003. Seasonal water balance of an Alpine catchment as evaluated by different methods for spatially distributed snowmelt modelling. Nordic Hydrology, 34(3): 179-202.

Zhang, Y.S., Suzuki, K., Kadota, T. and Ohata, T., 2004. Sublimation from snow surface in southern mountain taiga of eastern Siberia. Journal of Geophysical Research-Atmospheres, 109(D21): 1-10.

CHAPTER III: SUMMARY AND RECOMMENDATIONS

3.1 Introduction

In addition to the study completed in Chapter II, additional results were produced for further clarification and confirmation of model development, application and behavior. These results underline the conclusions of Chapter II, and, because of they necessarily repeat the major points, limited discussion of the results is included.

The additional results fall into three categories. First, a verification of the mass and energy balance of the snow pack scheme, and verification of the canopy dynamics are presented. Second, I present results confirming the dynamics of the sheltering and scattering of incoming shortwave radiation for three cases. Third, the results from additional scenarios are presented. These scenarios fall into two broad categories. One removes snow dynamics and uses uniform land-surface albedo in order to focus only on the catchment radiation distribution. All three hillslope albedo schemes are used and four cases of distant interaction are considered: (1) local sheltering; (2) local and remote sheltering; (3) local sheltering and remote scattering; and (4) local and remote sheltering, and remote scattering. The second scenario consists of considering two additional cases with snow dynamics. These are cases (2) and (3) listed above for the uniform albedo scenario.

After presenting the additional simulations, I review the results of the thesis. This includes a brief discussion of all of the conclusions presented in Chapter 2 as well as an integration of the results presented in the current chapter in support of these conclusions. The summary leads to recommendations for future work, which focus on additions to the model that may increase performance, additional modeling studies with the current model, and possible field measurements that can be made to inform the current understanding of radiation and snow dynamics.

3.2 Ancillary Results

For clarity, Figure 2.5 has been recreated in Figure 3.1. Recall the different zones: Zone 1 is the broad pediment at the outlet of La Jara; Zone 2 consists of the steeply incised valleys are low and middle elevations; Zone 3 are the broad ridge-tops with moderate to high sky-view factors; Zone 4 is the northern portion of the basin, with strong sheltering from the high elevations of Redondo; Zone 5 is at to the north of and at the base of the flank of Redondo peak; Zone 6 is the eastern slope of Redondo that is one of the highest features in catchment; and Zone 7 is the peak of Redondo, a regional high point. Results from Nodes 1196 and 1190 are presented. Node 1196, with its deeper snow pack, is used to confirm the dynamics of the snow pack. Node 1190, which is a forested node, is used to confirm the dynamics of the canopy. Basin averages are used to examine the radiation dynamics in the different scenarios.

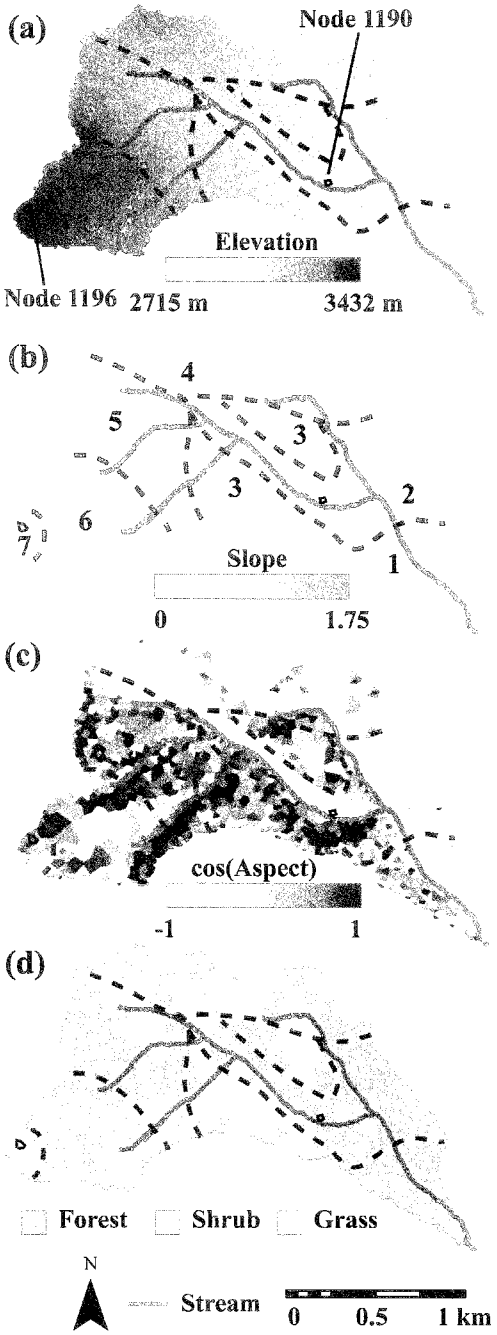

Figure 3.1. Distribution of topographic characteristics and vegetation in La Jara catchment as represented by Voronoi polygons. (a) Elevation (m). (b) Slope (ratio of y/x). (c) Cosine of the aspect (-). (d) Vegetation. In (c), south facing polygons ($\cos(A) < 0$) have light colors, depicting higher solar exposure, while north facing areas ($\cos(A) > 0$) have dark colors. East and west aspects are equivalent in color, but can be discerned relative to the streams derived from the DEM using a 500 m^2 constant area threshold. Zones with different responses to shortwave radiation have been delineated 1 through 7. Replicate of Figure 2.5.

3.2.1 Confirmation of Snow Dynamics

Figure 3.2 presents the snow and energy dynamics at Node 1196 from 5 March 2005 to 11 March 2005. Figure 3.2a depicts the transition from a dry cold ($T_{sn} < 0°C$) snow pack to a wet warm ($T_{sn} = 0°C$) snow pack. The snow pack becomes increasingly wet as the snow temperature oscillates from less then $0°C$ to $0°C$ with the diurnal cycles of air temperature and shortwave radiation. The increases in liquid water in the pack are initially lagged from the oscillations of snow temperature, until there is enough liquid water in the pack that it cannot all refreeze at night. Then, the diurnal cycle of air temperature and absorbed shortwave radiation is seen through the freezing and thawing of a portion of the liquid water equivalent. These increases and decreases are complimented by corresponding decreases and increases in the amount of ice in snow pack. As there is no precipitation, little latent heat flux and no routed melt occur during this period and the total amount of SWE remains nearly constant.

In Figure 3.2b, the energy balance is shown, which is manifested in the partitioning of water phases in the pack and snow temperature. As there is no ground heat flux in the model and there was no precipitation during the period, these sources of heat are not displayed. Incoming longwave radiation, absorbed shortwave radiation and sensible heat flux show the expected diurnal cycle. Deviations in shortwave radiation are caused by modeled cloud cover. The relative humidity during this period was modeled as being near saturation, leading to little latent heat flux. Outgoing longwave radiation displays a diurnal cycle concordant with snow temperature (Fig. 3.2a) until the snow temperature is at a constant 0°C. At this point, the outgoing longwave radiation remains constant. The internal energy also oscillates with the

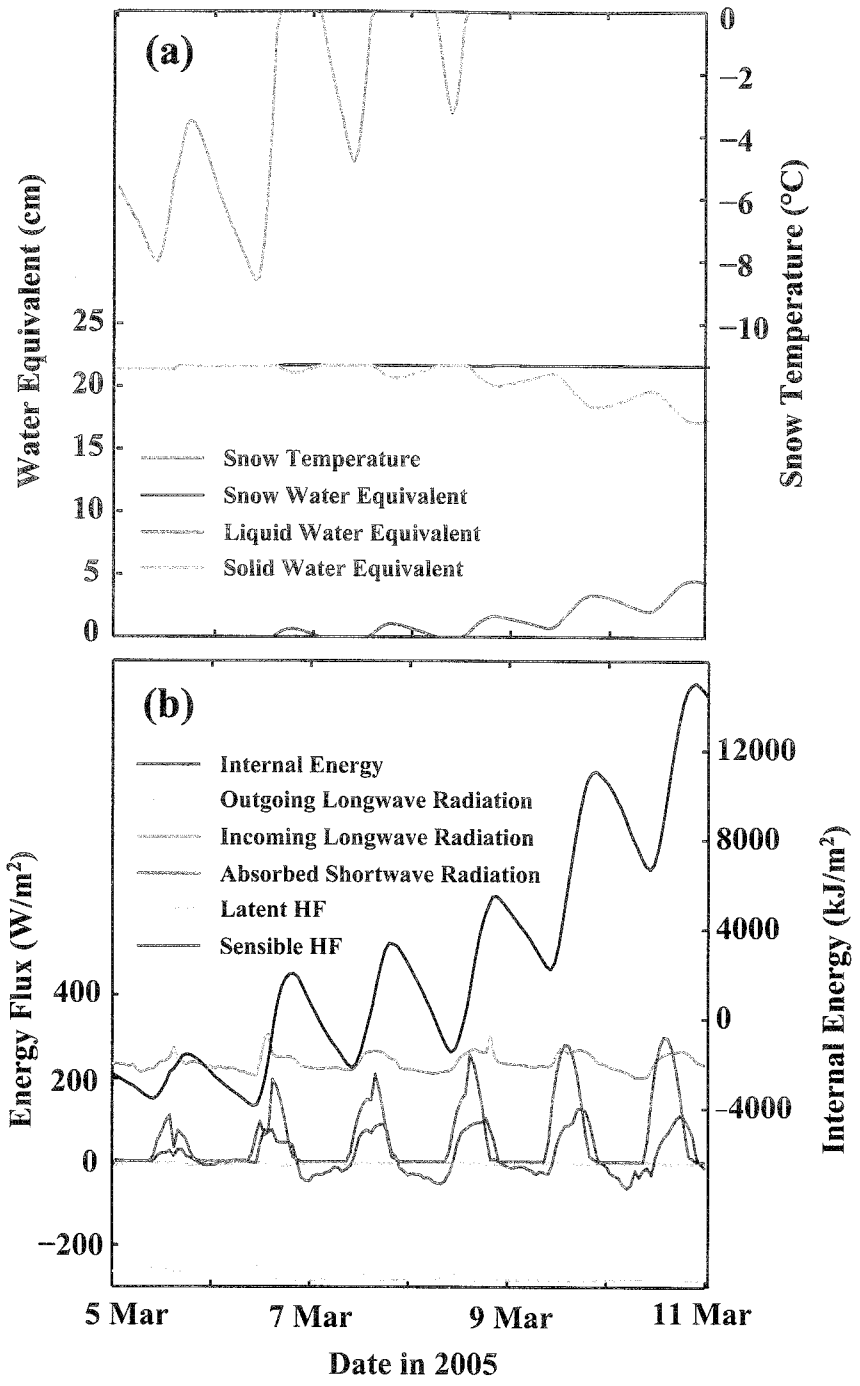

Figure 3.2. Confirmation of snow pack dynamics at Node 1196 from 5 March 2005 to 11 March 2005. (a) Mass partitioning of SWE (black) (cm) between ice (blue) (cm) and liquid water (red) (cm) as governed by snow temperature (green) (°C). (b) Energy balance with time series of outgoing longwave radiation (blue), incoming longwave radiation (green), absorbed shortwave radiation (red), latent heat flux (grey), and sensible heat flux (maroon) on the left axis in W/m^2; and total internal energy (black) on the right axis in kJ/m^2. The reference energy state (0 kJ/m^2) is an isothermal dry snow pack at 0°C.

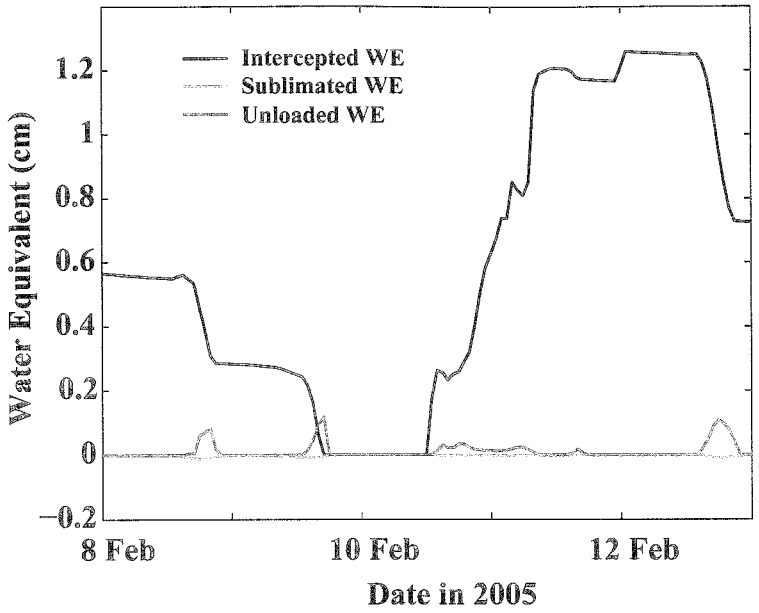

Figure 3.3 Dynamics of intercepted snow at Node 1196 from 8 February 2005 through 12 February 2005. Time series of intercepted water equivalent (black) (cm) captured in the canopy, sublimated water equivalent (blue) (cm), and water equivalent unloaded from the canopy (red) (cm) are shown.

diurnal cycle, gradually increasing through the displayed period. The energy goes above 0 kJ/m^2 only when the snow temperature is above 0°C and there is liquid water in the pack. When the liquid water refreezes and the snow temperature drops, the internal energy goes below 0 kJ/m^2. Late in the period, both snow temperature and internal energy remain above 0°C and 0 kJ/m^2, respectively. As demonstrated, the model is internally consistent, produces reasonable values and successfully couples and balances mass and energy.

3.2.2 Confirmation of Snow Interception Dynamics

Figure 3.3 shows the interception dynamics at Node 1196 from 8 February 2005 through 12 February 2005. At the beginning of this period, the canopy has snow captured in it that is gradually being sublimated (note the mild negative slope of intercepted WE). This snow is left from small events in early February. Late on 8

February and 9 February, the snow from the canopy is unloaded because of high temperatures. From 10 February through 11 February, a large snow event occurs, with mild temperatures and a cumulative precipitation of 5.2 cm. This is reflected in both the mild unloading (from warm air temperature) and rapid increase (from the large event) of snow in the canopy. Late on 12 February, there is an unloading event, with a corresponding decrease in intercepted snow.

3.2.3 Confirmation of Remotely-Controlled Radiation Dynamics

In order to examine the radiation dynamics of the model, four cases were examined: (1) local controls only (base case); (2) local and remote shading only; (3) local shading and remote scattering only; and (4) local and remote shading and remote scattering. In (3) and (4), all three hillslope albedo representations were used. In (1) and (2), the results are independent of hillslope albedo representation because there is no scattering. The uniform value of albedo for the land-surface (0.6) was used to calculate absorbed radation for the entire model domain. This does not include the scattering calculation. To calculate scattered radiation, the hillslope albedos were modeled by using the land-use input for vegetation albedo values, 0.6 for snow albedo, and a weighted-average of the land-use albedo and snow albedo for the mixed case.

Figure 3.4 shows the results of these different simulations for the basin-averaged absorbed radiation (W/m^2) from 7 March to 11 March. In the top row (Fig. 3.4a,c,e), the net values of radiation are reported, while the bottom row (Fig 3.4b,d,f) shows the difference between the remotely controlled cases and the base case. Figure 3.5 shows the relative controls of shading and scattering when snow hillslope albedo

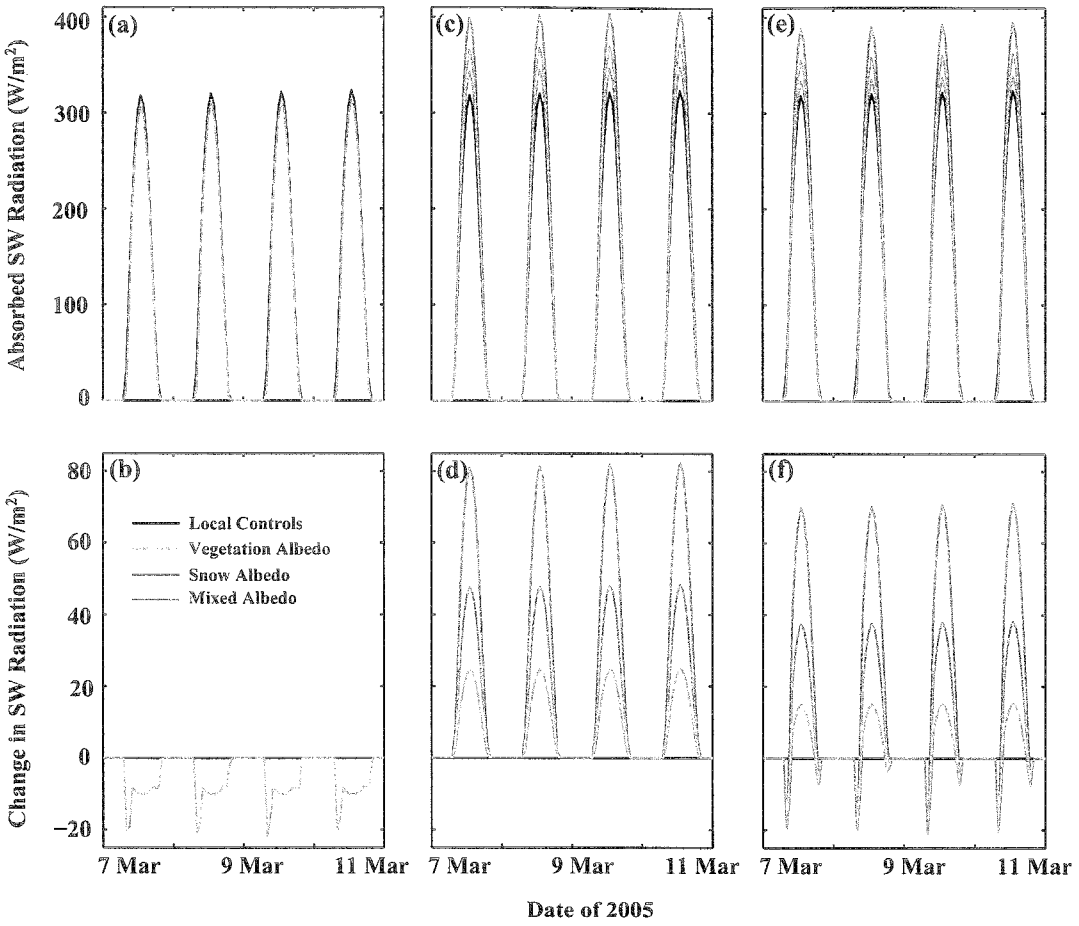

Figure 3.4 Time series of basin-average absorbed radiation (W/m^2) from 7 March 2005 to 11 March 2005. Four cases were simulated: local controls only (black); remote shading only (a,b); remote scattering only (c,d); and combined remote shading and scattering (e,f). The top row (a,c,e) are absolute values of absorbed radiation and the bottom row (b,d,f) are differences from the base case. Colors represent the hillslope albedo representation used: vegetation albedo in blue, snow albedo in red, and mixed albedo in green.

is used. As seen in Figures 3.4a and 3.4b, if only remote shading is used, the absorbed radiation is lower than the base case, with minima early in the morning and late in the afternoon when the sun angle is low. Figures 3.4c and d show the results for remote scattering only. As might be expected, all three hillslope albedo representations lead to more absorbed shortwave radiation. Specifically, snow hillslope albedo leads to the greatest amount of scattering and absorption, followed by the mixed and then vegetation hillslope albedo cases. Because scattering is proportional to the amount of

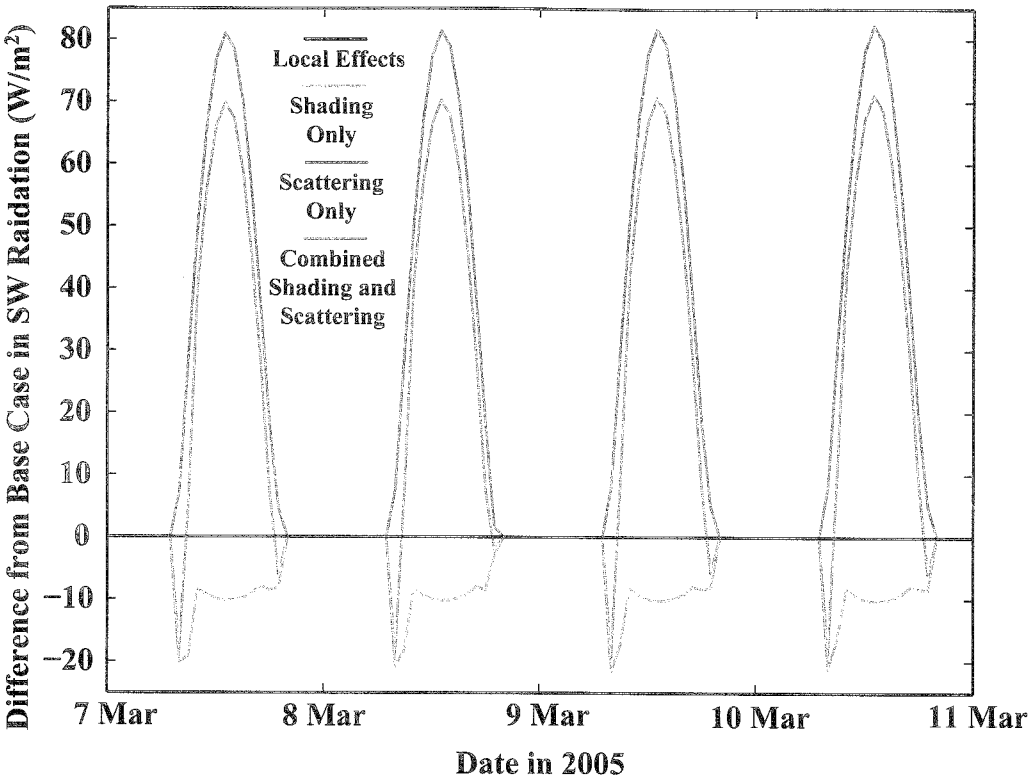

Figure 3.5 Deviation of basin-average absorbed radiation from base case (black) from 7 March 2005 to 11 March 2005 for simulations with remote shading only (blue), remote scattering only (red), and combined remote shading and scattering (green). Hillslope albedo was represented with snow albedo.incoming radiation, the deviations are greatest when the incoming radiation is greatest (i.e., at mid-day) and lowest when incoming radiation is lowest (i.e., in the early morning and late afternoon).

Figures 3.4e and f show the effects of accounting for both remote shading and scattering. Early in the morning and very late in the afternoon, remote shading dominates and lowers the absorbed radiation below the base case for all hillslope albedos. At mid-day, when incoming radiation is highest, scattering leads to a higher amount of absorption as compared to the base case. This scattering is still less than in the scattering-only case by approximately the amount of decreased absorption from shading. The positive deviations in absorption are greatest when snow hillslope albedo is used, followed by mixed albedo and by vegetation albedo. Early in the

morning, the negative deviation is independent of hillslope albedo representation because shading is caused by topography directly blocking the sun.

3.2.4 Results from Additional Radiation Representations

Simulations for two cases, one with uniform surface albedo and the other with dynamic snow cover, were completed for four subcases: (1) local sheltering only; (2) remote sheltering only; (3) remote scattering only; (4) remote sheltering and scattering combined. The hillslope albedo used to calculate scattering was represented in three distinct ways, as vegetation albedo, snow albedo, and a combination of snow and vegetation albedo, for each subcase. I begin by examining the spatial distribution of absorbed radiation for the different cases when uniform surface albedo is used. For dynamic snow cover, I examine the spatial distribution of absorbed radiation, peak SWE, cumulative snow-covered days, and the day of year of the peak SWE (DOYP). In order to present a coherent story, I will replicate some of the results from Chapter II.

3.2.4.1 Absorbed Radiation with Uniform Surface Albedo

Four cases were examined with a uniform surface albedo and varying radiations schemes: (1) local effects only; (2) local and remote shading; (3) local shading and remote scattering; and (4) local shading, and remote shading and scattering. Because these simulations do not have dynamic snow cover, only the average absorbed shortwave radiation are examined for the different cases.

In the locally sheltered case, the south-facing portions of Zones 1, 2 and 4 receive a large amount of radiation (~100 W/m^2) (Fig. 3.6a). Zones 3, 6 and 7, with

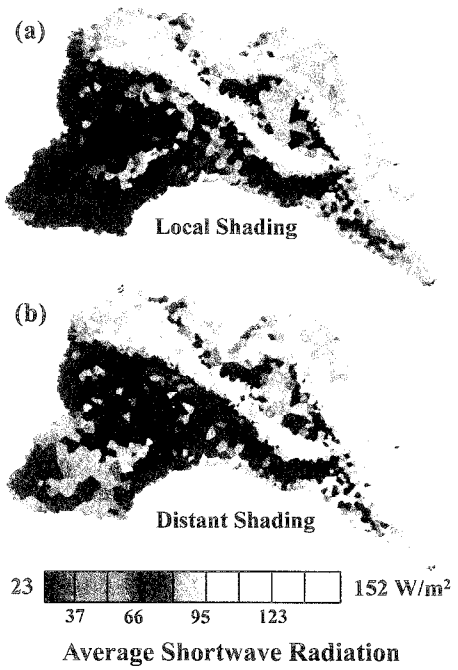

Figure 3.6 Distribution of average absorbed shortwave radiation (W/m^2) in La Jara when uniform surface albedo (0.6) is used over the simulation period. (a) Only local sheltering is applied and (b) local and remote shading are used.

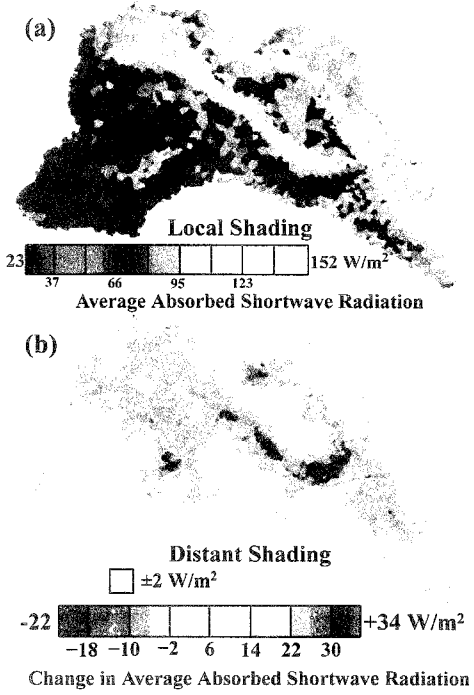

Figure 3.7 (a) Distribution of average absorbed shortwave radiation (W/m^2) over the simulation period when only local sheltering is applied with uniform albedo. (b) Difference between the base case (a) and when remote and local shading are used. The teal color implies that only ± 2 W/m^2 difference is found between the local case and the remotely shaded case.

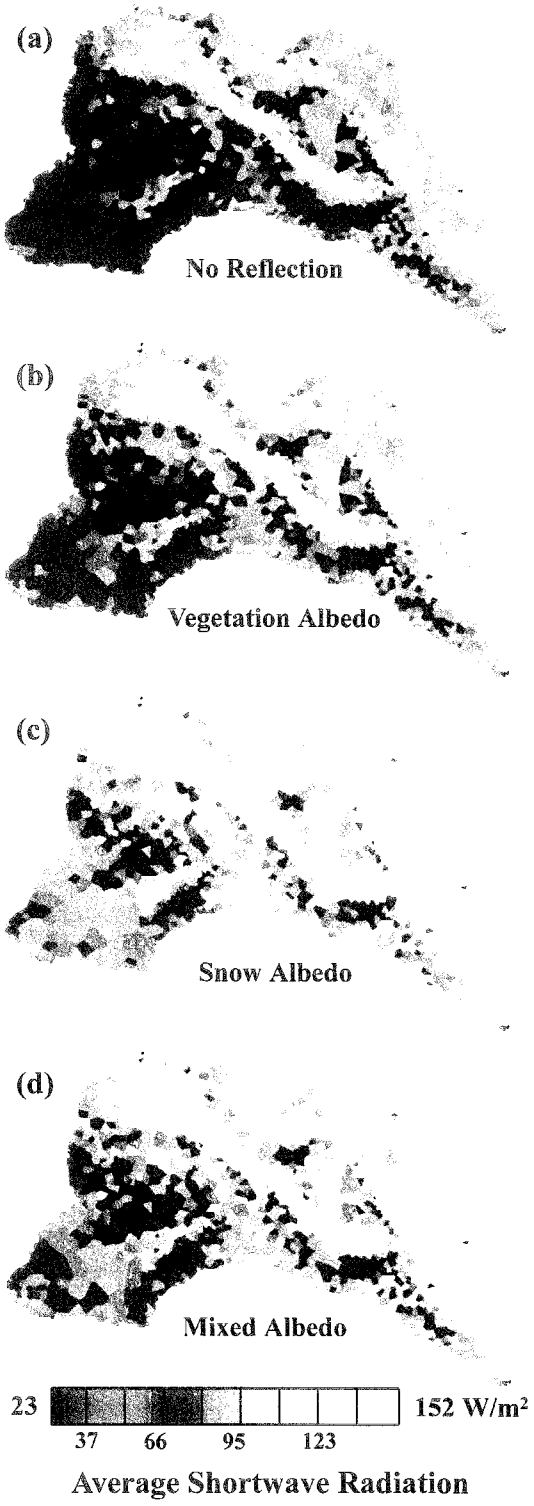

Figure 3.8 Average absorbed shortwave radiation (W/m^2) over the simulation period with uniform surface albedo when the sheltering scheme applied is (a) only local controls; and when local shading and remote scattering is applied with (b) vegetation hillslope albedo, (c) snow hillslope albedo, and (d) mixed hillslope albedo.

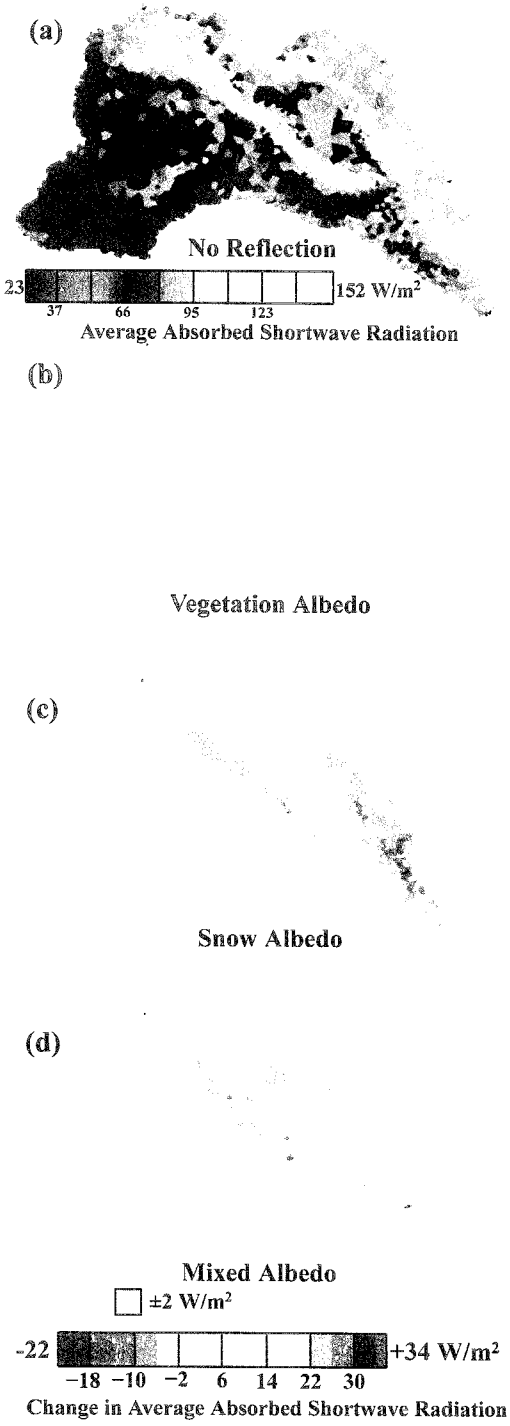

Figure 3.9 (a) Average absorbed shortwave radiation (W/m^2) over the simulation period with uniform surface albedo with local sheltering. The difference between the base case (a) and the cases with local shading and remote scattering, and (b) vegetation hillslope albedo, (c) snow hillslope albedo, and (d) mixed hillslope albedo. The teal color implies that only ± 2 W/m^2 difference is found between the local case and the remote case.

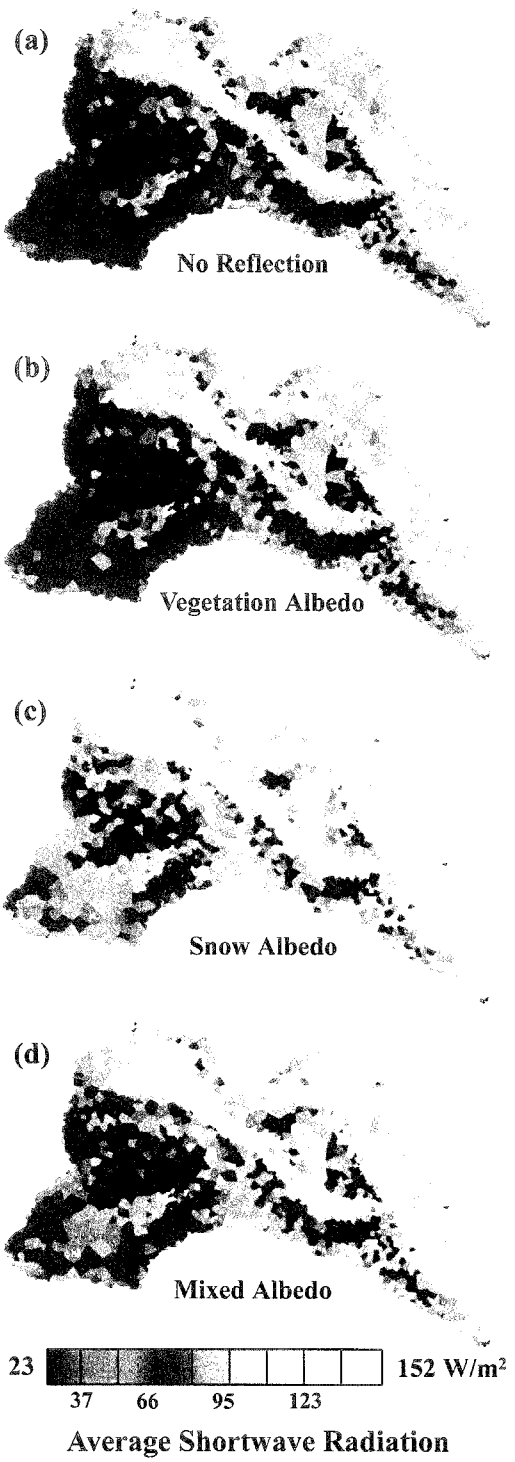

Figure 3.10 Average absorbed shortwave radiation (W/m^2) over the simulation period with uniform surface albedo when the sheltering scheme applied is (a) only local controls; and when local shading, and remote shading and scattering with (b) vegetation hillslope albedo, (c) snow hillslope albedo, and (d) mixed hillslope albedo.

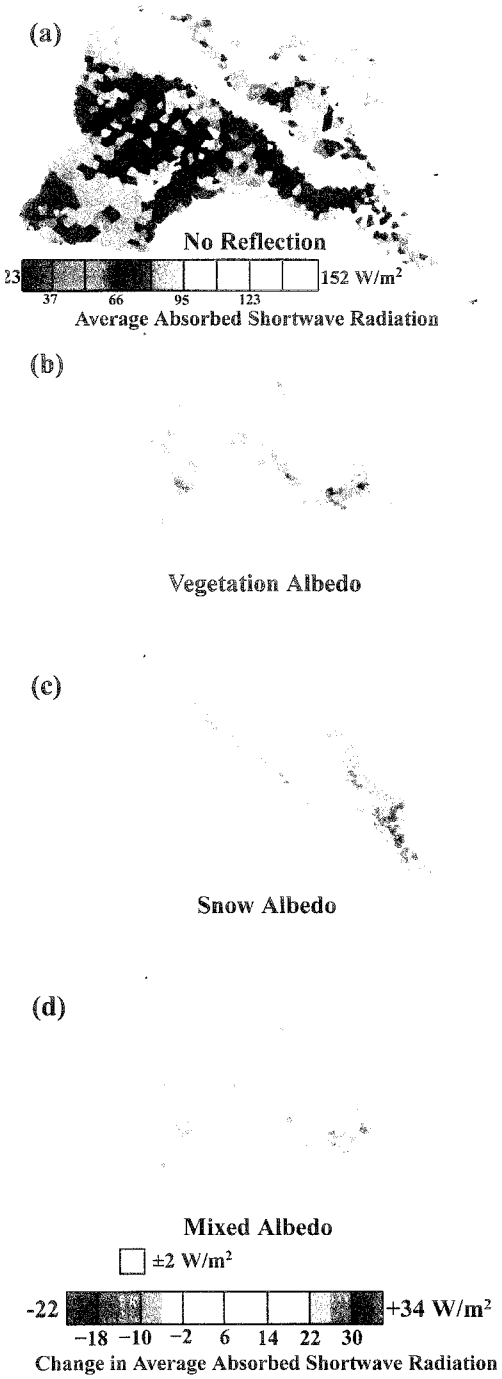

Figure 3.11 (a) Average absorbed shortwave radiation (W/m^2) over the simulation period with uniform surface albedo with local sheltering. The difference between the base case (a) and the case with local shading, and remote shading and scattering with (b) vegetation hillslope albedo (c) snow hillslope albedo, and (d) mixed hillslope albedo. The teal color implies that only ± 2 W/m^2 difference is found between the local case and the remotely shaded case.

their smooth non-south facing slopes, receive moderate amounts of radation (~80 W/m^2). Zone 5 is the most sheltered (~60 W/m^2) because of its north aspect and steep slopes. When remote shading is used (Figs. 3.6b and 3.7b), then the poorly shaded Zones 1, 3, 6 and 7 have at most a decrease in radiation of –6 W/m^2. The rugged Zones 2, 4 and 5, which are either deeply incised or on the north side of higher topography, are significantly shaded with decreases in absorbed radiation averaging – 10 W/m^2.

When local shading and scattering from distant hillslopes is modeled, a general increase in absorbed shortwave radiation is seen for all cases of hillslope albedos (Figs. 3.8b,c,d and 3.9b,c,d). The primary difference is in terms of the magnitude of the increase. With vegetation albedos (Figs. 3.8b and 3.9b), Zones 2 and 4, with their high land-view factors, are the only regions to show large deviations with increases of up to +18 W/m^2. The other zones have mild increases of up to +6 W/m^2. When snow hillslope albedos are applied (Figs. 3.8c and 3.9c), then zones 2 and 4 have extremely large increases averaging +26 W/m^2. The other zones have large increases averaging 14 W/m^2. When mixed albedos are applied (Figs. 3.8d and 3.9d), the same spatial pattern emerges as in the case with snow hillslope albedos, but with lower magnitudes.

If both scattering and shading are accounted for, the importance of the hillslope albedo representation becomes clear (Figs 3.10b,c,d and 3.11b,c,d). When vegetation hillslope albedo is applied (Figs. 3.10b and 3.11b), then most of the catchment (Zones 1, 3, 6 and 7) has little change in absorbed shortwave radiation. Zone 4 receives slightly more than the base case (+6 W/m^2). Zones 2 and 5 generally have little

change but have regions of large decreases (-14 W/m^2). This mild effect is contrasted by the large increases in radiation when snow hillslope albedo is used (Figs. 3.10c and 3.11c). For this case, Zones 1, 3, 6 and 7 absorb approximately +14 W/m^2 more shortwave radiation than in the base case. Zones 4 and portions of Zones 1, 2 and 3 show large increases (+26 W/m^2). Only in Zone 5 and portions of Zone 2 are deviations either slightly positive (+6 W/m^2), neutral or slightly negative (-6 W/m^2). In the mixed case (Figs. 3.10d and 3.11d), Zones 3, 6, and 7 see slight increases or small deviations from the base case. Zones 2 and 5 show mild decreases (-10 W/m^2). The only large positive deviations from the base case are found in Zones 1 and 4, with increases averaging +6 to +10 W/m^2.

3.2.4.2 Absorbed Shortwave Radiation with Snow Dynamics Modeled

The same set of cases of local and remote controls have been simulated with snow dynamics modeled. In each case, all three hillslope albedo schemes were applied (i.e., vegetation, snow and mixed hillslope albedo representations).

If only local controls are considered (Fig. 3.12a), then Zones 1 and 4, and the south-facing portions of Zone 2 absorb the greatest average shortwave radiation (180 -195 W/m^2). Zones 3 and 5, with their north aspects, receive the lowest amounts (60-100 W/m^2). Zones 6 and 7, with moderate slopes but east-north-east aspects, receive an intermediate amount of shortwave radiation (100-150 W/m^2). If remote shading is applied (Figs. 3.12b and 3.13b), then the entire basin receives less radiation. The decreases are small in Zones 1, 3, 6 and 7 (-6 W/m^2). In Zones 2, 4 and 5, the decreases are much larger, averaging –20 W/m^2.

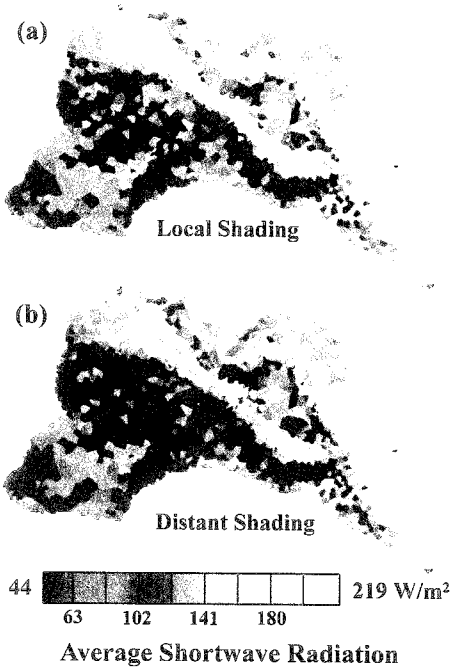

Figure 3.12 Distribution of average absorbed shortwave radiation (W/m^2) in La Jara with snow dynamics used over the simulation period. (a) Only local sheltering is applied and (b) local and remote shading are used.

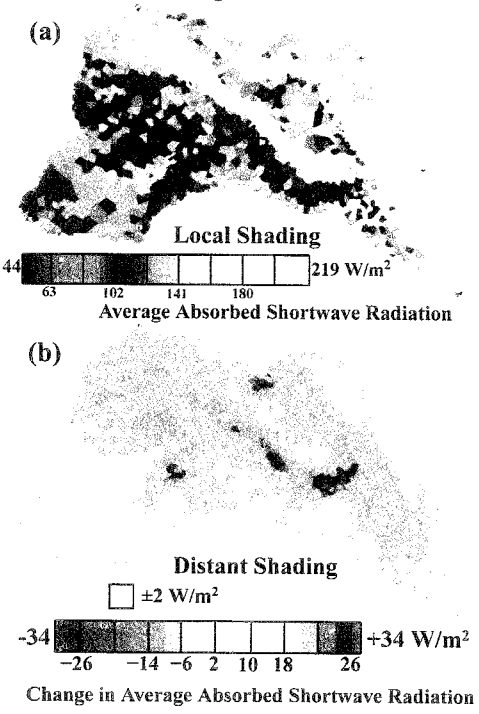

Figure 3.13 (a) Distribution of average absorbed shortwave radiation (W/m^2) over the simulation period when only local sheltering is applied and snow dynamics are modeled. (b) Difference between the base case (a) and when remote and local shading are used. The teal color implies that only ± 2 W/m^2 difference is found between the local case and the remotely shaded case.

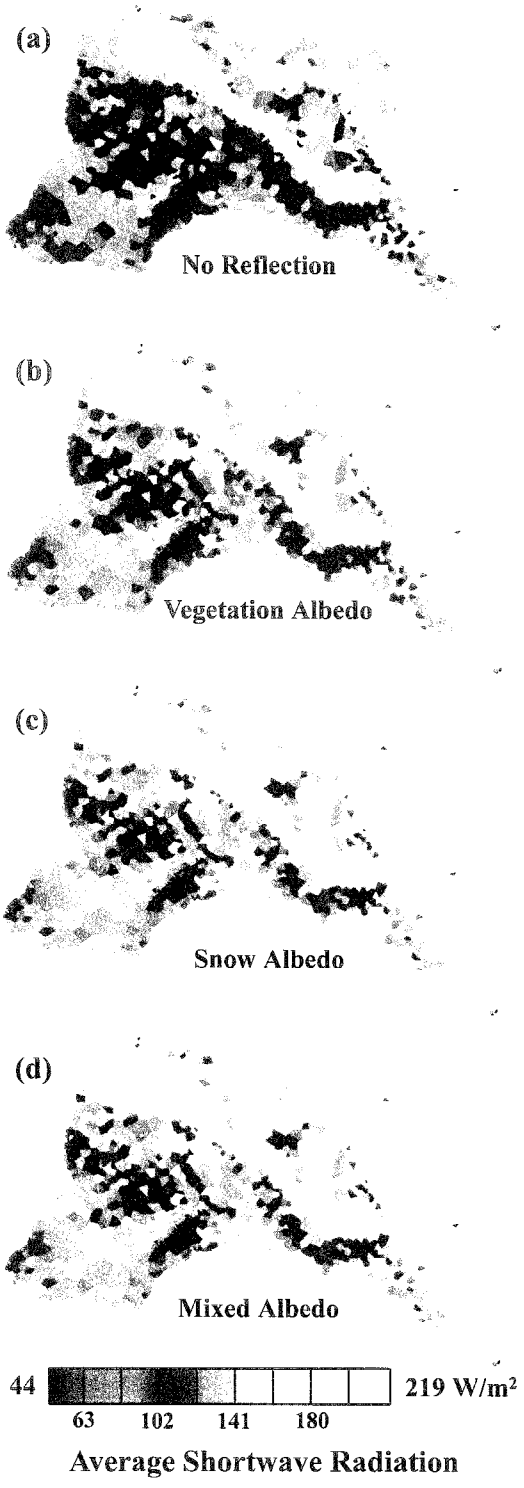

Figure 3.14 Average absorbed shortwave radiation (W/m^2) over the simulation period with snow dynamics modeled when the sheltering scheme applied is (a) only local controls; and local shading and remote scattering with (b) vegetation hillslope albedo; (c) snow hillslope albedo; and (d) mixed hillslope albedo.

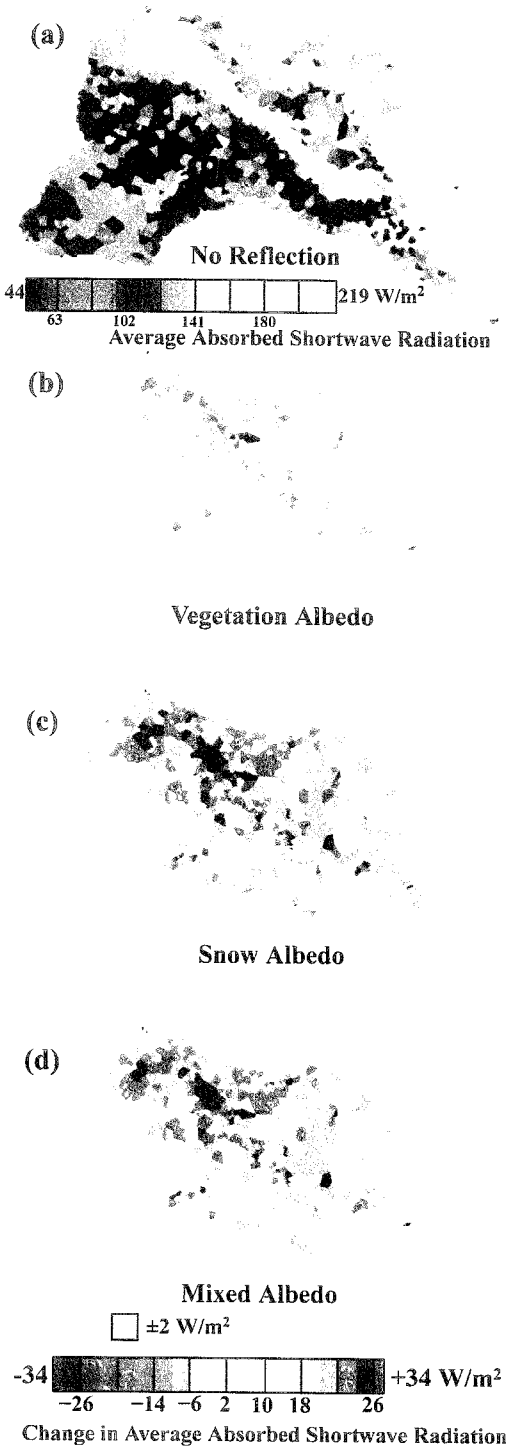

Figure 3.15 (a) Average absorbed shortwave radiation (W/m^2) over the simulation period with snow dynamics modeled with local sheltering. The difference between the base case (a) and the case with local sheltering and remote scattering with (b) with vegetation hillslope albedo; (c) snow hillslope albedo; and (d) mixed hillslope albedo. The teal color implies that only ± 2 W/m^2 difference is found between the local case and the remote case.

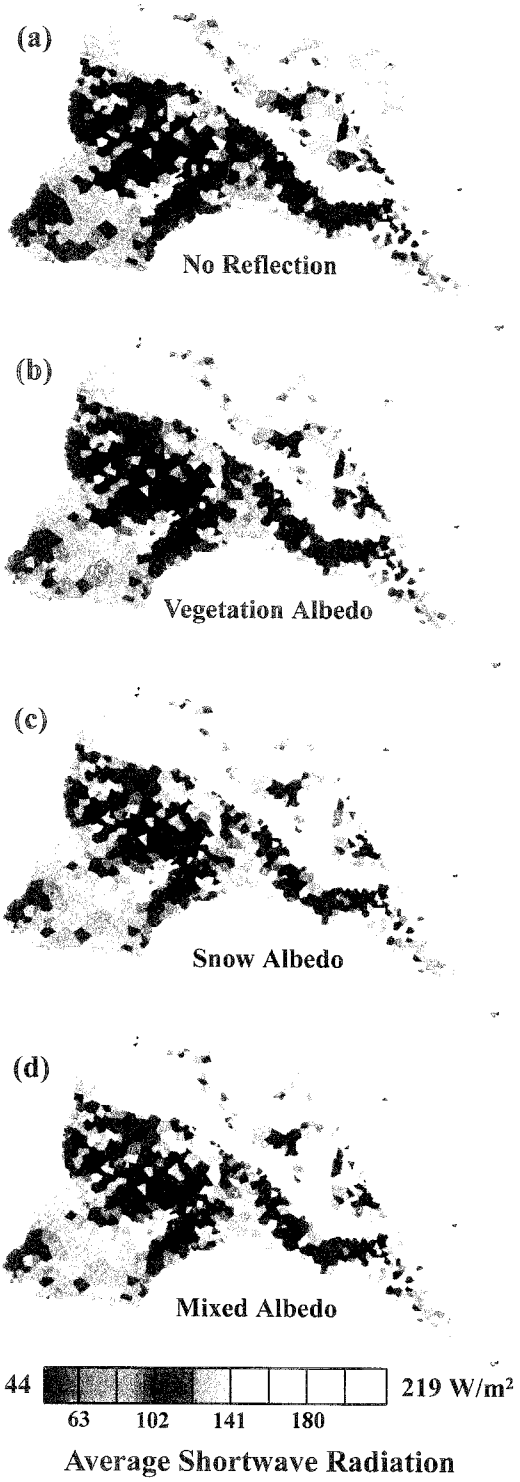

Figure 3.16 Average absorbed shortwave radiation (W/m^2) over the simulation period with snow dynamics modeled when the sheltering scheme applied is (a) only local controls; and local shading, and remote shading and scattering with (b) vegetation hillslope albedo; (c) snow hillslope albedo; and (d) mixed hillslope albedo.

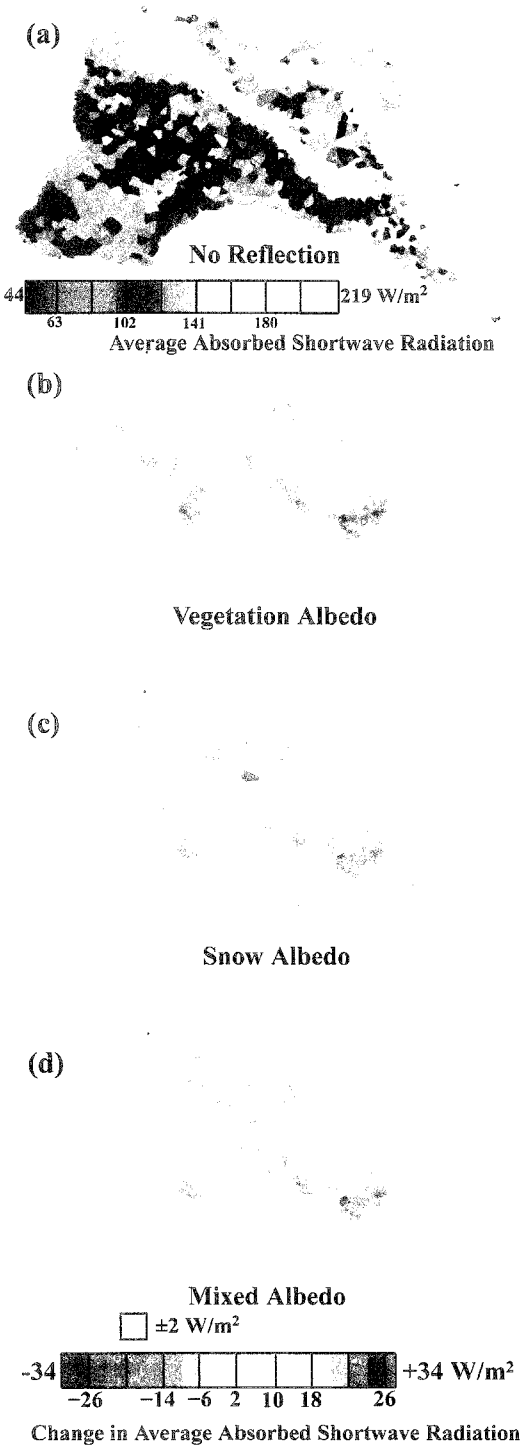

Figure 3.17 (a) Average absorbed shortwave radiation (W/m^2) over the simulation period with snow dynamics and local sheltering. The difference between the base case (a) and the case with local shading, and remote shading and scattering with (b) vegetation hillslope albedo; (c) snow hillslope albedo; and (d) mixed hillslope albedo. The teal color implies that only ± 2 W/m^2 difference is found between the local case and the remote case. (Replicate of Figure 2.8)

If there is no remote sheltering and only remote scattering, then the absorbed radiation increases throughout the basin for all cases of hillslope albedo (Figs. 3.14b,c,d and 3.15b,c,d). If vegetation hillslope albedo is applied (Figs. 3.14b and 3.15c), then Zones 1, 2 and 4 have the greatest increases (+20 W/m^2), while Zones 3, 5, 6 and 7 all have moderate increases in absorbed shortwave radiation (+10 W/m^2). When snow hillslope albedo is used (Figs. 3.14c and 3.15c), then Zones 1, 2, 3, and 4 all absorb much more radiation than the base case (+25 W/m^2). The remaining zones are do not absorb as much, but still more than in the other cases (+16 W/m^2). If mixed albedo is used (Figs. 3.14d and 3.15d), the distribution is similar to when snow albedo is used, but of slightly lesser magnitude.

When both scattering and remote shading are accounted for (Figs. 3.16b,c,d and 3.17b,c,d), then the importance of hillslope albedo representation is emphasized. Using vegetation hillslope albedo (Figs. 3.16b and 3.17b), there are regions of significant change, but overall the effects of incorporating remote controls are fairly minor. The patterns of absorbed radiation with snow albedo (Figs. 3.16c and 3.17c) or mixed albedo (Figs. 3.16d and 3.17d) are similar. In Zones 1, 3, 6 and 7, there is little change from the base case (±4 W/m^2). In the highly sheltered Zones 2 and 5, there is a distinct decrease in absorbed radiation (-15 W/m^2) in some areas when compared to the base case. In Zone 4, there is a large increase of absorbed radiation (+10 W/m^2), but not nearly as large as when there was no remote sheltering.

3.2.4.3 Peak SWE with Snow Dynamics Modeled

The control of remote shading and scattering are pronounced in the spatial distribution of peak SWE, reflecting the close relationship between absorbed

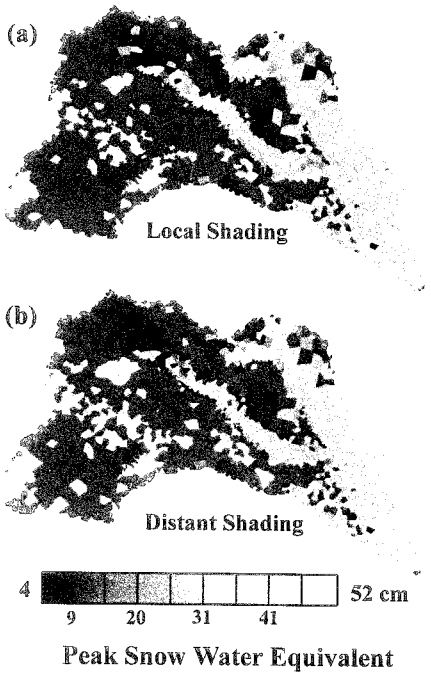

Figure 3.18 Distribution of peak SWE (cm) in La Jara over the simulation period. (a) Only local sheltering is applied and (b) local and remote shading are used.

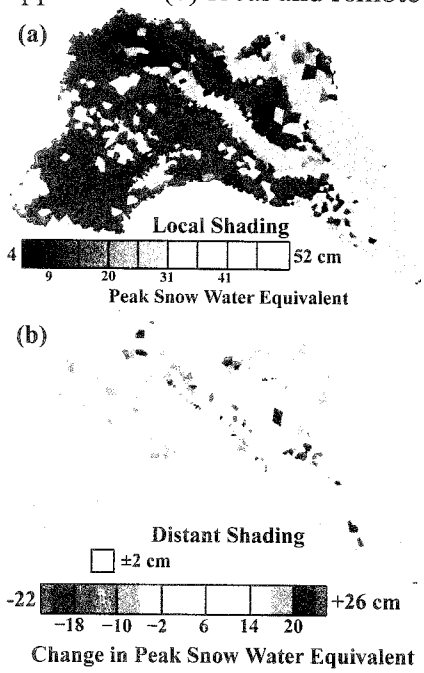

Figure 3.19 (a) Distribution of peak SWE over the simulation period when only local sheltering is applied. (b) Difference in peak SWE between the base case (a) and when remote and local shading are used. The teal color implies that only ± 2 cm difference is found between the local case and the remotely shaded case.

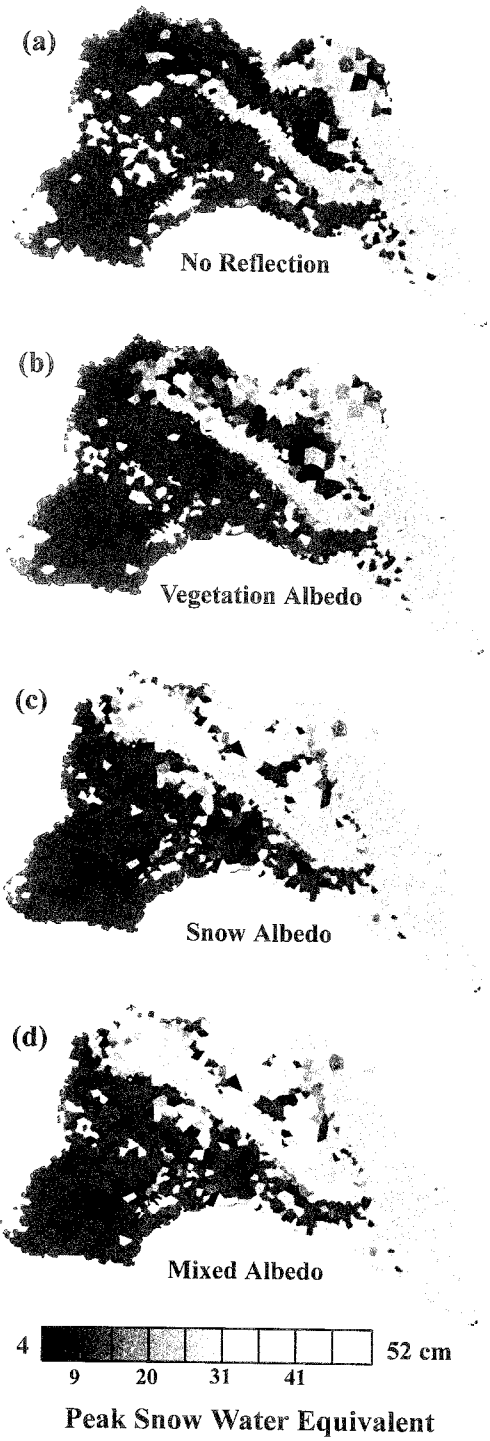

Figure 3.20 Peak SWE (cm) of the simulation period when the sheltering scheme applied is (a) only local controls; and local shading and remote scattering with (b) vegetation hillslope albedo; (c) snow hillslope albedo; and (d) mixed hillslope albedo.

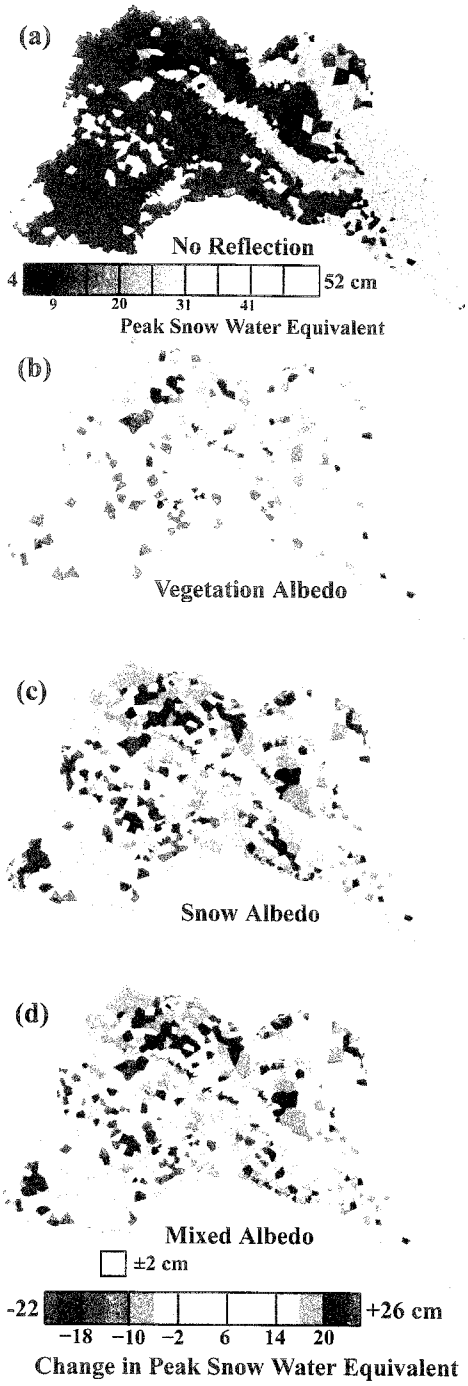

Figure 3.21 (a) Peak SWE (cm) of the simulation period with local sheltering. The difference in peak SWE between the base case (a) and the case with local sheltering and remote scattering with (b) with vegetation hillslope albedo; (c) snow hillslope albedo; and (d) mixed hillslope albedo. The teal color implies that only ± 2 cm difference is found between the local case and the remote case.

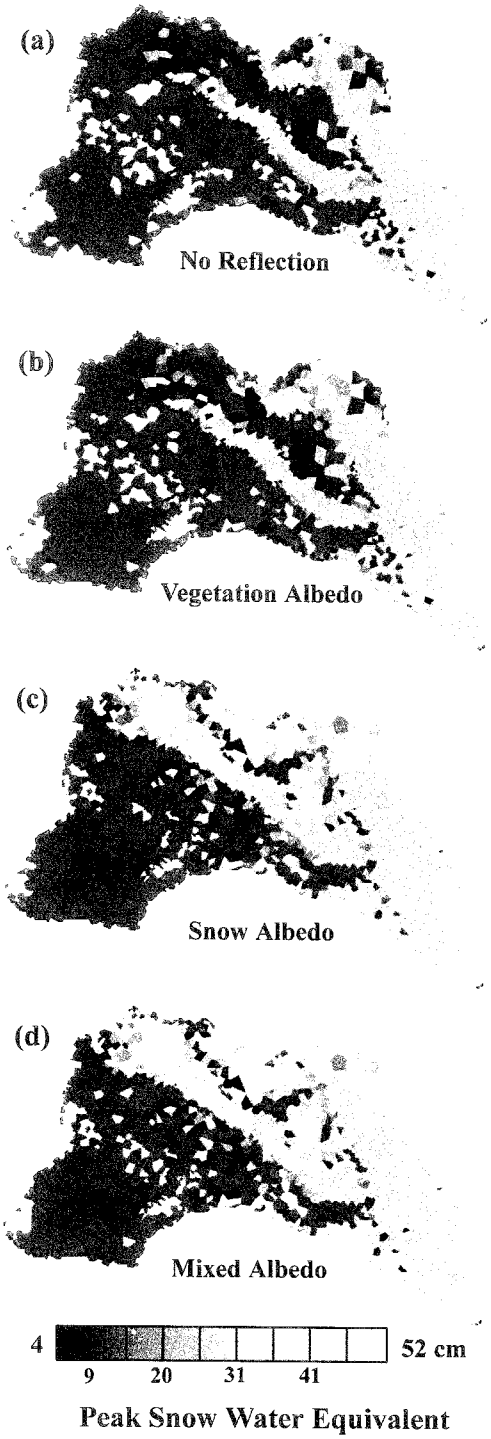

Figure 3.22 Peak SWE (cm) of the simulation period when the sheltering scheme applied is (a) only local controls; and local shading, and remote shading and scattering with (b) vegetation hillslope albedo; (c) snow hillslope albedo; and (d) mixed hillslope albedo.

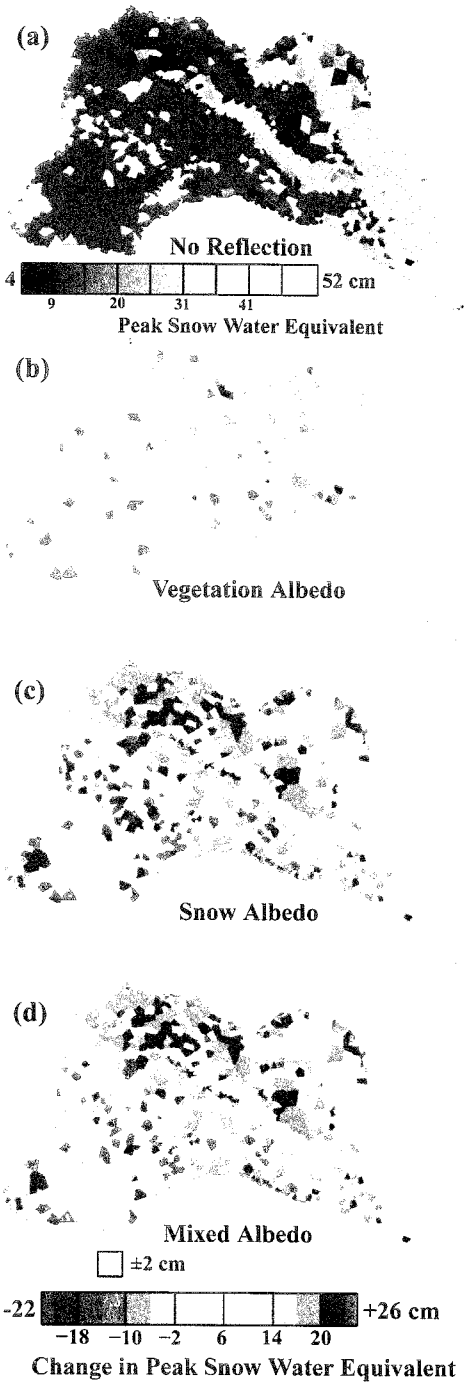

Figure 3.23 (a) Peak SWE (cm) of the simulation period with snow dynamics and local sheltering. The difference of peak SWE between the base case (a) and the case with local shading, and remote shading and scattering with (b) vegetation hillslope albedo; (c) snow hillslope albedo; and (d) mixed hillslope albedo. The teal color implies that only ± 2 cm difference is found between the local case and the remote case. (Replicate of Figure 2.9)

shortwave radiation and snow dynamics. We present the spatial distribution of peak SWE for the cases of local sheltering only; local and remote shading; local shading and remote scattering; and local and remote shading and remote scattering.

The distribution of peak SWE when local controls are considered (Fig. 3.18a) breaks into specific areas. Zones 1 and 2, and the eastern portion of Zone 4 form a contiguous zone of peak SWE of 30 cm. Zone 3 and the western portion of Zone 4 form another zone with an average peak SWE of 18 cm. Zone 5 has two distinct values of peak SWE. The steep north-facing polygons have peak SWEs of 30 cm. The remainder of Zone 5 and the most of Zone 6 has a peak SWE of 18 m. Zone 7 has the maximum accumulation of the entire basin, with a peak SWE of 49 cm. When remote shading is also incorporated (Figs. 3.18b and 3.19b), there are specific areas of difference from the base case. Specifically, portions of Zones 2 and 4 deviate from the base case by –10 cm, while areas in Zones 5 and 6 show increases over the base case of +10 cm.

When local shading and remote scattering are represented, the deviations from the base case are more marked (Figs. 3.20b,c,d and 3.21b,c,d). The effects of hillslope albedo representation are emphasized. Using vegetation hillslope albedo (Figs. 3.20b and 3.21b) to calculate scattered light causes the peak SWE in Zone 4 to mostly increase by +8 to +20 cm. Zones 1, 2, and 3 have little change from the base case. Zone 5 and 7 have decreases in peak SWE (-6 to –20 cm). Snow hillslope albedo (Figs. 3.20c and 3.21c) leads to more dramatic deviations. Western Zone 4 has large increases in peak SWE (8 to 20 cm), causing the peak SWE of all of Zone 4 to be continous with Zones 1 and 2. The northern portion of Zone 3 has similar increases to

that of Zone 4. Zones 5, 6 and 7 show a general decrease in peak SWE (-6 to –18 cm). The distribution of peak SWE when a mixed albedo (Figs. 3.20d and 3.21d) is used is nearly identical to the snow case.

When local and remote shading are included with remote scattering, a distribution of peak SWE similar to the scattering only case emerges, but the strength of the deviation is slightly damped by including remote shading (Figs. 3.22b,c,d and 3.23b,c,d). The changes in peak SWE when vegetation albedo is used are small throughout La Jara, except for Zone 1 (Figs. 3.22b and 3.23b). When snow albedo is used (Figs. 3.22c and 3.23c), the increases in Zones 3 and 4 are similar to those in the scattering-only case. They lead to Zone 4 and northern Zone 3 having the same peak SWE as Zones 1 and 2. The decreases in peak SWE in Zones 5 and 6 are slightly less than in the scattering-only case (-2 to –14 cm), but the decreases in Zone 7 are identical. When mixed hillslope albedo is used (Figs. 3.22c and 3.23c), the distribution of peak SWE is almost identical to the snow case, except that some of the decreases in peak SWE in the northern portion of Zone 5 are slightly smaller.

3.2.4.4 Cumulative Snow-Covered Time with Snow Dynamics Modeled

The simulation using local sheltering has a distinctive pattern to the cumulative snow-covered time during the study period (Fig. 3.24a). Zones 1 and 2 have the most ephemeral snow pack (40-50 days). Zones 3, 4 and 5 have reaches of both high (100 days) and low (60 days) snow-covered time, but generally have moderate snow covered time (80 days). Zone 6 is has a fairly homogeneous distribution of snow-covered time (80 days). Zone 7 has some of the most persistent snow pack in La Jara (90-124 days). When remote shading is added (Figs. 3.24b and 3.25b), the differences

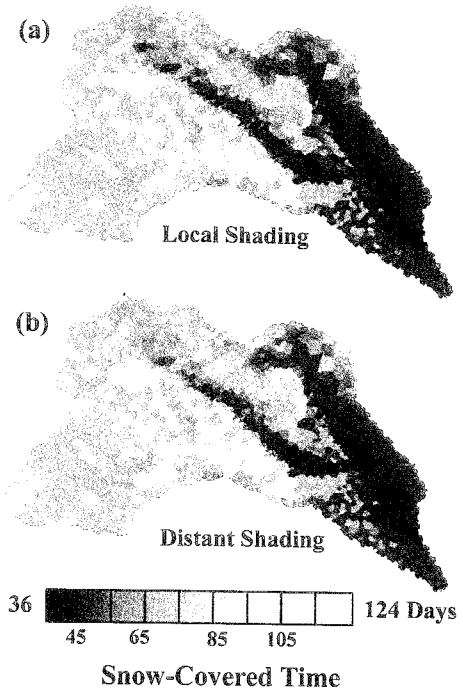

Figure 3.24 Distribution of snow-covered time (days) in La Jara over the simulation period. (a) Only local sheltering is applied and (b) local and remote shading are used.

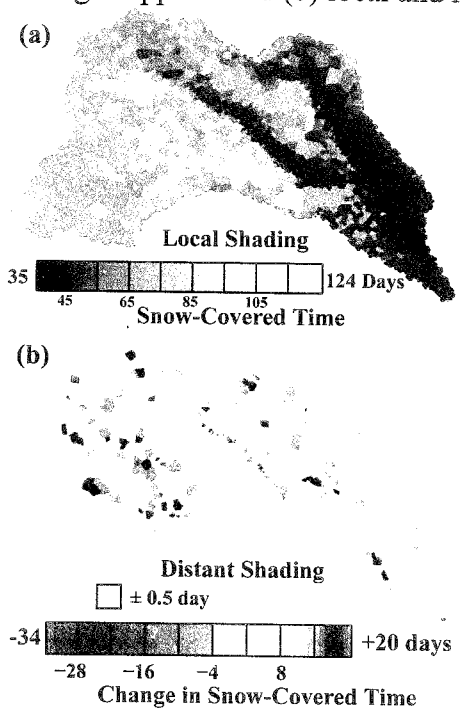

Figure 3.25 (a) Distribution of snow-covered time (days) during the simulation period when only local sheltering is applied. (b) Difference in snow-covered time between the base case (a) and when remote and local shading are used. The teal color implies that only ± 0.5 day difference is found between the local case and the remotely shaded case.

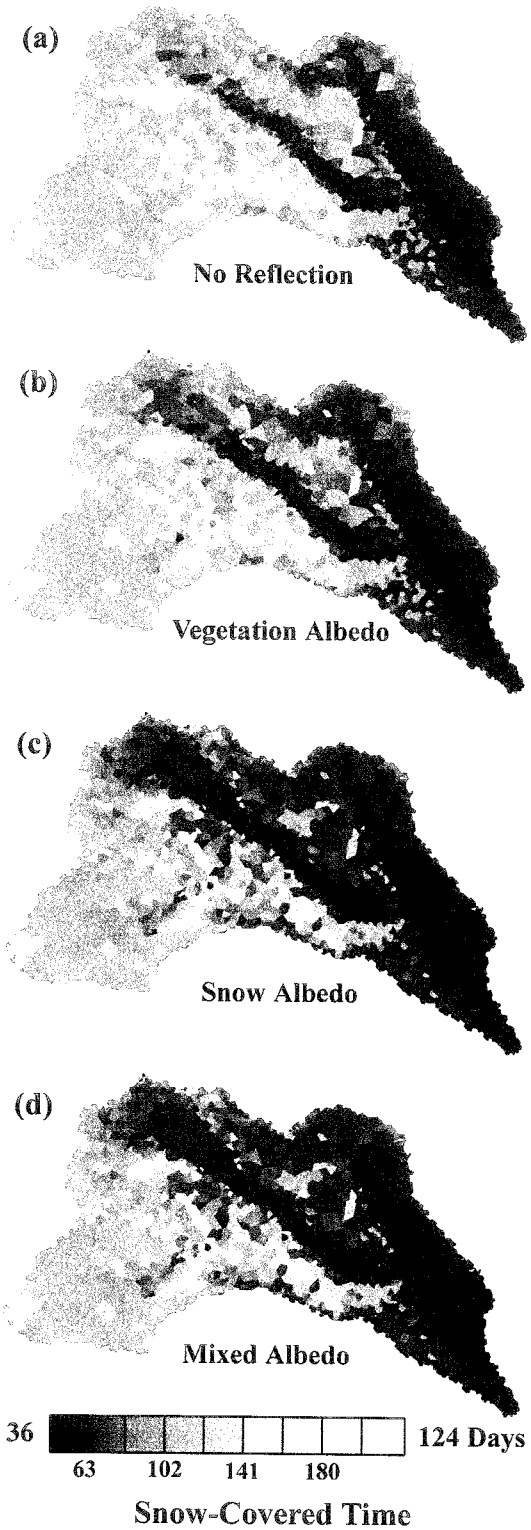

Figure 3.26 Snow-covered time (days) during the simulation period when the sheltering scheme applied is (a) only local controls; and local shading and remote scattering with (b) vegetation hillslope albedo; (c) snow hillslope albedo; and (d) mixed hillslope albedo.

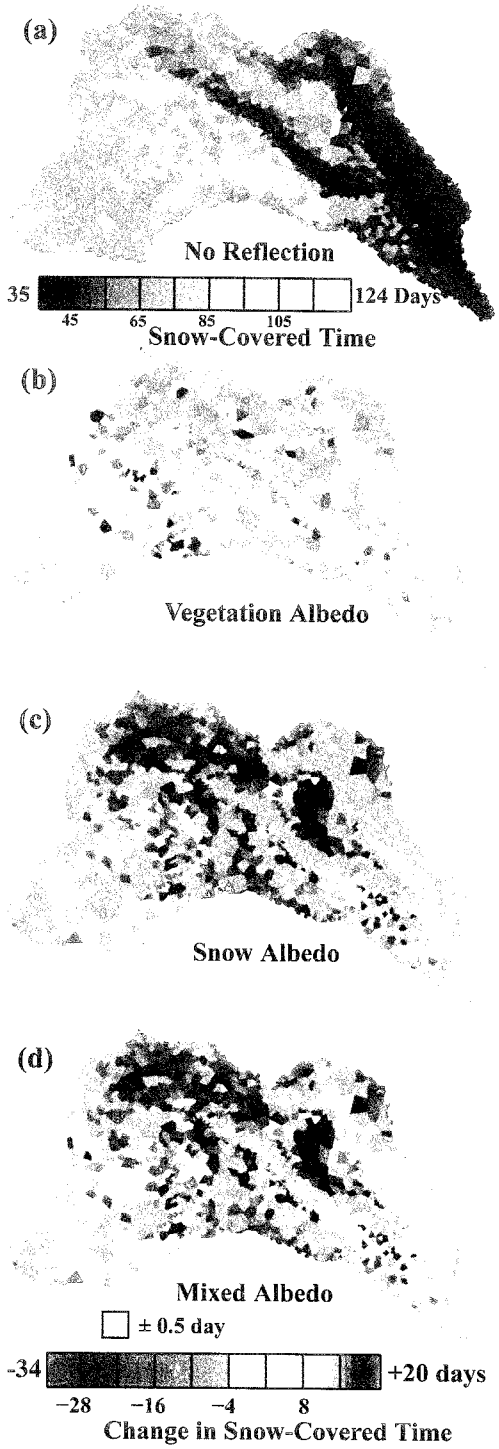

Figure 3.27 (a) Snow-covered time (days) during the simulation period with local sheltering. The difference in snow-covered time between the base case (a) and the case with local sheltering and remote scattering with (b) with vegetation hillslope albedo; (c) snow hillslope albedo; and (d) mixed hillslope albedo. The teal color implies that only ± 0.5 day difference is found between the local case and the remote case.

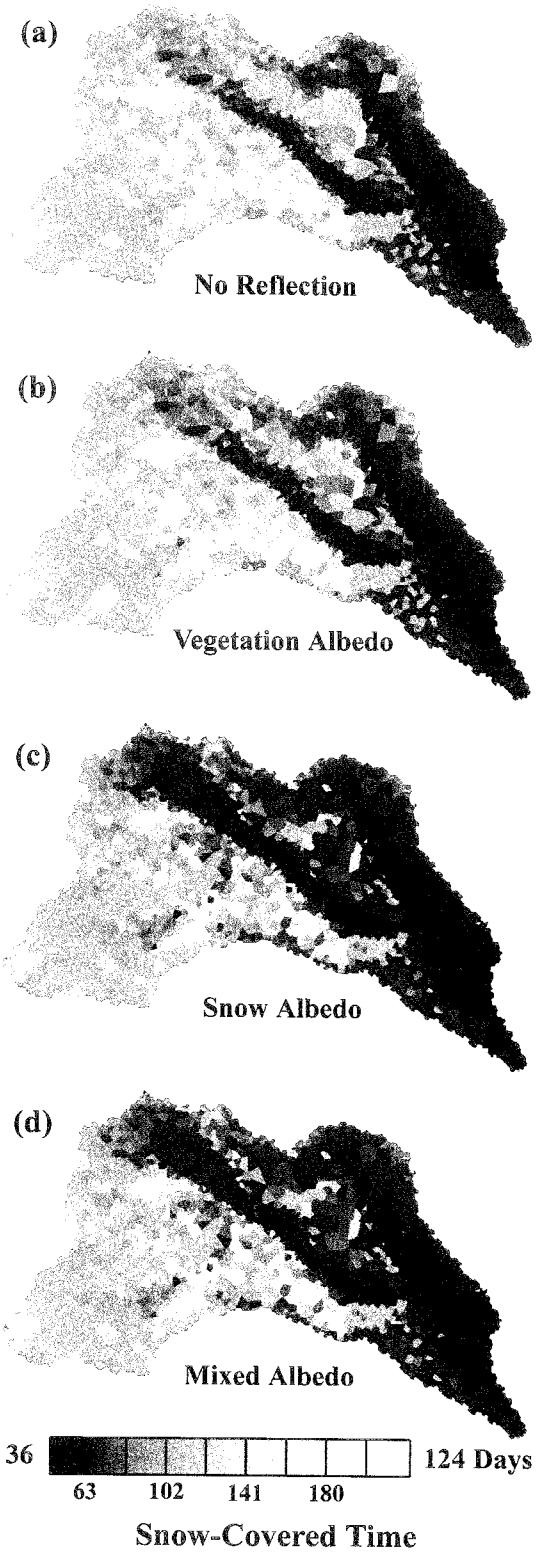

Figure 3.28 Snow-covered time (days) during the simulation period when the sheltering scheme applied is (a) only local controls; and local shading, and remote shading and scattering with (b) vegetation hillslope albedo; (c) snow hillslope albedo; and (d) mixed hillslope albedo.

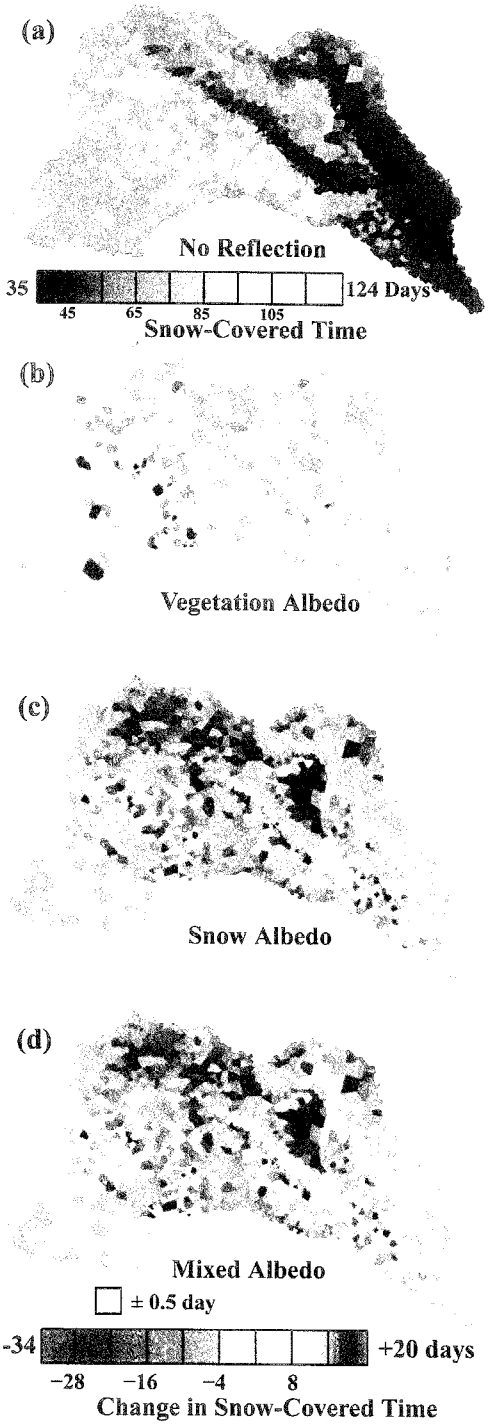

Figure 3.29 (a) Snow-covered time (days) during the simulation period with snow dynamics and local sheltering. The difference of snow-covered time between the base case (a) and the case with local shading, and remote shading and scattering with (b) vegetation hillslope albedo; (c) snow hillslope albedo; and (d) mixed hillslope albedo. The teal color implies that only ± 0.5 day difference is found between the local case and the remote case. (Replicate of Figure 2.10)

in snow-covered time between the shaded case and the base case are generally positive (8-18 days) and spread throughout Zones 2, 3, 4, 5, 6 and 7. Zone 1 shows little change.

When compared to local controls, the cases that incorporate only remote scattering all have less persistent snow packs, independent of the hillslope albedo parameterization (Figs. 3.26b,c,d and 3.27b,c,d). The hillslope albedo representation, however, controls the exact distribution and magnitude of decrease in persistence. When vegetation albedo is used (Figs. 3.26c and 3.27c), Zones 3 and 4 have the greatest decreases in persistence from the base case (-4 to –16 days). The other zones change little. The changes are larger and more spatially frequent when snow albedo is used for hillslope albedo (Figs. 3.26c and 3.27c). Here, Zones 3 and 4 once again show the greatest decreases in snow-covered time (-16 to –28 days), but Zones 2, 5, 6 and 7 all have moderate decreases (-4 to –12 days). The distribution of snow-covered days is similar for the mixed hillslope albedo (Figs. 3.26d and 3.27d) and the snow hillslope albedo case. The loss of persistence is slightly less in the mixed case than in the snow case, but only by a small amount.

3.2.4.5 Day of Peak SWE with Snow Dynamics Modeled

Another metric of the temporal character of the snow pack is at what day of year the peak SWE occurs (DOYP). When local controls are implemented (Fig. 3.30a), Zones 1 and 2, and eastern Zone 4 have a late peak (~84 days), which is when the large snow event occurred in March. Zones 3, 5, and 6, and eastern Zone 4 all have earlier DOYP in mid- to late February. Zone 7 has the latest DOYB of 90 days, consistent with its deep accumulation.

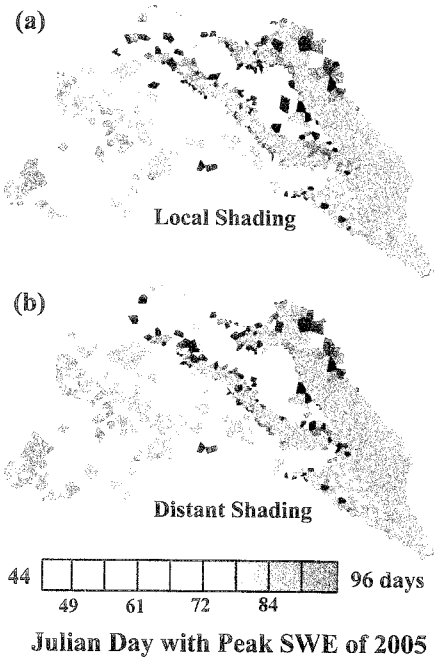

Figure 3.30 Distribution of Julian snow-covered time (days) in La Jara over the simulation period. (a) Only local sheltering is applied and (b) local and remote shading are used.

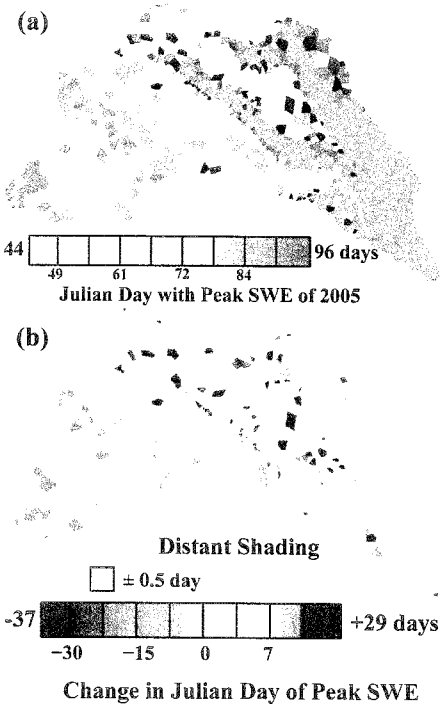

Figure 3.31 (a) Distribution of Julian day of Peak SWE during the simulation period when only local sheltering is applied. (b) Difference in snow-covered time between the base case (a) and when remote and local shading are used. The teal color implies that only ± 0.5 day difference is found between the local case and the remotely shaded case.

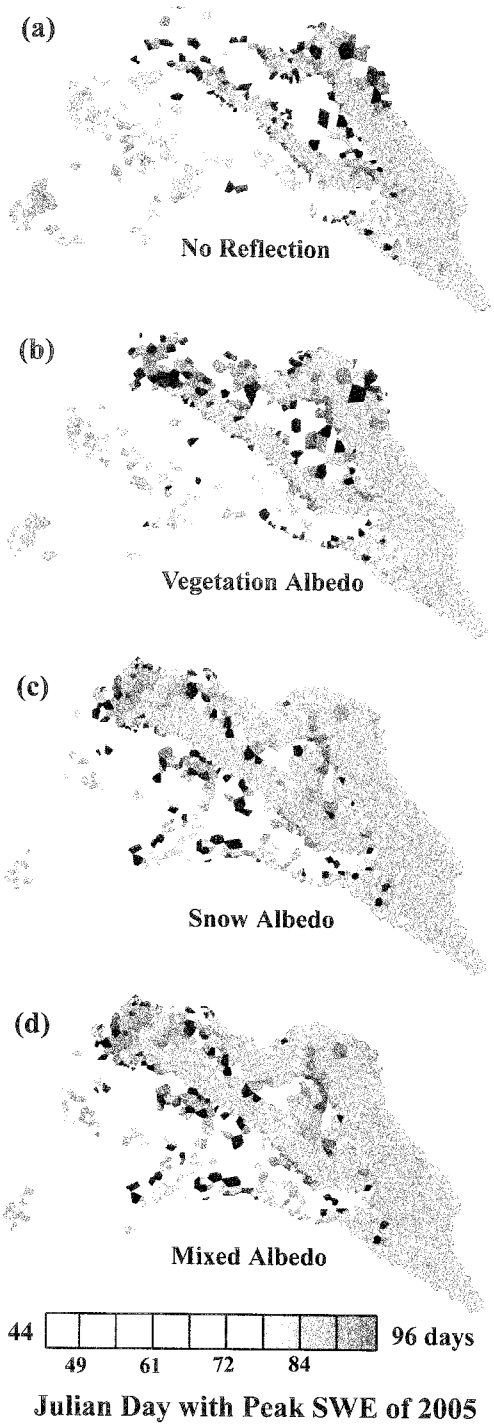

Figure 3.32 Julian day with peak SWE during the simulation period when the sheltering scheme applied is (a) only local controls; and local shading and remote scattering with (b) vegetation hillslope albedo; (c) snow hillslope albedo; and (d) mixed hillslope albedo.

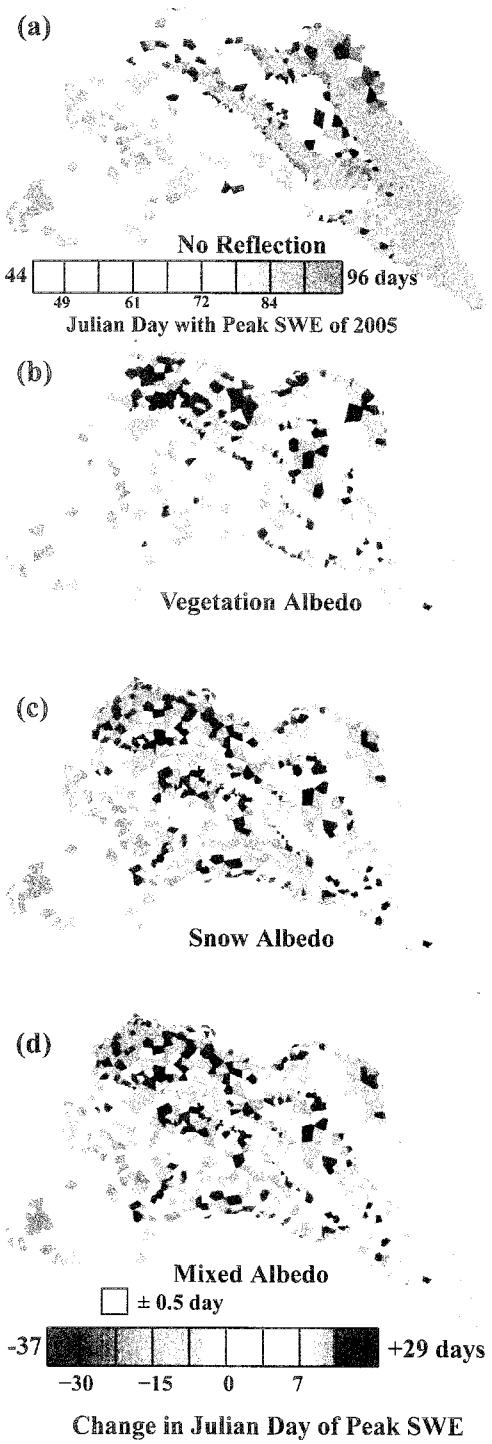

Figure 3.33 (a) Julian day of peak SWE during the simulation period with local sheltering. The difference in Julian days between the base case (a) and the case with local sheltering and remote scattering with (b) with vegetation hillslope albedo; (c) snow hillslope albedo; and (d) mixed hillslope albedo. The teal color implies that only ± 0.5 day difference is found between the local case and the remote case.

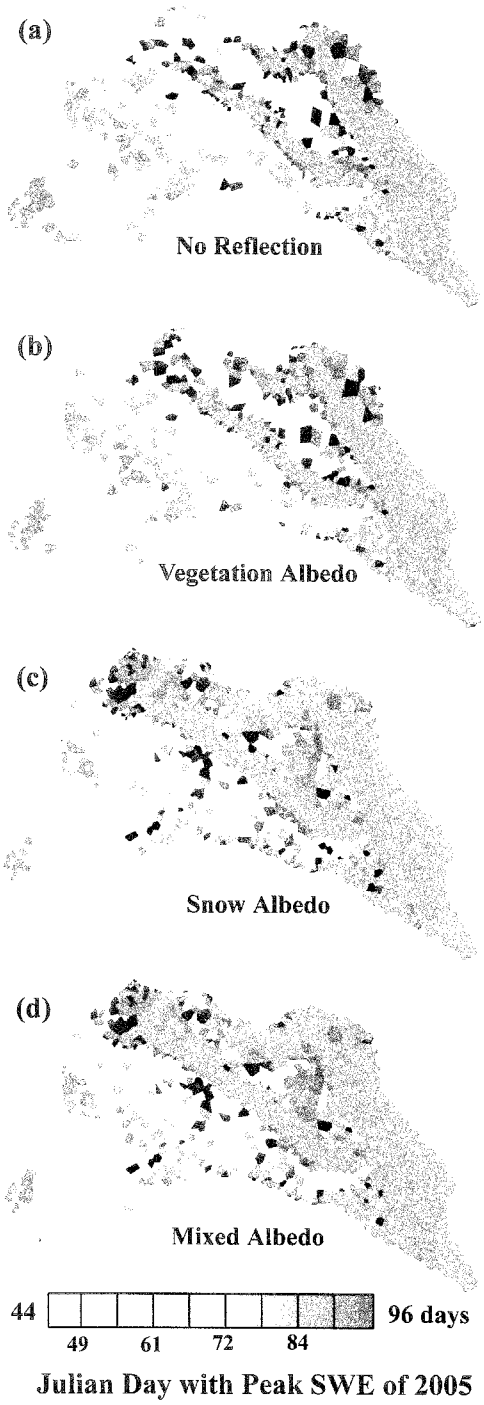

Figure 3.34 Julian day of peak SWE during the simulation period when the sheltering scheme applied is (a) only local controls; and local shading, and remote shading and scattering with (b) vegetation hillslope albedo; (c) snow hillslope albedo; and (d) mixed hillslope albedo.

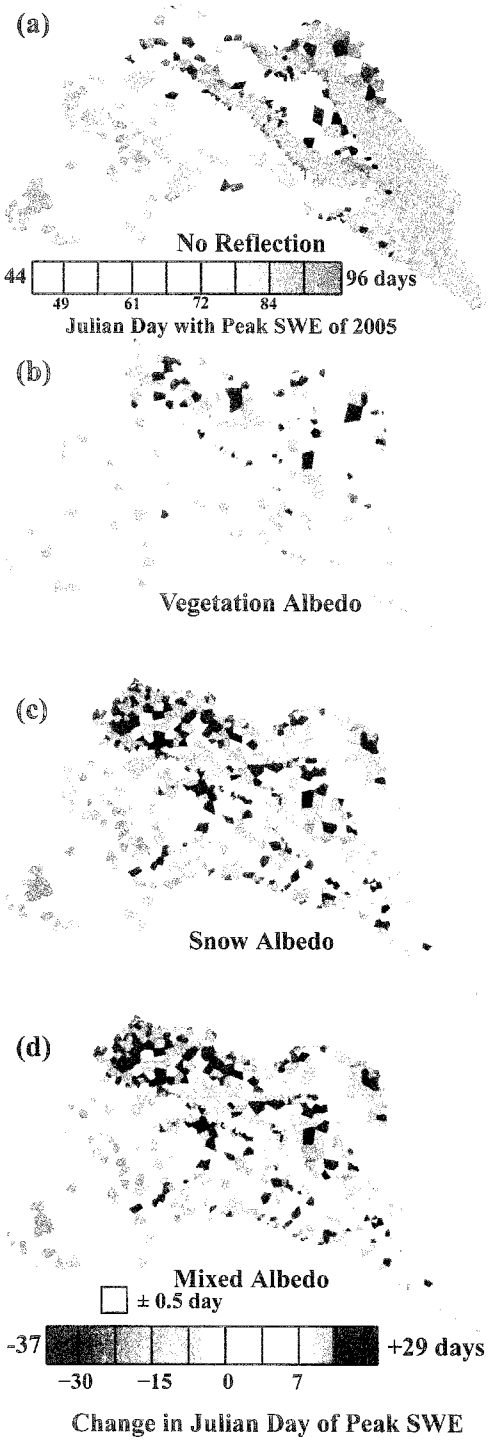

Figure 3.35 (a) Julian day of peak SWE during the simulation period with snow dynamics and local sheltering. The difference of Julian day between the base case (a) and the case with local shading, and remote shading and scattering with (b) vegetation hillslope albedo; (c) snow hillslope albedo; and (d) mixed hillslope albedo. The teal color implies that only ± 0.5 day difference is found between the local case and the remote case. (Replicate of Figure 2.11)

If remote shading is applied (Figs. 3.30b and 3.31b), then relatively little change occurs. In Zones 2 and 4, there are some regions of mild increases (5 days), but these regions also have decreases in DOYP (-15 days). Zones 5 and 6 have scattered regions that show positive deviations from the base case (+10 days), but the majority of these zones and the remainder of the catchment have less than ± 0.5 day difference in DOYP than the base case.

When scattering with no remote shading is used (Figs. 3.31b,c,d and 3.32b,c,d), larger deviations appear. The location of the differences remains the same independent of hillslope albedo representation, but magnitude and pervasiveness of the differences changes. When vegetation hillslope albedo is used (Figs. 3.31b and 3.32b), Zones 3 and 4 have large increases in DOYP compared to the base case (+20 to +29 days). The rest of La Jara sees little change except for some mild decreases in Zone 5. When snow (Figs. 3.31c and 3.32c) or mixed (Figs. 3.31d and 3.32d) hillslope albedo is used, then the deviations are identical between the cases and are larger than when the vegetation hillslope albedo is used. Specifically, all of Zones 3 and 4 and a portion of north-western Zone 2 all see large increases in DOYP (+15 to +29 days). The decreases in Zones 5 and 7 are more widespread and pronounced (-15 to -20 days). The remaining zones have little change.

When both remote shading and scattering are used (Figs. 3.33b,c,d and 3.34b,c,d), the importance of accurately representing hillslope albedo is emphasized. In the vegetation albedo case (Figs. 3.33b and 3.34b), little change is seen from the base case, with the greatest changes occurring in isolated regions of Zone 4, where the changes from shading and scattering were positive and additive. The rest of the

catchment sees little change except for some isolated negative deviations. This is contrasted by the large increases seen in Zones 3 and 4 and northwestern Zone 2 when either snow (Figs. 3.33c and 3.34c) or mixed (Figs. 3.33d and 3.34c) are used. Also, then negative deviations in Zones 5 and 7 are of the same order as in the scattering-only case.

3.2.4.6 Simulated Basin-Average and Point Simulated SWE

Figure 3.36 presents time series of basin-average SWE (cm), SWE at Node 1190 (in Zone 7), and SWE at Node 1196 (on a south-facing slope in Zone 3) for all of the cases simulated. In all cases, Node 1190 and Node 1196 present end members of behavior in the catchment, with Node 1190 having a deep persistent snow pack and Node 1196 having a shallow ephemeral pack. The basin-average SWE generally lies between these end-members, except in early March when a large melt event removed much of the snow pack in the basin. In all cases, little change between cases is seen at Node 1196. This is in an invariant region of Zone 3.

When remote shading only is considered (Fig. 3.36b), Node 1190 has a slightly large maximum than the other cases. The basin-average SWE is nearly the same as the base case. When scattering only is considered (Figs. 3.36c,d,e), there are small deviations in the melt after the maximum SWE. In all cases, a small step immediately after the maximum occurs that is not modeled in the base case. The lower maximum basin-average and Node 1190 SWE and a smaller rise of basin-average SWE early in the simulation than in the base case are most pronounced when snow hillslope albedo is applied (Fig. 3.36d). The deviations are slightly smaller when the mixed albedo is

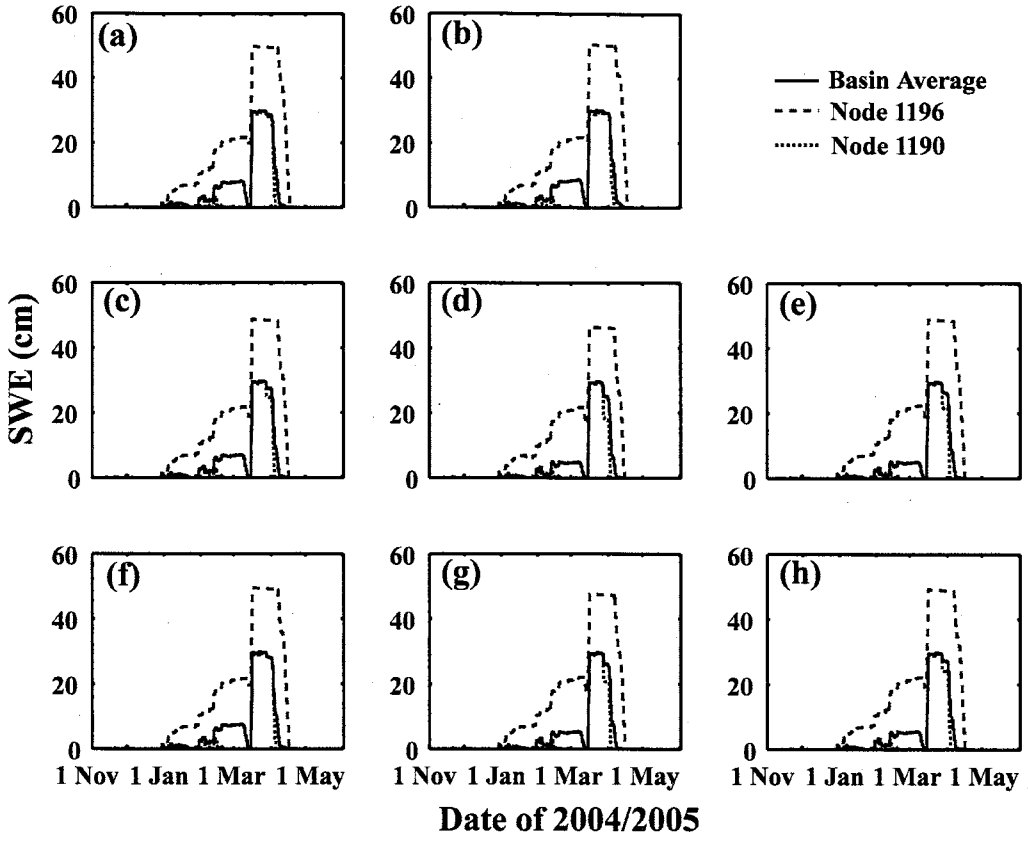

Figure 3.36 Time series of basin average SWE (solid) (cm), SWE at Node 1196 (dashed) (cm), and SWE at Node 1190 (dotted) (cm). These time series are replicated for (a) local sheltering only; (b) local and remote shading; local shading and remote scattering for hillslope representation using (c) vegetation albedo, (d) snow albedo, and (e) mixed albedo; and local and remote shading, and remote scattering with the hillslope representation using (f) vegetation albedo, (g) snow albedo, and (h) mixed albedo.

used (Fig. 3.36e), followed by fairly mild deviations when the vegetation albedo is used (Fig. 3.36c).

When both remote shading and scattering are used (Figs. 3.36f,g,h), some features of both the shading and scattering cases are seen. The use of vegetation hillslope albedo (Fig. 3.36f) produces time-series very similar to the base case in all features except that the maximum SWE at Node 1190 is slightly less than in the base case. When snow hillslope albedo (Fig. 3.36g) or mixed hillslope albedo (Fig. 3.36h)

is used, the behavior of basin-average SWE, and the SWE at Node 1190 and 1196 is similar to the scattering only case.

3.3 Discussion of Ancillary Results

The major findings of Chapter II are confirmed by the ancillary results of Chapter III. In particular, confidence has been affirmed in the model representations of snow pack energy and mass balance, canopy dynamics and the various radiation schemes. Two distinct scenarios related to the radiation schemes were presented. The first, with a uniformly applied surface albedo of 0.6, clearly demonstrated the effects of remote shading, remote scattering and the combination of the two on the amount of absorbed shortwave radiation by removing varying albedo that is introduced by modeling snow dynamics. In the remote sheltering case, Zones 2 and 5 had significant decreases in radiation. When scattering only was applied, then increases throughout the basin were found, especially in Zones 2, 3 and 4. Snow hillsope albedo produced the largest increases in absorbed shortwave radiation, followed by the representation using mixed albedo and the vegetation albedo. When both scattering and shading were applied, the snow hillslope albedo produced a pattern of absorbed radiation nearly identical to that found in the scattering-only case. The vegetation hillslope albedo produced a muted pattern of absorbed radiation of the shading-only case with small positive deviations from scattering primarily occuring in Zone 4. The mixed hillslope albedo representation produced a mix of the shading-only and scattering-only cases, but the dominance of scattering from snow-covered surfaces was emphasized by the prevalence of positive deviations.

In short, when a uniform albedo is applied, a clear picture of the interaction between topography and radiation appears. Shading, which is dependent only on topography, becomes important only in areas of large topographic relief or when the albedo of the surrounding landscape is low. Shading also serves to decrease the amount of light that is scattered in all cases. Scattering is very sensitive to hillslope albedo representation, and, when the landscape albedo is high, can dominate the shading signal.

The second scenario examined the interaction of snow and radiation by modeling both remote controls on radiation and snow dynamics. This leads to time-varying surface and hillslope albedos, complicating the results. The distribution of absorbed radiation in all cases is similar in pattern, though different in magnitude, to that of the uniform albedo scenario. The increase in magnitude is due to the non-snow-covered periods of time when lower surface albedos are used, increasing absorption. These changes from the base case in absorbed shortwave raditation manifest themselves in the distribution of snow-related variables in the basin. In the shading-only case, the deviations in peak SWE and DOYP are small but are correlated with the distribution of radiation. The strong relationship between radiation and cumulative time snow-covered is more instructive. When comparing these two maps, the regions with decreases in radiation have increases in snow-covered time.

In the scattering-only case, the importance to the spatiotemporal distribution of hillslope albedo and the significance of scattering are emphasized. Here, the region of peak SWE and DOYP that was restricted to Zones 1 and 2 are extended into Zone 4. This corresponds to the largest increases in absorbed radiation in the catchment. The

same is true for snow-covered time, with the areas of largest decreases in snow-covered time corresponding to the regions of largest increases in absorbed radiation. This related shift of radiation and snow variables is largest when snow albedo is used for the hillslope albedo, with similar results for the mixed albedo. When vegetation albedo is used, the regions affected are similar, and, given the smaller deviations of radiation, the differences of snow variables is correspondingly small.

When both scattering and shading are modeled, the distribution of snow variables is once again related to the distribution of absorbed radiation in the same way that it was in the shading-only and scattering-only case; when both are modeled, the results are a composite. If vegetation hillslope albedo is applied, then the decreases in Zones 2 and 5 lead to increased snow-covered time and mild deviations in peak SWE and DOYP. Overall, when vegetation hillslope albedo is used, the results are remarkably similar to the base case. Representing the landscape albedo with snow or mixed albedo leads to the dominance of scattering, as seen in increased radiation, large deviations in peak SWE and DOYP, and decreased snow-covered time. All of these deviations are correlated in space and related to the high albedo of snow. In Zone 2, however, there remained regions of decreased absorbed radiation and increased snow-covered time. The effects on peak SWE and DOYP are minor, similar to the shading-only case.

The primary difference between the two scenarios (uniform cover and dynamic albedo) is in the magnitude of absorbed radiation. The visual patterns, which are constrained by topography, remain nearly the same. The change in magnitude of

absorbed radiation is due to the lower albedo durings time with no snow cover when snow is modeled.

To summarize, the incorporation of shading leads to less absorbed radiation, and, when snow dynamics are modeled, correspondingly more persistent snow pack. When scattering only is modeled, then radiation increases and the persistence of the snow pack decreases. Snow hillslope albedo leads to the largest deviations, followed by mixed and then vegetation albedo representations. If both scattering and shading are incorporated, the results are a composite of the results from the two other cases. If vegetation albedo is used, some areas (e.g., Zone 4) reflect the increase in radiation from scattering, while others (e.g., Zone 2) reflect large decreases in radiation. Much of the catchment displays small changes from the local case, as the scattering is balanced out by remote shading. If snow or mixed hillslope albedo is applied, then the component of scattering dominates over shading. These effects are significant, decreasing snow-covered time by weeks. Only in deeply incised regions (Zones 2 and 5) are the effects of shading prevalent.

3.4 Summary

I have presented a single-layer energy-balance snow model that incorporates snow-vegetation-terrain interactions by representing local interception of snow by vegetation canopy and controls on incoming shortwave radiation through sheltering and scattering from distant topography. I presented four different representations of topographic controls on incoming shortwave radiation: local controls of slope and aspect; local and remote shading; local shading and remote scattering; and local and remote shading with remote scattering. In the remote cases incorporating scattering,

three subcases were presented, where I changed the representation of the albedo of distant slopes among (1) vegetation albedo, (2) snow albedo, (3) a dynamic mix of vegetation and snow albedo. I applied these models to the La Jara catchment in the Valles Caldera National Preserve in the Jemez Mountains of north central New Mexico between 1 November 2004 and 5 June 2005. After completing the simulations, their results were compared, specifically the different simulated absorbed shortwave radiation, maximum SWE, and temporal persistence of snow in the catchment.

The simulations led to some interesting and unexpected results. When the landscape albedo (i.e., the albedo of the distant hillslope) was taken to be that of vegetation, it appears that the scattered radiation and the radiation blocked by topography balance in such a way that the effective incoming shortwave radiation was similar to the local case. In other words, at least for La Jara, only minor deviations from the local case have been seen when the remote sheltering and vegetation landscape albedo was used.

This near equivalence between the base case and the vegetative case was in stark contrast to the case when snow albedo is used. Here, the deviations in radiation from the local case were dramatic, generally causing a more ephemeral snow pack. The increases in radiation led to less persistent snow cover throughout the catchment. The decreases in snow-cover persistence led to a less persistent snow pack earlier in the season. We defined peak SWE to be the maximum of the most persistent (longest continuous snow cover) portion of the simulation. Because of this definition the earlier portions of the season where peak SWE occurred previously were no longer

the most persistent snow cover of the simulation, changing both the date of peak and the peak SWE amount to a later date and a greater amount.

When the dynamic snow-vegetation albedo was applied, the results are nearly identical to when snow albedo is used. This results from the temperature-index based unloading scheme used. The cold temperatures forcing the model cause snow to remain in the canopy for extended periods of time, leading to snow-only albedo, and not a combination of snow and vegetation albedo, for most of the modeled period.

3.5 Recommendations for Future Work

My recommendations fall into three categories. The first consists of improvements to the snow algorithm. The second consists of possible numerical studies that directly address the local and remote controls of vegetation. The third consists of field studies that examine the issues of distant vegetative, snow, and topography interactions.

There are some immediate additions that can be made to the snow model. First, the single layer scheme needs to be extended to at least a two-layer and possibly a multi-layer scheme. Either of these extensions may lead to significant improvements with respect to model accuracy. The model needs to incorporate at least the active-inactive zones of a two-layer model to be more accurate (Marks et al., 1999). If more emphasis were placed on understanding effects of radiation, a multiple layer scheme incorporating extinction depths, detailed snow and ice microphysics, and adjustments made to the albedo for litter and dust is preferable, though more computationally expensive (Anderson, 1976).

Similarly, shallow ground heat flux needs to be included in the modeled energy balance, even in the single-layer model (Tarboton and Luce, 1997). This would allow the accumulation periods of the season to be better captured, which then ensures an accurate portrayal of the ablation season. Some of framework for the computation of ground heat flux is already in place in tRIBS that should allow for a relatively fast implementation (Ivanov et al., 2004).

A more accurate snowmelt algorithm is also needed. Currently, a threshold method is used because of its simplicity. Either the algorithm used by Tarboton and Luce (1997) or by Albert and Krajeski (1998) is recommended. Either model would help ensure more realistic melt periods and downstream hydrographs.

Currently, there is no truly satisfactory model for unloading of snow captured in the canopy. The two competing models are presented in Pomeroy et al. (1998) and Liston and Elder (2006). The latter is used here. Pomeroy et al. (1998), unfortunately, does not allow for preexisting snow in the canopy. For single interception events, it can be made to fit the unloading of individual trees through expensive field experiments and calibration. Liston and Elder (2006) present an empirical model without clearly justifiable parameters. This model, however, does allow for loading of snow in an already partially filled canopy and has some physical reasoning (in warmer temperatures, the viscosity of snow decreases and the elasticity of branches increase, leading to faster unloading). This problem should be looked at in greater detail and approached from basic stress-strain relationships that would hopefully scale up to a simple set of relationships involving temperature, vapor pressure, and wind speed.

Additional numerical studies can be performed based on the developed applications for the Quemazon SNOTEL station and La Jara catchment. These studies focus on the effects of vegetation on the partitioning of water and energy under the current model assumptions.

A detailed sensitivity study of the parameters of the loading, sublimation and unloading scheme needs to be performed, with the primary focus not necessarily on the impact to the state of the canopy, but, instead, on the effect of different parameterizations on the state of snow on the ground (i.e., changes in distribution of SWE). I do not believe these generally accepted models have been tested in this way. Additionally, a full sensitivity analysis of the impact of landscape albedo on the distribution of radiation and SWE needs to be carried out. This study focused on two end-members (snow albedo vs. vegetation albedo). This leads to a gap in specific knowledge of the different regimes possibly due to variations in landscape albedo.

Currently, a component of the tRIBS is being developed that will allow dynamically varying albedo, vegetation fraction, LAI, and other vegetation parameters. This, in the context of snow-cover, should be examined both with actual data sets and synthetic data in order to clearly show the relationships in time of the state of vegetation and snow-cover.

Finally, a well-paremeterized warm-season tRIBS application in La Jara needs to be developed. As this study focused only on the snow-cover, the groundwater table, soil parameters, and some of the vegetation parameters were not focused on, leading to an unexplored representation of runoff and groundwater flow.

My recommendations for field studies are focused on quantifying the actual contributions of terrain-scattered radiation as well as the controls of sheltering, and how are these effects are distributed in space. A series of criterion can be set in order to, first, identify suitable areas of work and, second, guide the experimental design to examine the temporal and spatial variations of scattered and sheltered light.

In terms of the field locations, some basic criteria can be specified. The overall geometry of the setting must be relatively simple (e.g., lone peak, u-shaped valley, or bowl-shaped) and contain relatively homogeneous vegetation, at least near the measurement locations. These two considerations ensure that the observations made are interpretable. One possibility is to examine the spatial decay of scattered light from a mountain out onto a plain. To the best of my knowledge, this study has not been performed. Such a study is needed to clearly conceptualize and model the scattering processes. Another, though harder, approach would incorporate different landscape elements (e.g., peaks, bowls and valleys) and measure their contributions to the shading and scattering of light.

Given the current emphasis on non-glaciated sub-alpine to alpine setting, I would recommend to retain focus on these regions at first. There is no reason not to examine glaciers, except for that the model presented in this work does not consider those dynamics. In fact, the changing albedo of perennial snow-cover and ice may yield some interesting results. For example, the long-term exposure of snow may increase the effects of dust, leading to higher degrees of surface melt that then cause ice-layers to form in deeper in the pack, aiding the conversion of snow into ice.

The instrumentation for a radiation-specific study is more complicated. A design would need to be constructed that could isolate a radiometer from scattered light, while maintained portability and retaining the possibility of removing the 'shelter' efficiently in order to get a base measurement. One possible simple design is similar to a lamp with an upturned shade. It should have an adjustable angle in order to mimic the sky-view sheltering of the region. A measurement without the shade should also be taken. As the first measurement would focus on the incoming radiation from the atmosphere, the difference between the total radiation measure and the first measurement would yield an estimate of the scattered radiation.

One of the other subtle points of these studies lie in the fact that the conditions on distant surfaces change the scattering of light. To incorporate this, spatially distributed proxies of albedo need to be found. Possibilities include remotely sensed proxies as well as site-specific measurements. One possibility is to incorporate concurrent photography from the radiation-measurement locations. This would allow the remote surface conditions to be evaluated, especially with respect to visible snow-covered area. Coincident measurements of soil moisture, during the warm season, and snow depth, during the cold season, should be taken as well in order to examine the degree of coupling of scattered light and the surface hydrology.

Closely located permanent stations across different terrain features and ecosystems that measure radiation, surface hydrologic conditions, and other hydrometeorologic variables would provide a more reliable and temporally dense set of measurements than the approach outlined above. The cost of this could be

prohibitive. In order to balance the two approaches, a sparse permanent network could be constructed with periodic intermediate measurements.

This study has led not only to some findings that point to the need to consider the landscape as a whole instead of as a collection of independent points, but also to a recommended series of numerical and field studies. All of these studies are focused, either directly or indirectly, at examining the relative importance of different portions of the energy budget on the distribution of snow. While many studies have looked at a specific process in a particular location, relatively few studies appear to consider snow-cover for what it is—a delicate manifestation of everything around it.

3.6 References

Albert, M. and Krajeski, G., 1998. A fast, physically based point snowmelt model for use in distributed applications. Hydrological Processes, 12: 1809-1824.

Anderson, E.A., 1976. Point energy and mass balance model of a snow cover. NOAA Technical Report NWS 19. 150 pp.

Benjamin, S.G., and Carlson, T.N., 1986. Some effects of surface heating and topography on the regional severe storm environment: (1) 3-Dimensional simulations. Monthly Weather Review, 114(2): 307-329

Ivanov, V.Y., Vivoni, E.R., Bras, R.L. and Entekhabi, D., 2004. Preserving high resolution surface and rainfall data in operational-scale basin hydrology: a fully distributed physically-based approach. Journal of Hydrology, 298(1-4): 80-111.

Liston, G.E. and Elder, K., 2006. A distributed snow-evolution modeling system (SnowModel). Journal of Hydrometeorology, 7(6): 1259-1276.

Marks, D., Domingo, J., Susong, D., Link, T. and Garen, D., 1999. A spatially distributed energy balance snowmelt model for application in mountain basins. Hydrological Processes, 13(12-13): 1935-1959.

Pomeroy, J.W., Parviainen, J., Hedstrom, N. and Gray, D.M., 1998. Coupled modelling of forest snow interception and sublimation. Hydrological Processes, 12(15): 2317-2337.

Tarboton, D.G. and Luce, C.H., 1996. Utah Energy Balance Snow Accumulation and Melt Model (UEB), USFS. 64 pp.

APPENDIX: IMPLEMENTATION OF SNOW DYNAMICS AND REMOTE RADIATION CONTROLS IN TRIBS AND CONTENTS OF ATTACHED DVD-ROM

A.1 Introduction

In order to provide structure for future model developers and users, extensive documentation has been constructed for the new components. The goal of this is to provide perspective and verification of the research results, introduce future authors smoothly to the model architecture (both tRIBS and snow model), facilitate version control and updates, and introduce the additional requirements and capabilities of the tRIBS to future users.

A.2 Existing Model Structure

I am incorporating snow physics and remote topographic sheltering into the tRIBS model described in Ivanov et al., (2004) and Vivoni et al. (2007). The computational mesh is based on an irregular mesh that is resampled from a gridded digital elevation model (DEM), the implementation of which is described in Tucker et al. (2001) and Vivoni et al. (2004). The existing model, including ancillary functionality and model physics, is object-oriented and written in C^{++}. Objects are abstract numerical entities that have linked functionality and properties. In tRIBS,

each single object contains a large set of functionality. For example, energy and mass balance at the surface is handled by the *tEvapoTrans* object, while infiltration processes are represented in *tHydroModel*. A hierarchy of interconnected objects forms the spatial mesh (or discretization), culminating in the pervasive *tCNode* derived class that stores the state variables, fluxes and output variables of each node in the mesh. A class is an instance of an object (e.g., an integer variable is an instance of an integer type).

The classes of the model can be classified into those relevant to (a) the discretization, (b) the routing, (c) the land-surface, (d) the subsurface, (e) the input and output (I/O) for meteorological, soils and land-use data, (f) the input/output (I/O) for model options, and (g) organizing and sequencing other classes. As snow processes are surface processes, I added two objects to (c). In order to represent shading from remote topography, however, another class was required in (e). Numerous minor changes were also needed in classes relevant to (a) the discretization, (g) ancillary classes, (d) subsurface classes and (f) I/O for model options, as documented in Table A.1.

Table A.1 A list of the changes to existing classes. The noted changes are added functions, added variables and modified functions. Within the code, changes can be tracked by searching the function for *AJR 2007*.

Class (Class Type)	Added Functions	Added Variables	Modified Functions
tOutput *(I/O)*			*void* CreateAndOpenPixel() *void* CreateAndOpenDynVar()
tCOutput (I/O)			*void* WritePixelInfo(*double*) *void* WriteDynamicVar(*double)* *void* WriteDynamicVars(*double)* *void* WriteIntegrVars(*double*)
tFlowResults *(I/O)*			*void* write_inter_hyd(*char **, *char *, int*)
tFlowNet *(Routing)*			*void* SurfaceFlow()
tCNode (Discretization)	*double* getLiqWE() *double* getIceWE() *double*getDU() *double*getLiqRouted() *double* getSnTempC() *double* getCrustAge() *double* getDensityAge() *double* getEvapoTransAge() *double* getSnLHF() *double* getSnSHF() *double* getSnGHF() *double* getSnPHF() *double* getSnRLin() *double* getSnRLout() *double* getRSin() *double* getUnode() *double* getUerror() *double* getCumLHF() *double* getCumSHF() *double* getCumPHF()	*Double* liqWEg *double* iceWEq *double* dU *Double* liqroute *double* snTemperC *double* crAge *double* densAge *double* ETage *Double* snLHF *Double* snSHF *Double* snGHF *Double* snPHF *double* snRLout *Double* snRLin *Double* snRSin *Double* Unode *double* Uerror *double* intSWEq *Double* intPrec *double* intSnUnload	tCNode() tCNode(tInput &)

Table A.1 Continued

	double getCumRLin()	*double* intSub	
	double getCumRLout()	*double* horizonAngle0000	
	double getCumRLin()	*double* horizonAngle0225	
	double getCumRSin()	*double* horizonAngle0450	
	double getCumGHF()	*double* horizonAngle0675	
	double getCumHrsSun()	*double* horizonAngle0900	
	double getCumHrsSnow()	*double* horizonAngle1125	
	double getCumUerror()	*double* horizonAngle1350	
	double getIntSWE()	*double* horizonAngle1575	
	double getIntPrec()	*double* horizonAngle1800	
	double getIntSnUnload()	*double* horizonAngle2025	
	double getIntSub()	*double* horizonAngle2250	
	double getCumIntSub()	*double* horizonAngle2475	
	double getCumIntUnl()	*double* horizonAngle2700	
	double getHorAngle0000()	*double* horizonAngle2925	
	double getHorAngle0225()	*double* horizonAngle3150	
	double getHorAngle0450()	*double* horizonAngle3375	
	double getHorAngle0675()	*double* sfact	
	double getHorAngle0900()	*double* lfact	
	double getHorAngle1125()		
	double getHorAngle1350()		
	double getHorAngle1575()		
	double getHorAngle1800()		
	double getHorAngle2025()		

Table A.1 Continued

	double getHorAngle2250() *double* getHorAngle2475() *double* getHorAngle2700() *double* getHorAngle2925() *double* getHorAngle3150() *double* getHorAngle3375() *double* getSheltFact() *double* getLandFact() *void* setLiqWE(*double*) *void* setIceWE(*double*) *void* setDU(*double*) *void* setLiqRouted(*double*) *void* setSnTempC(*double*) *void* setCrustAge(*double*) *void* setDensityAge(*double*) *void* setEvapoTransAge(*double*) *void* setSnLHF(*double*) *void* setSnSHF(*double*) *void* setSnGHF(*double*) *void* setSnPHF(*double*) *void* setSnRLin(*double*) *void* setSnRLout(*double*) *void* setRSin(*double*) *void* setUnode(*double*) *void* setUerror(*double*) *void* setIntSWE(*double*) *void* setIntPrec(*double*) *void* setIntSnUnload(*double*) *void* setIntSub(*double*) *void* setHorAngle0000(*double*) *void* setHorAngle0225(*double*) *void* setHorAngle0450(*double*) *void* setHorAngle0675(*double*)		

Table A.1 Continued

	void setHorAngle0900(*double*) *void* setHorAngle1125(*double*) *void* setHorAngle1350(*double*) *void* setHorAngle1575(*double*) *void* setHorAngle1800(*double*) *void* setHorAngle2025(*double*) *void* setHorAngle2250(*double*) *void* setHorAngle2475(*double*) *void* setHorAngle2700(*double*) *void* setHorAngle2925(*double*) *void* setHorAngle3150(*double*) *void* setHorAngle3375(*double*) *void* setSheltFact(*double*) *void* setLandFact(*double*) *void* addLHF(*double*) *void* addSHF(*double*) *void* addPHF(*double*) *void* addRLin(*double*) *void* addRLout(*double*) *void* addRLin(*double*) *void* addRSin(*double*) *void* addGHF(*double*) *void* addHrsSun(*double*) *void* addHrsSnow(*double*) *void* addUerror(*double*) *void* addIntSub(*double*) *void* addIntUnl(*double*)		

tPreprocess (Ancillary)			*void* CheckInputFile(tInputFile &)
tSimulator (Ancillary)			*void* simulation_loop(tHydroModel*, tKinemat*, tEvapoTrans*, tIntercept*, tWaterBalance*, tSnowPack*, tSnowIntercept*) *void* RunItAgain(tInputFile &, tHydroModel*, tKinemat*, tEvapoTrans*, tIntercept*, tWaterBalance*, tSnowPack*, tSnowIntercept*) *void* SurfaceHydryoProcesses(tEvapoTrans*, tIntercept*, tSnowPack*, tSnowIntercept*)
tHydroModel (Subsurface)			*void* UnSaturatedZone(*double*)
VCell (Discretization)	*int* findDirectionIntersectionPoint(*in, double, double, double*, double*, double*, double*, int)*		*void* convertToVoronoiFormat(*int*)

Table A.2 The inheritance structure of the new classes (*tShelter, tSnowPack, tSnowIntercept*) from base classes (*tResample, tSnowPack, tSnowIntercept*).

Base Class	*tResample*	*tEvapoTrans*	*TEvapoTrans*
Derived Class	*tShelter*	*tSnowPack*	*tSnowIntercept*

A.3 Added Classes

I have added three new classes: *tSnowPack*, *tSnowIntercept* and *tShelter*. All three are derived classes (Table A.2). Of these, *tSnowPack* and *tSnowIntercept* add physics to model. Snow pack dynamics are included in *tSnowPack* and snow-canopy interactions are included in *tSnowIntercept*. Both of these classes inherit from *tEvapoTrans* as they require much of the same functionality. The class *tShelter* derives gridded maps of horizon angles at 16 azimuths and subsequently resamples the grids to the Voronoi polygon mesh via areally weighted averaging. Because of their similar functions, *tShelter* is derived from *tResample*. The sky-view and land-view factors are calculated before any physical calculations (i.e. incoming radiation) are performed. A list of functions and variables for each added class is found in Tables A.3.

A.4 Guide to DVD-ROM

The attached DVD-ROM consists of several sets of files. These consist of (a) the entire source code (tRIBS and the snow model), (b) site-specific and option specific models, (c) flow charts of the algorithm, and (d) adjusted tRIBS user manuals.

Table A.3 The architecture of added classes (*tShelter*, *tSnowPack* and *tSnowIntercept*) with added functions and variables.

Class (Class Type)	Added Functions	Added Variables
tShelter	tShelter()	*double* GridInPath[50]
(Ancillary)	tShelter(*tSimulationControl**,*tMesh<tCNode>**, *tInputFile&*)	*double* angleDiv
	~tShelter	*double* horAngle
		double maxTan
		double tempTan
		double maxRow
		double maxCol
		double maxZ
		double tempZ
		double initZ
		double sv
		double lv
		double slope
		double aspect
		double elevation
		double **horAngleX
		double **tempGrid
		int radSheltOpt
		int windSheltOpt
tSnowPack	tSnowPack()	*double* densityAge
(Surface)	tSnowPack(*tSimulationControl**, *tMesh<tCNode>**, *tInputFile&*, *tRunTimer**, *tResample**, *tHydroModel**, *tRainfall**)	*double* rainTemp
	~tSnowPack()	*double* ETAge
	void SetSnowPackVariables(*tInput&*, *tHydroModel**)	*double* timeSteph
	void SetSnowVariables(*tInput &*, *tHydroModel**)	*double* timeStepm
	void callSnowPack(*tIntercept**, *int*, *tSnowIntercept**, *double*, *double*)	*double* timeSteps
	void getFrNodeSnP(*tCNode**)	*double* minutelyTimeStep
	void setToNodeSnP(*tCNode**)	*double*liqWE
	void SetSunVariablesSn()	*double* iceWE
	void snowEB(*int*)	*double* snWE
	int getSnowOpt()	*double* liqRoute
	double densityFromAge()	*double* liqWEm

Table A.3 Continued

	double latentHFCalc(*double*) *double* sensibleHFCalc(*double*) *double* snowFracCalc() *double* precipiationHFCalc() *double* latHeatVapCalc() *double* latHeatFreezeCalc() *double* latHeatSubCalc() *double* heatCapAirCalc() *double* heatCapSolCalc() *double* heatCapLiqCalc() *double* vaporPressSnowSurfCalc() *double* agingAlbedo() *double* resFactCalc() *double* inShortWaveSn() *double* inLongWaveSn() *double* emmisSn() *double* CtoK() *double* KtoC()	*double* iceWEm *double* snWEm *double*Utot *double* Usn *double* Uwat *double* Utotold *double* liqWatCont *double* liqTempC *double* iceTempC *double* snTempC *double* liqTempK *double* iceTempK *double* snTempK *double* crustAge *double* H *double* L *double* G *double* Prec *double* Rn *double*dUint *double* Rlin *double* Rlout *double* Rsin *double* Uerr *double* snPrec *double* liqPrec *double* snPrecm *double* liqPrecm *double* snPrecmm *double* liqPrecmm *double* snUnl *double* vapPressSmb *double* vapPresskSPa *double* rholiqcgs *double* rhoicecgs *double* rhosncgs *double* rholiqkg *double* rhoicekg *double* rhosnkg *double* rhoAir

Table A.3 Continued

		double phfOnOff *double* cpsnowkJ *double* cpicekJ *double* cpwaterkJ *double* cpairkJ *double* latFreezekJ *double* latVapkJ *double* latSubkJ *double* resFact *double* hillalbedo *double* albedo *double* compactParam *double* rhoSnFreshkg *double* snDepth *double* snDepthm *double* snOnOff *double* naughttokilo *double*kilotonaught *double* cgsRHOtomks *double* mksRHOtocgs *double* naughttocm *double* cmtonaught *double* ctom *double* mtoc
tSnowIntercept (Surface)	tSnowIntercept() tSnowIntercept(*tSimulationControl**, *tMesh<tCNode>**, *tInputFile&*, *tRunTimer**, *tResample**, *tHydroModel**, *tRainfall**) ~tSnowIntercept() *void* SetSnowInterceptVariables(*tInput&*, *tHydroModel**) *void* SetSnowVariables(*tInput &*, *tHydroModel**) *void* callSnowIntercept(*tCNode**, *tIntercept**) *void* getFrNodeSnP(*tCNode**) *void* setToNodeSnP(*tCNode**)	*int* nID *double* timeSteph *double* timeStepm *double* timeSteps *double* minutelyTimeStep *double*liqWE *double* iceWE *double* snWE

Table A.3 Continued

	void SetSunVariablesSn()	*double* liqRoute
	void snowEB(*int*)	*double* liqWEm
	void computeSub()	*double* iceWEm
	void computeUnload()	*double* snWEm
	int getSnowOpt()	*double*Utot
	double densityFromAge()	*double* Usn
	double latentHFCalc(*double*)	*double* Uwat
	double snowFracCalc()	*double* Utotold
	double latHeatVapCalc()	*double* liqWatCont
	double latHeatFreezeCalc()	*double* liqTempC
	double latHeatSubCalc()	*double* iceTempC
	double heatCapAirCalc()	*double* snTempC
	double heatCapSolCalc()	*double* liqTempK
	double heatCapLiqCalc()	*double* iceTempK
	double inShortWaveSn()	*double* snTempK
	double CtoK()	*double* crustAge
	double KtoC()	*double* H
		double L
		double G
		double Prec
		double Rn
		*double*dUint
		double Rlin
		double Rlout
		double Rsin
		double Uerr
		double snPrec
		double liqPrec
		double snPrecm
		double liqPrecm
		double snPrecmm
		double liqPrecmm
		double snUnl
		double vapPressSmb
		double vapPresskSPa
		double rholiqcgs
		double rhoicecgs
		double rhosncgs
		double rholiqkg
		double rhoicekg

Table A.3 Continued

		double rhosnkg
		double rhoAir
		double phfOnOff
		double cpsnowkJ
		double cpicekJ
		double cpwaterkJ
		double cpairkJ
		double latFreezekJ
		double latVapkJ
		double latSubkJ
		double resFact
		double hillalbedo
		double albedo
		double compactParam
		double rhoSnFreshkg
		double snDepth
		double snDepthm
		double snOnOff
		double naughttokilo
		*double*kilotonaught
		double cgsRHOtomks
		double mksRHOtocgs
		double naughttocm
		double cmtonaught
		double ctom
		double mtoc
		double htos
		double Qcs
		double Ce
		double I
		double Iold
		double psiS
		double Imax
		double prec
		double LAI
		double kc
		double iceRad
		double dmdt
		double Omega
		double Sp

Table A.3 Continued

		double RH *double* D *double* rhoVap *double* Sh *double* Nu *double* Re *double* Ktatm *double* Ta *double* Mwater *double* R *double* RdryAir *double* esatIce *double* nu *double* beta *double* acoefficient *double* Lm *double* airTempK *double* effPrecip

A.4.1 Source Code

The entirety of the source code is found in *./Code*. Tables A.1 and A.3 have a list of new classes, new and altered functions and new and altered variables. Each new or adjusted group of code begins with a description and is marked with *AJR 2007* to indicate its addition. The comments found in the code form an adequate description of the architecture and algorithms of the new modules. The general style mimics that of the pre-existing source code. In the physical classes (i.e., *tSnowPack* and *tSnowIntercept*), this consists of constructors and destructors with associated initialization functions, calling functions, functions that interact with the discretization objects (*tCNode*), unit conversion functions, physical subroutines for computation of fluxes and parameters, and miscellaneous auxiliary functions. In

tShelter, an ancillary class, there is only one set of functions, the constructor, as this class only derives and resamples horizon angles and sky-view factors. As *tShelter* inherits from *tResample*, most of the functions and variables used are already present in the base class.

To run the uniform case, the code was hardwired to run with the appropriate albedos (see Chapter 3). This is done in the function *inShortWave()* in *tEvapoTrans.cpp*. Then , the code needs to be recompiled.

A.4.2 Makefile, Compilation and Executable

The compilation process of the modified code is the same as before: in order to compile the code, use the command *make –f makeLINUX* at the prompt with the needed make file in the same directory. The makefile, *makeLINUX* , is found in *./Code*. The executable used for the simulations, *tribs.exe,* are also found in *./Code*. To run all of the simulations, use the runfile, *tribs0405_multi*.

A.4.3 Site Models

Two site specific model applications are found in the directories *./quemazon* and *./lj20*. The meteorological data, including rainfall, for the Quemazon and La Jara models are found under *./quemazon/Weather* and *./lj07/Weather*, respectively. The *.in files are found in *./quemazon* and *./lj20*. The files associated with land-use, soils, and digital elevation maps, and point files are found in *./quemazon/Input* and *lj20/Input*. In the *Output** directories the**.aml* scripts and MATLAB **.m* files needed to process the various map outputs are found. The point outputs are found in

the same directory with the extension **.pixel*. Integrated average basin responses from **.mrf* files are found in *Output*/hyd*.

In order to run the model applications, export the file directory into an appropriate directory, adjust the needed file pathnames in the **.in* file, and start the simulations according to the instructions in the user manual, which is also found on the DVD-ROM.

A number of **.in* files are used in the simulations from this thesis. In *quemazon*, there is only *quem0405.in*. In *lj20*, a number of **.in* files are found for the different cases. For each, the base name is *lj_Winter0405_a#s%&*. The # is a wildcard for the hillslope albedo option (0 => snow albedo, 1 => land-use albedo, and 2=> mixed temporally varying albedo) used in the **.in* file. The *%* is a wildcard for the shelter option used (0 => local with no hillslope scattering, 1 => remote control on diffuse shading and scattering, 2 => remote control on direct and diffuse shading and scattering, and 3 => no sheltering or scattering). The & is whether a uniform albedo (1) or snow dynamics was used (&).

The same nomenclature used for specifying the **.in* files for the La Jara model are used to specify the *Output* directories. There are four *Output_a#s%* directories with # representing the user-selected hillslope albedo option and *%* representing the user-selected sheltering option. The outputs used in this work are also included, the base name specified in the *.in file (*lj* or quem**) with *_base* appended.

The scripts used to visualize model spatial output are also included in each output directory. In order to visualize snow variables in *ArcGIS*, it is necessary to truncate the spatial output files. This is done by using *findZeros_tRIBSmap.m* and

findZeros_DYNmap.m. These output *temp.** files that can then be changed appropriately (e.g. from temp to lj) and inputted into *createtribsmap_crip.aml* (for integrated output) and *createtribsmap_drip.aml* (for dynamic output) to construct the Arc coverages used for visualization of results. The scripts *createvoicover.aml* and *createrchcover.aml* do not require any preprocessing to use.

A point worth mentioning concerns the meshes and parameterization used in the two models. The Quemazon SNOTEL station corresponds to node 100 of the Quemazon model. With the current version of tRIBS, a small headwater basin containing the site was delineated. This mesh includes concave polygons that are constructed improperly by tRIBS. These polygons were not corrected as each node acts independently, and the node of interest was not concave.

The model developed for La Jara catchment is developed using a 10 m DEM. An allowed disparity (z_r error tolerance) of 2.0 m was allowed between the DEM and the derived TIN. A stream threshold of 500 m^2 was used to derive the network. This means that the model treats a polygon that has a contributing area of 500 m^2 or more as a stream polygon. The boundary and stream reaches were manually checked for consistency and nodes associated with concave polygons were corrected. There were four concave polygons derived by the mesh generator. Given that this is less than 0.1% of the total number of polygons and the concave polygons were small, these nodes were deleted from the nodes file.

A.4.4 Flowcharts

Linked flowcharts (Table A.4) are found in *./FlowCharts* and fall into three groups. The general approach was to provide a broad map of the flow of execution

and logic in the program, beginning with *main.cpp* and progressing through detailed physical and geometric algorithms. This warranted including details of code that was not constructed in this work and, in order to only show the most pertinent portions of the program, to leave out some of the details of the added modules.

Excluding *main.cpp*, the flowcharts fall into three groups. The first group is the flowchart of *cVell::convertToVoronoiFormat()*. The case of small grid cell size and large Voronoi polygons was not accounted for in the original function. I have added this functionality. The second group is the *tShelter::tShelter()* constructor. To easily access needed functionality, *tShelter* inherits from *tResample*. Lastly, a sequence of flowcharts detailing the physics of the snow algorithm, both of the snow pack (*tSnowPack*) and snow interception (*tSnowIntercept*), is included. The organization of flow charts is summarized in Table A.4.

A.4.5 User Manual

The existing model already has an extensive user manual that lists input parameters, classes, data sources, among other information. Changes have been made to include the addition of the remote shading and snow physics. These changes are mostly consolidated in the description of the classes, and input options, pathnames and parameters. The updated **.html* files are included under *usermanual.html, modelinfo.html* and *modeloutput.html* in the home directory.

Table A.4 A list of the pages and their links. The list is naturally repetitive and also characterizes the modular nature of the programming style.

Page	Link
main.cpp	convertToVoronoiFormat tShelter callSnowPack
convertToVoronoiFormat	main.cpp
tShelter	main.cpp
callSnowPack	main.cpp callSnowIntercept snowFracCalc resFactCalc latentHFCalc precipitationHFCalc agingAlbedo snowEB
callSnowIntercept	callSnowPack computeSub computeUnload snowFracCalc
snowFracCalc	callSnowPack callSnowIntercept precipitationHFCalc
resFactCalc	callSnowPack snowEB
compSkyCover	inShortWaveSn inLongWaveSn

Page	Link
latentHFCalc	callSnowPack snowEB
precipitationHFCalc	callSnowPack snowFracCalc snowEB
agingAlbedo	callSnowPack
snowEB	callSnowPack latentHFCalc sensibleHFCalc inShortWaveSn inLongWaveSn
computeSub	callSnowIntercept inShortWaveSn
computeUnload	callSnowIntercept
sensibleHFCalc	snowEB
inShortWaveSn	snowEB computeSub aboveHorizon compSkyCover
inLongWaveSn	snowEB compSkyCover
aboveHorizon	inShortWaveSn

A.6 References

Ivanov, V.Y., Vivoni, E.R., Bras, R.L. and Entekhabi, D., 2004. Preserving high-resolution surface and rainfall data in operational-scale basin hydrology: a fully-distributed physically-based approach. Journal of Hydrology, 298(1-4): 80-111.

Tucker, G.E., Lancaster, S.T., Gasparini, N.M., Bras, R.L. and Rybarczyk, S.M., 2001. An object-oriented framework for distributed hydrologic and geomorphic modeling using triangulated irregular networks. Computers & Geosciences, 27(8): 959-973.

Vivoni, E.R., Ivanov, V.Y., Bras, R.L. and Entekhabi, D., 2004. Generation of triangulated irregular networks based on hydrological similarity. Journal of Hydrologic Engineering, 9(4): 288-302.

Vivoni, E.R., Entekhabi, D., Bras R.L., and Ivanov, V.Y., 2007. Controls on runoff generation and scale dependence in a distributed hydrologic model. Hydrology and Earth Systems Science, 11: 1683-1701.

Wyckoff, R.L., 2007. Sensitivity to Arroyo Development Scenarios: Insights from a Distributed Hydrologic Model, New Mexico Institute of Mining and Technology, Socorro, NM, 208 pp.